UNIVERSITY OF COPENHAGEN
FACULTY OF SCIENCE

PhD thesis

Alexandra Messerli

Surface velocities and hydrology at Engabreen:

Observations from feature tracking and hydro-meteorological measurements

Academic advisors:

Aslak Grinsted
Dorthe Dahl-Jensen
Nanna Karlsson
Centre for Ice and Climate, Niels Bohr Institute, University of Copenhagen, Denmark

Miriam Jackson
Norwegian Water Resources and Energy Directorate (NVE), Oslo, Norway

This thesis has been submitted to the PhD school of the Faculty of Science, University of Copenhagen
Submitted: 11/03/15

Abstract

Recent studies have likened the seasonal observations of ice flow at the marginal regions of the Greenland Ice Sheet (GrIS) to those found on smaller alpine and valley counterparts. These similarities highlight the need for further small scale studies of seasonal evolution in the hydrological and dynamic structure of valley glaciers, to aid interpretation of observations from the margins of the GrIS. This thesis aims to collate a large suit of glacio-hydrological data from the outlet glacier Engabreen, Norway, in order to better understand the role the subglacial drainage configuration has on surface velocities recorded at the site.

The Svartisen Subglacial Laboratory (SSL) under Engabreen, augmented by additional subglacial pressure and hydrological measurements, provides a invaluable observations for detailed process-oriented studies. However, the lack of complementary surface velocity data complicates comparisons with other surface-oriented glacio-hydrological studies. One major aim of this thesis is to provide a longer record of surface velocity, enabling a more complete understanding of the glacial hydro-mechanical relationship at Engabreen. In order to extend the velocity dataset here, a time-lapse camera based study was carried out, providing seasonal velocity maps over a large portion of an inaccessible region of the glacier. The processing and feature tracking of terrestrially based imagery, in order to obtain quantitative velocity measurements, is challenging. Whilst optical feature tracking has a relatively long history in glaciology, the availability of adaptable terrestrial georectifiaction and feature tracking tools is somewhat limited. A key achievement of this thesis is the development of a new, comprehensive, georectification and feature tracking toolbox, ImGRAFT. This adaptable tool performs both rectification of the time-lapse camera imagery, and feature tracking. The resulting velocity estimates are able to capture seasonal changes in velocity structure at Engabreen, as well as short-term speed-up events, in response to hydro-meteorological forcings.

GPS velocity data from the lower tongue of Engabreen are analysed in detail alongside the hydro-meteorological time-series. The higher temporal resolution of the GPS allows the effect of short-term hydrological forcings on ice flow to be assessed. Two key events: the spring-speed up event (P1a) and a short-term rain induced event (P1b), provide the focus for the analysis, where causal relationships between the changes in the surface velocities are discussed within the context of changes in the subglacial hydrological system. Engabreen exhibits a classic spring-speed up event, but appears insensitive to subsequent pulse inputs of meltwater.

Interpretation of these data are aided by examining geomorphologial evidence at Engabreen. The recent deglaciation at the margin of the glacier provides insight into the detailed structure of the former, and current, subglacial drainage system. The

unique geomorphology observed on the bedrock at Engabreen, characterised by deeply incised perpendicular cutting canyons, suggests a mixed Nye-channel linked-cavity drainage configuration. These prominent features are likely to explain the lower sensitivity of Engabreen to pulse inputs of meltwater.

Resumè

Nye studier har sammenlignet observationer af isflydningen ved randen af den grønlandske indlandsis (GrIS), med isflydningen ved randen af små alpine og dal gletchere. Lighederne fra disse sammenligninger, fremhæver nødvendigheden af yderligere studier af den årstids afhængige evolution i den hydrologiske og dynamiske struktur af dal gletchere. Dermed vil en bedre forståelse af observationerne fra randen af GrIS blive opnået. Formålet med denne afhandling, er at sammenligne en stor mængde glacial-hydrologisk data fra "outlet" gletcheren Engabreen i Norge. Dermed kan afsmeltningens rolle, under geltcheren, på de overflade hastigheder der er blevet fundet bedre at forstås.
Betydningen af Svartisen Subglacial Laboratory (SSL), beliggende under Engabreen, samt det store net af trykmålinger og hydrologiske målinger under isen, gør lokationen fordelagtig for yderligere detaljerede process-orienterede studier. Det er imidlertid en udfordring med manglende overflade-hastigheds målinger. Denne mangel gœr sammenligningen med andre glacio-hydrologiske overflade-studier udfordrende. En stor del af denne afhandling er, at fremskaffe en længere optegnelse af overflade-hastigheder. Dette muliggœr en mere komplet forståelse for det glaciologiske-hydrologiske-makaniske forhold på Engabreen. Hastigheds-optegnelsen af Engabreen blev udfærdiget, ved at udfœre et time-lapse kamera baseret studie. Dermed kunne hastigheds-kort, for et stort ufremkommeligt område af gletcheren, fastlægges for hver sæson. Processen med, at behandle og feature tracking af de terrastisk baserede billeder, for derved at fremskaffe kvantitative hastighedes målinger, er udfordrende. Dette skyldes ikke midst den meget begrænsede mængde af værktœjer der findes til behandlingen af terestisk georektifikation og feature tracking. Dette er på trods af den relativt lange historie for optisk feature tracking inden for glaciologien. En af de primære bedrifter beskrevet i denne afhandling, er udviklingen af en ny omfattende georektifikation og feature tracking programmœrværktœjskasse, ImGRAFT. Med dette fleksible værktœj kan der både udfœres vanskelige korrektioner af billederne fra time-lapse kameraet samt feature tracking. De beregnede hastigheder kan både opfange sæson-afhængige ændringer i strukturen af hastighederne ved Engabreen, samt kortvarige hastighedsændringer i forbindelse med hydrologisk-meteorologiske drivkrafter.
GPS hastigheds-data fra Engabreens nederste tunge er analyseret ned til minste detalje, sidelœbende med de hydrologiske-meteorologiske tids-serier. Den hœje tidslige oplœsning af GPSen tillader vurdering af effekten af de kortvarige hydrologiske drivkrafter på is-strœmmen. I sammenhæng med ændringer i det hydrologiske system under gletcheren, danner to centrale begivender, forårs-accelerationen (P1a) og en kortvarrig regn-periode (P1b), baggrund for analysen af det kausale forhold mellem ændringerne i overflade-hastighederne. Mens Engabreen demonstrerede en klassisk forårs-acceleration, viser den ingen tegn på det efterfœlgende kortvarrige input af smeltevand. Fortolkningen af disse data bliver i denne afhandling understœttet af geomorfologiske

undersøgelser ved Engabreen. Den seneste afsmeltning ved randen af gletcheren giver en dyb insigt i den detaljerede struktur af tidligere, og nuværende, smeltevands-afløb under gletcheren. Den enestående geomorfologi der er observeret på grundfjeldet ved Engabreen, karakteriseret ved dybe lodrette fjeldklæfter, antyder et afløb af en Nye-channel linked-cavity sammensætning. Disse prominente strukturer forklarer sandsynligvis den lave følsomhed Engabreen viste overfor kortvarrige input af smeltevand.

Acknowledgements

Firstly I would like to thank all of my supervisors of which there are many! I would especially like to thank Aslak and Dorthe, for giving me this amazing opportunity and continuously pushing me to learn and explore avenues I would never have anticipated 3 years ago. Aslak: I am, and always will be in awe of your speed of coding and knowledge, they know no bounds. Finally, your coffee consumption never ceases to amaze me. Thanks to Nanna, for all your humour, friendship and red pen. It has been a delight to work with you, you always manage to keep track of the overview, of both people and the project. Thank you for always listening and coming up with cunning plans, I will miss the *comfy chair* times. Thank you to Miriam and all the NVE HB department; Hallgeir and Dick for all the help with logistics and Engabreen challenges. Thank you for allowing me to work in and explore this amazing place, both above it and below it. It truly has been a unique experience that has taught me so much, not least about myself. PiM you are a special, wonderful human being. I am so glad to have got to know you and share this roller-coaster of a journey with. I can't imagine doing all the work at Engabreen with anyone else. I look forward to many more adventures with you. I think *globally*, we made a pretty excellent team Engabreen!
To all my other adopted Norwegian family, you made me feel so welcome in your homes and I thoroughly enjoyed all the fun times with you all. Thank you to Solveig for being such a great friend and support throughout my PhD, I have really enjoyed getting to know you and enjoying many adventures with you, especially the Engabreen field trip. I can't wait for more soon! To all the my wonderful colleagues at CIC, past and present, I have loved working in this wonderful place with such inspiring and kind people. Thank you all for making me feel so welcome and at home here in Copenhagen. I didn't think it possible for a mountain, hobbit like me to feel so at home in such a flat country.
Special thanks to Anne my other Engabreen buddy, thanks for always being there to talk drainage networks and velocity fields, and of course being a key part of the Jokihop team with Paul! Thanks to Paul and Ali (and Bean) for all your great friendship throughout my time here. Pizza nights are always a highlight with you guys. Thanks to hobbit Ak, Our NEEM time was memorable, and the continuous humour a highlight in my day, Corentin for the "waaater", Mai for the tea-breaks, to new friend Joel and Laura, who have only known me in my "special" state, I look forward to fun times ahead.

A big thank to all the wonderful and crazy people who helped me in the field at Engabreen, this thesis would have looked a lot thinner without you!. Lyndsey, Maxime, Torben, Coline, Mathieu, Sofie. Thank you to Anneke for teaching me so much about Engabreen and mountaineering skills! To Heidi, thanks for all the crazy adventures we had, particularly in our first few years. The Björndalen and Svea were truly amazing and of course the New years trips to "our" mountains. Thank you for your help at

Engabreen what a team we made, the fight through the forest with ablation poles was one of the most amusing (in hindsight) moments at Engabreen! A big thanks to all of the SVALI team, I feel privileged to have been a part of such a wonderful project. In particular thank you for giving us the opportunity to travel all over the nordic countries, to collaborate with great researchers and friends. I can't wait for the final conference in Ilulissat! I will miss being a part of this close knit group of amazing people, but look forward to the prospects of future collaborations.

Finally a huge thank you to all my close friends near and far, old and new. None of this would have been possible without your humour, unwavering support and friendship. I look forward to seeing many of you more often, and thank you all for your patience whilst I embarked on my biggest adventure yet. A very special thank you to a few people who have been true, rocks over the years, some joined the journey and some were there before the craziness began. Jan, your support has been amazing from Cambridge and beyond. Holly, for always being there and keeping me going, with humour and an ear. To my birthday twin Kaitlin, thanks for the all fun times, its great to have you back. A big thanks to Helen, I can't wait for the adventures and I am not sure I would have managed without you a true rock to have around. To Felicia, thank you for your patience, and belief in me this last year, your support (and design skills) got me through.

Finally the biggest thanks to my family. To Hanni, Jürg and Maja, for always being there and believing in me! My greatest thanks to Mum and Philip, thank you for always supporting me, in everything I have done and believing in me, even when I thought it wasn't possible.

Contents

Chapter 1

Introduction

It has long been understood that water at the base of the glacier plays a fundamental role in the motion of the ice mass (e.g Weertman, 1972), through the process of basal lubrication. The interaction between glacial meltwater and ice flow, has been the focus of numerous glacial research investigations for over half a century (Iken et al., 1983; Flowers, 2010). The complex nature of the interaction and associated feedbacks between meltwater and sliding remain illusive. Whilst significant advances have been made at both small and large ice masses, key feedbacks and processes continue to elude glaciologists (Clarke, 2005; Chandler et al., 2013). In a warming climate where the availability of meltwater is changing, both spatially and temporally, the response of large ice masses, such a the Greenland ice sheet (GrIS) is of substantial glaciological and societal importance. The response of glaciers to seasonal variations in meltwater availability is well documented in an alpine and valley glacier system (e.g. Iken et al., 1983; Iken and Bindschadler, 1986; Mair et al., 2001, 2002), and more recently on the GrIS (e.g. Zwally et al., 2002; Sundal et al., 2009; Hoffman et al., 2011; Bartholomew et al., 2012; Meierbachtol et al., 2013). Evermore similarities are being drawn between the two settings as more data reveal similar responses (Andrews et al., 2014; Chandler et al., 2013). Most of the measurements on the large ice masses come from indirect measurements of changes in basal conditions, compared to the more direct approach possible on smaller valley glaciers (Chandler et al., 2013). This highlights the importance, for continued observations on valley glacier systems, where a more complete, multi-faceted approach is plausible. Engabreen, and the Svartisen Subglacial Laboratory (discussed in detail in Chapter 2), provides an optimal setting for such process-based investigations. It is evident that a more complete understanding of the link between the indirect surface measurements and the changing basal conditions at smaller ice masses, would offer yet further insights into the conditions under the marginal regions of the GrIS.

Most glaciological investigations revolve around measurements taken at or of the surface of the glacier or ice sheet. These indirect measurements are often used to infer what conditions are present at the base of the glacier. Recently, larger, extensive campaigns have successfully managed to drill to the base of the ice sheets where the borehole has been instrumented from the surface to the base with a suite of borehole logging instruments. Pressure transducers are a common feature in borehole data logging. The aim of this dataset is to estimate the basal water pressure variations throughout the season, and analyse the dataset alongside other fundamental datasets, such as surface velocity data. One recent project that has produced a number of key

studies (e.g Andrews et al., 2014; Ryser et al., 2014) is the Real-time Observations of Greenland's Under-ice Environment (ROGUE) project [1]. The collaborative project focused on the Paakitsoq region of west Greenland, just north of Jakobshavn Isbræ. These recent advances in the understanding of the motion of the GrIS highlight the usefulness of simultaneous surface and basal measurements to further explore the complex relationship between meltwater input and ice flow. The exact dynamics that take place at the base of glaciers and ice sheets during the connection of meltwater with the basal environment, at the beginning and throughout the meltseason are still not fully understood (Hoffman et al., 2011; Clarke, 2005). These complex processes also form parts of multi-sign feedback mechanisms that are to date still poorly constrained.

1.1 Motivation

The main motivation for this body of work, is to help to further constrain complex relationships acting at the glacier bed. Most of these processes are driven by changes in basal water pressure, that operate on range of scales; from small scale sliding over bedrock obstacles to entire drainage network configurations. One of larger implications of these feedbacks is the uncertainty in the future evolution of ice masses in response to changes in meltwater input to the subglacial environment. Meltwater has the ability to affect influence rates of ice motion, transporting ice from the accumulation zone via longitudinal stresses, into the ablation zone, where yet further melt is expected. The impact of the spatial and temporal extension of melt at the surface of glaciers and ice sheets is of much debate, particularly as the complex feedbacks within these systems have potential to lead to increased dynamic mass loss, that directly contributes to sea level rise (Rignot and Kanagaratnam, 2006; Hanna et al., 2008; Moon et al., 2012). The extension of the ablation zone on the GrIS, leads to a greater, more widespread area of melt. In-turn this water makes its way to the subglaial system, where it immobilises the overlying ice, through the dynamic feedbacks at ice-bed interface. In a warming climate the area of the ice sheet affected by meltwater and its associated feedbacks is increasing, therefore more of these complex feedbacks have the ability to affect large areas of the GrIS.

1.2 Objectives

A part of the wider collaborative project *Stability and Variations in Arctic Land Ice* (SVALI)[2], is to apply a range of methods to investigate observations and process oriented research to understand the changes in Arctic land-ice in relation climate change. The main goal of this thesis is to apply a multidisciplinary approach to to examine the role of hydrological forcings on short-term velocity changes at Engabreen. The process based approaches to answering these questions, provides a further understanding of glacial-hydological interaction. These findings can be used to further constrain predictive models of small and large scale ice flow behaviour, in response to changes in climatic forcings. Aside from the process-based investigations, further development of methods for observing ice surface velocities at Engabreen are made.
The broad aims of the study are as follows:

[1] http://www.ig.utexas.edu/people/staff/gcatania/rogue.html
[2] http://ncoe-svali.org/

- Develop methods to spatially and temporally extend the surface velocity measurements at Engabreen, in order to complement the continuous datasets collected at and beneath the glacier.
- Use these surface velocity datasets in combination with other hydrological and geomorphological observations, to investigate the relationship and response of ice flow to short-term variations in hydrological forcings.
- Assess the ability of small scale, process-based studies of the relationship between hydrology and ice flow at Engabreen, to be applied to other glacial settings

1.3 Thesis outline

The thesis is split into the flowing series of chapters:

Site and Data

Chapter 2 provides an extensive introduction to the study site at Engabreen. It also provides a complete overview of the suit of methods used to observe and analyse seasonal and short term changes in the hydro-mechanical relationship at Engabreen.

Optical Feature Tracking

Chapter 3 introduces a major part of the thesis, that presents the time-lapse optical feature tracking toolbox developed during this study in the associated publication. The chapter discusses the ImGRAFT toolbox in great detail with applications to both the study site at Engabreen using two forms of remotely -sensed data; terrestrial time-lapse imagery, and optical satellite imagery. The imagery and velocity data presented in this chapter are used extensively throughout the thesis, particularly in Chapter 5, where they complement the large range of velocity and hydro-meteorological time-series data. Finally, a new study using ImGRAFT, presents the first extensive results from applying the tool to five large, marine terminating outlet glaciers in Greenland.

Geomorphological Evidence at Engabreen

Chapter 4 presents a variety of geomorphological data collected at Engabreen. This data takes the form of two themed geomorphological maps and a comprehensive photo series of the wealth geomorphological evidence of the former subglacial drainage system. Specific features indicative of distinct processes are presented in greater detail. These are used as indications of fundamental former and contemporary fluvioglacial and ice -contact processes. This evidence is used extensively to support the findings of Chapter 5 and associated hypotheses proposed and discussed in Chapter 6.

Hydrology and Dynamics at Engabreen

Chapter 5 analyses an extensive set of time-series data, covering the 2013 meltseason. During this period two key events (P1a and P1b) are discussed how they appear in the

time-series. An assessment of the relationships between key hydrological, meteorlogical and ice flow data are analysed, in order to highlight causal links between the datasets. These relationships found the basis of the discussion presented in Chapter 6.

Discussion: controls on Hydrology and Dynamics at Engabreen

Chapter 6 provides a detailed discussion of all the presented data in Chapters 4 and 5. Many of the exposed relationships between the subglacial drainage system and the associated time-series of surface velocity are discussed, which provide an overall assessment of the importance of the configuration of the subglacial drainage system on the hydro-mechanical response. Particular attention is made to the detailed geomorphology at Engabreen, that supports many of the observed relationships. Furthermore, a discussion of the results in the context of the previous work is explored.

Conclusions and Outlook

Chapter 7 summarises the key findings of the thesis within the greater context, and presents avenues for future work at Engabreen. Particular attention is paid to the further development and application of the ImGRAFT toolbox, as an all round monitoring system with extremely useful quantifiable outputs, such as velocity estimates. This chapter highlight the benefits of a multi-disciplinary approach to investigating glacial systems.

Chapter 2

Site and Data

This chapter presents an overview of the study site at Engabreen, where the majority of the work in this thesis was carried out. The aim is to provide an overview of the area and to highlight the reason for choosing this particular glacial setting for the investigations presented in the following chapters. Finally, an outline of the data existing at the site is presented with a particular focus on the data that is explored within the thesis. Much of the information in this chapter will set the scene for the following chapters and will be refereed to throughout with regards to specific measurement station locations and properties.

2.1 Engabreen

Engabreen is a valley outlet glacier of the West Svartisen Ice Cap. It is a temperate, hard-bedded, maritime glacier located on the north-west coast of Norway, just within the Arctic circle (66° 41' 02 N 13° 46' 03 E) (Figure 2.1).

Figure 2.1: *The location of Engabreen, just north of the Arctic circle, northern Norway*

Engabreen lies in an asymmetric valley with steep slopes on the western margin of the glacier and somewhat shallower slopes on the eastern margin (Figure 2.2). It flows out of the main ice cap and drains in between two high ridges, Møsbrømtuva and Midnatsoltind. The terminus lies at the head of a small canyon that funnels the proglacial

river into a proglacial lake, Engabrevatn. The terminus elevation is currently approximately 100 m.a.s.l. The exposed bedrock flanking the glacier margin is characterised by deep cross-cutting channel like structures. Many of these collect water from the surrounding catchments and form small streams that feed directly under the glacier, confined by the complex geology. These features are discussed in detail in chapter 4.

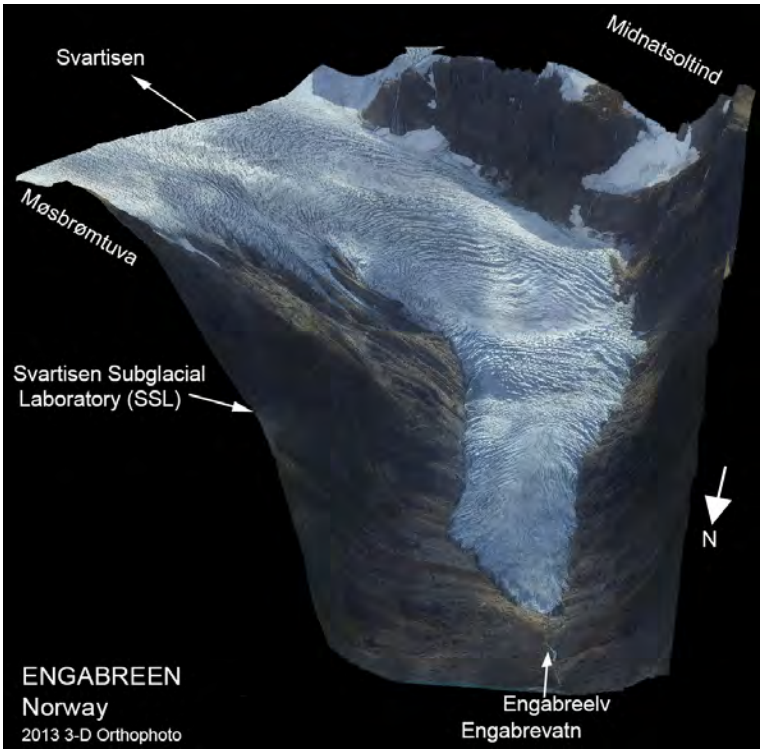

Figure 2.2: *A 3-D map of Engabreen with overlaid airborne image (September 2013). The change in flow direction is clearly seen where the upper section flows in an almost direct westerly direction and turns to flow almost directly north. Key locations areas are annotated such as the SSL entrance and the proglacial river Engabreelv.*

The flow of Engabreen is dominated by a sharp bend around the foot of Møsbrømtuva, where it changes flow direction from westward to northward (Figure 2.2). As it flows out of the main Svartisen Ice cap it enters into an icefall (upper icefall), which ends in a small overdeepening in the middle of the bend at approximately 550 m a.s.l.. As the ice flows out of the overdeepening it enters into a second smaller, yet steeper icefall (lower icefall), which terminates at the base of Møsbrømtuva, before entering the flatter terminus.

2.2 Svartisen Subglacial Laboratory (SSL)

The Svartisen Subglacial Laboratory (SSL) (Figure 2.3) is a permanent research laboratory 200 m under the glacier at approximately 850m.a.s.l.

Currently, there are only two active subglacial laboratories in the world; the SSL, and a laboratory under Glacier d'Argentière. A subglacial laboratory under Bondhusbreen, an outlet glacier of Folgefonna ice cap also in Norway, was active during the

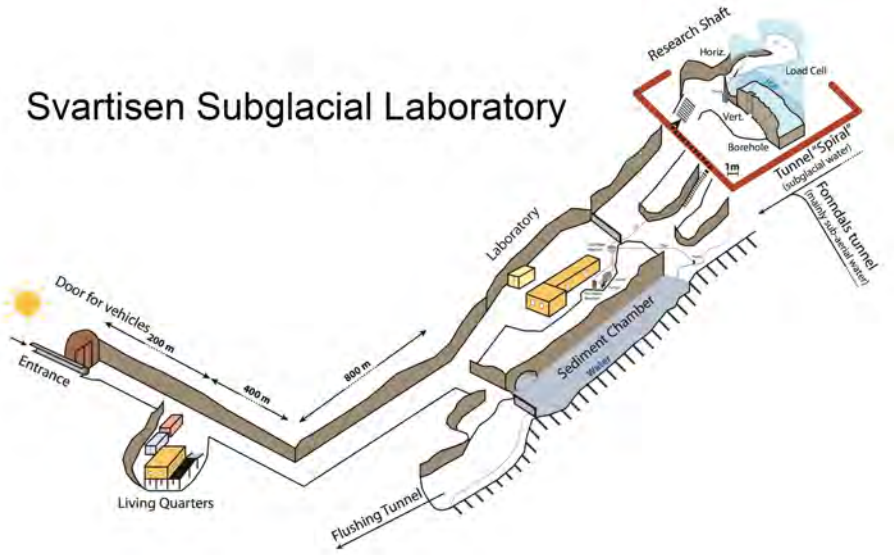

Figure 2.3: *Detailed layout of the Svartisen Subglacial Laboratory (SSL). The figure courtesy of P-M. Lefeuvre*

1970's and 80's, but is now disused. All these subglacial laboratories have a common origin; they are all in existence as a part of hydroelectric power plants. The SSL and Bondhusbreen laboratory are similar in that they both had designated tunnels excavated in order to reach the base of the glacier. The laboratory under Glacier d'Argentière, exists in a natural bedrock cavity, nevertheless man-made tunnels allow access to the cavity. Both SSL and Bondhusbreen are examples of where the ice is in full contact with the bed. In order to gain access to the subglacial environment, a hot water hose is needed to melt the ice around the entrance and allow full access to the ice-bed interface.
The SSL is a part of the Svartisen hydroelectric power project, owned by Statkraft. They began to excavate the tunnels for the hydropower project in 1989 and the plant began operating in 1993. During construction two research oriented access shafts were drilled, separate to the main access and water routing tunnels (Figures 2.4 and 2.3). In order to reach the SSL access is made through the main tunnel that enters the mountain at an elevation of 600 m.a.s.l. The stairway that provides access to the research shaft is approximately 1.5 km along the main tunnel from the entrance. Access to the ice-bed interface is through either a vertical or a horizontal research shaft, where the overlying ice is approximately 200 m thick (Figure 2.3). Once access to the ice-bed interface is made, numerous research activities can be undertaken in the direct subglacial environment. The SSL has both continuous and periodic measurements taking place. This direct access has allowed for many detailed studies investigating subglacial process and the subglacial environment. Additionally the SSL has provided invaluable insights into the subglacial hydrology, through the subglacial water intakes feeding the hydropower plant. A large volume of subglacial meltwater is tapped from beneath Svartisen/Engabreen andis routed via a sedimentation chamber (Figure 2.4) and then to the Storglomvatnet reservoir via the tunnel network. A more detailed description of the measurements taken in the SSL and the datasets is presented in section 2.5.

The SSL offers researchers a unique insight into the subglacial environment below

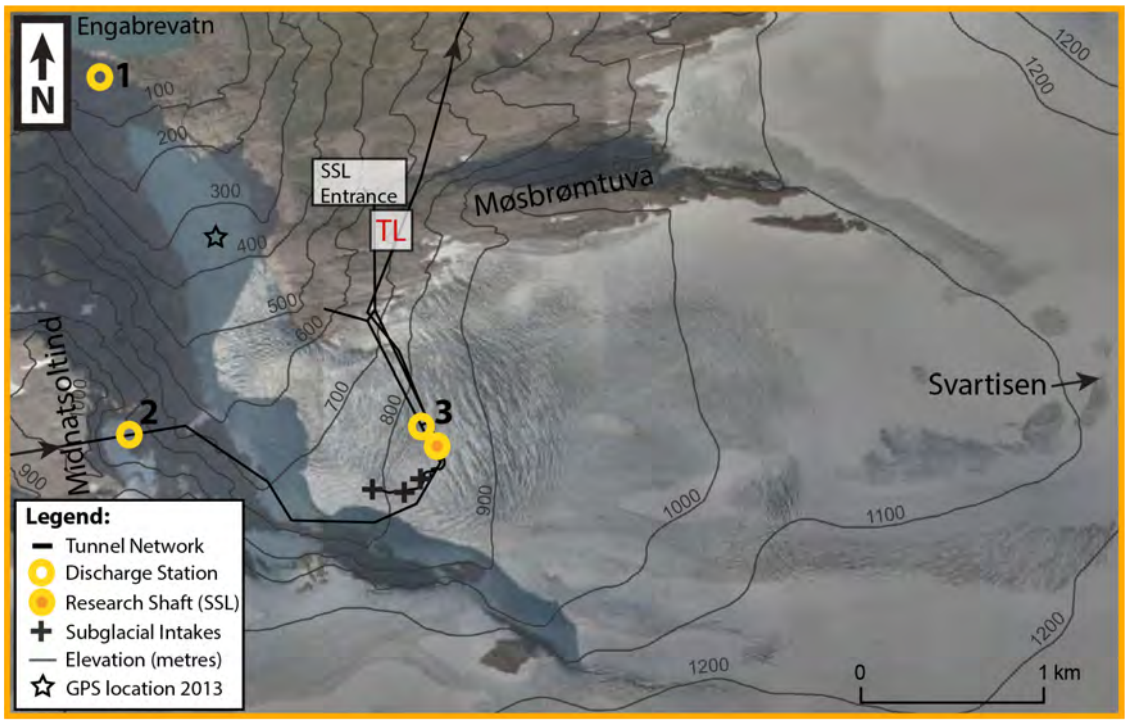

Figure 2.4: *Aerial overview of the key sites at Engabreen referenced throughout the thesis. Discharge station 1 is the proglacial station at Engabreelv, station 2, is the one in Fonndal and 3 is the Sediment chamber station. The star on the lower tongue shows the approximate location of the four GPS in 2013. The red label (**TL**) is the location of the time-lapse camera that faces south-west. The figure is adapted from (Lefeuvre et al., 2015).*

an active, temperate valley glacier. It is possible to witness first hand many fundamental subglacial processes such as basal sliding, erosion, creep closure, varying pressure conditions at the ice-bed interface. Not only does the SSL offer such useful access the basal environment, but also provides the hydro-meteorological data needed to link the glacier surface and bed conditions. The ability to simultaneously collect surface and subglacial data makes this an extremely useful laboratory when trying to interpret surface data. Furthermore, results from the SSL offer useful insights in interpreting surface data from other valley glaciers where direct basal data are unavailable.

2.3 Previous work

2.3.1 Historic overview

A short historic overview of the previous work at Engabreen and SSL is presented here. One of the first recorded investigations at Engabreen was documented by Worsley (2007), who provides a narrative of an expedition to Engabreen in 1865. The expedition was run by three young men (Archibald Geikie, James Geikie and William Whitaker) from the British Geological Survey (BGS) Worsley (2007). As far a the records state, they were on a quest to gain first hand field experience and to collect evidence to support the theory that glacier originated on land as proposed by Agassiz in the mid-18th centuary (land-ice theory). The competing theory proposed at the time was of the marine-iceberg theory. This topic was under much discussion during this

period and whilst it was fairly well established in that the land-ice theory Alpine glacial landscapes, they sought additional examples that could explain the "glacial" features in Scotland. They travelled to Norway to undertake studies around the margins of both Engabreen and Fonndalsbreen Worsley (2007). After careful observation of abrasive processes around the margin of the two glaciers, the BGS expedition concluded that there was sufficient evidence in support of the land-ice theory . In some areas they were able to crawl underneath the ice and observe the ice resting on the polished, striated bedrock. Observing these processes in action left the party with very little doubt that the rock formations they observed in their native Britain had the very same origin as these examples at Engabreen and Fonndalsbreen (Worsley, 2007). The observations they noted and subsequently published was a driving factor in convincing geologists of the day that the land-ice theory was the most likely explanation for the sculpturing of the distinct landscapes in Scotland and England

2.3.2 Present day overview

Today, many of these processes are still observed in the SSL over 150 years after the BGS expedition. The relatively easy accessibility which had lead previous early expeditions to Engabreen (e.g. von Buch in 1908/1909, and later Geikie in 1865 and Rekstad in the 1890's Worsley, 2007), is still very much the same today, albeit that the glacier terminus is now over two kilometres from Holandsfjord. The SSL has attracted many researchers, not only glaciologists, to examine and investigate the subglacial environment and to witness and measure some of the same process observed many years before at Engabreen Worsley (2007). Many of the following studies are subglacial-process oriented, and to this day are regarded as benchmark observations of fundamental basal processes, their role and mechanisms (e.g. Jansson et al., 1996; Cohen, 2000; Iverson et al., 2007; Lappegard and Kohler, 2005; Lappegard et al., 2006; Moore et al., 2013; Lefeuvre et al., 2015).

The surface environment at Engabreen is also well studied, particularly from a mass balance and glacial change perspective (e.g Andreassen et al., 2005, 2006; Engeset et al., 2000; Schuler et al., 2005). Many of these studies include a modelling approach to explore climate sensitivity. However, surface velocity measurements remain sparse, only one peer-reviewed study exists (Jackson et al., 2005) that solely investigates the velocity of Engabreen. Some older NVE reports exist documenting changes in surface velocities around the time of the subglacial intake construction in the early 1990's (Kohler, 1998). Interestingly, almost all of the surface velocity measurements at Engabreen have been derived from optical feature tracking of aerial imagery (Kohler, 1998; Jackson et al., 2005).

The aim of this thesis was to measure surface velocity continuously for periods longer than a few days or weeks in order to assess the seasonal changes and short-term speed-up events at Engabreen, as well as complement sublgacial and hydro-meteorological data.

2.4 Field study and methods

During the course of this project two major field campaigns were carried out at Engabreen and SSL, during 2012 and 2013, both of which were independently or-

ganised. As stated above most of the previous studies at Engabreen were undertaken in the SSL and as a result very few, sporadic surface measurements exist.

2.4.1 Global Positioning Systems (GPS)

Surveys using GPS were carried out at Engabreen during the two field campaigns in 2012 and 2013. The aim of the GPS measurements was to obtain a long, continuous data series of surface velocities, that overlap with the numerous other datasets presented in this section. Three main GPS campaigns were carried out at Engabreen, two short campaigns of approximately 1 month in 2012, and a longer campaign of approximately three months in 2013. In 2012 the five dual frequency GPS' were place along the glacier two on the high plateau at existing mass balance stakes above the upper icefall, one in the slight surface depression between the two icefalls and two on the lower tongue. A local base station was also deployed near the tunnel entrance. These GPS' were retrieved on June 1st 2012. No long data series was obtained from these GPS as heavy snowfall after deployment buried the solar panels and power supply was quickly depleted. In August 2012 three GPS' were deployed on the lower tongue, these were retrieved on September 23rd 2012. TAs a result of a significantly warm and rainy late summer, There has been substantial melt of the glacier surface between August and September 2012 (within a few days, melt rates at Engabreen are likely to have exceeded 15cm of melt due to a heavy rainfall event). As a result, the GPS platforms melted out quickly, thereby reducing the stability of the GPS antenna and the quality of the signal. As a result it was decided no further assessment of this data would be made due to the uncertainty on the positioning introduced from large motion in the antenna.
A successful GPS campaign was carried out from April to the end of July in 2013. Four dual frequency GPS were placed on the lower tongue only, on a GPS platform. These new platforms were based on a modified design from the Icelandic Met Office(IMO), which were built prior to the 2013 season. The main modification was the addition of telescopic legs on the platform that allowed for on site adjustment to ensure a stable and horizontal positioning of the antenna. An example of the GPS platform can be seen in figure 2.5.

Two GPS (JB and JL), (see Figure 2.4 for location) recorded continuously from the beginning of May to the end of July in 2013. These two long time-series of velocity data are presented and discussed in chapter 5. The two other GPS (TT and TR) suffered from internal hardware and software failure throughout the season and only short periods of reliable data were recorded. As a result of their extremely short interrupted time-series the data are not included in this thesis.

The GPS data was processed with TRACK/GAMIT (http://www-gpsg.mit.edu/~simon/gtgk/) kinematic GPS processing software for 2012 and with RTKLIB (http://www.rtklib.com/) for 2013. The base station data used for all the kinematic processing was the Ørnes base station, approximately 20 km away from Engabreen. The one second interval base station data was provided by Satref[1]. The final processed data that are presented in chapter 5 has had a, 1st order robust variant of the Savitsky-Golay filter applied with a three-day time window, in order to remove the high frequency noise in the raw processed data.

[1]Satref (http://www.satref.no) data provided from from the Norwegian Mapping Authority (http://www.kartverkt.no)

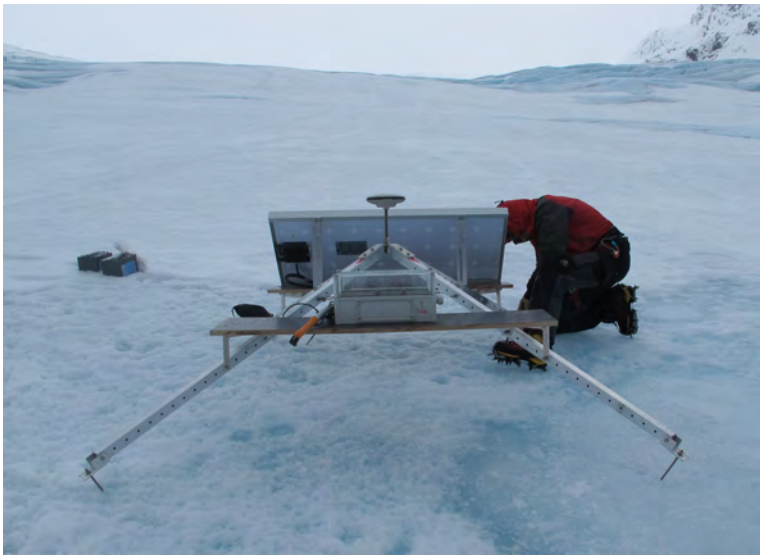

Figure 2.5: *An example of the modified GPS platform with telescopic legs at Engabreen. The shortening of the up-slope platform legs ensures a horizontal position for the antenna in regions with steeper slopes. The short spikes visible on the base of the platform "feet" act as spikes that melt into the ice surface preventing it from sliding. The system was powered with two 1 V, 44 Ah batteries and a single 80 W solar panel. The GPS was housed in a watertight enclosure mounted on the frontal wooden panel.*

The GPS data are presented and interpreted alongside key supra-,pro- and subglacial time-series data collected at Engabreen during 2013. This data in combination with time-lapse velocity data provides vital insights into the relationship between the motion of Engabreen in relation to changes in the water volume and structure of the subglacial hydrological system and is discussed in Chapter 5.

2.4.2 Time-Lapse

A time-lapse camera is a camera with a timer (intervalometer) that allows the user to program the camera to take images at a given interval. A time-lapse camera can provide a wealth of information about environmental change particularly in a dynamic environment such as the cryosphere. Previous studies have demonstrated the ability to monitor glacier flow from time-lapse imagery and so the decision was made to deploy a camera system at Engabreen. The nature of the glacier surface provides challenges to record velocity measurements using traditional techniques such as GPS or stake networks. The camera was used in order to obtain a large spatial coverage of ice flow measurements, from a low power, cost effective system. The camera system was mounted on a stable disused metal meteorological tower (Figure 2.6), that was cemented into the bedrock at an elevation of approximately 700 m.a.s.l on Møsbrømtuva ridge (see Figures Figure 2.4 and 2.2). The camera had a three hour recording interval and was continuously running from April until the end of September 2013. Regular maintenance checks and data download visits to the site were carried out throughout the summer of 2013. The camera system was powered by two 11.1 V, 9 Ah Li-ion polymer batteries, supported by a small 10 W solar panel (Figure 2.6).

The time-lapse imagery from 2013 was processed using the Image GeoRectification And Feature Tracking (ImGRAFT) toolbox (Messerli and Grinsted, 2015), developed

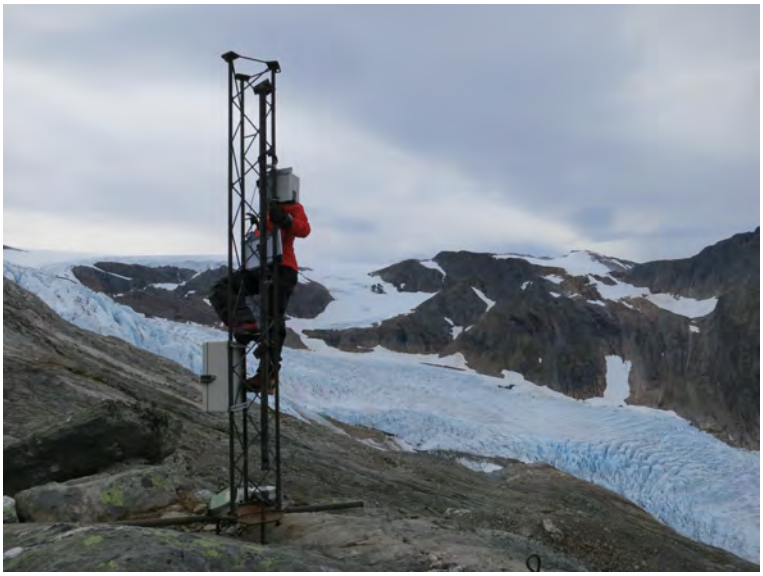

Figure 2.6: *The time-lapse camera mounted to the disused meteorological station platform on Møsbrømtuva. Numerous key features and crevasses on the ice surface can be seen in the image with the icefall and bend of Engabreen. Photo taken by. H. Sevestre.*

as part of this thesis are discussed extensively in Chapter 3. ImGRAFT is an optical feature tracking tool that can be used on both ground based and aerial/satellite imagery. This is presented and discussed extensively in chapter 3. The processed time-lapse imagery produced a long time-series of velocity maps over the icefall region of Engabreen. The time-lapse velocity data are presented in chapters 3 and 5. This velocity dataset complements and expands the GPS (point) dataset presented in the previous section both spatially and temporally throughout 2013. As seen in chapter 5, the time-lapse imagery provided additional valuable information (e.g. snow cover, melt-lake development) about the site and useful validation of other meteorological and hydrological datasets.

2.4.3 Hydrology

The hydrological network at Engabreen is extensive and well maintained, with stations monitoring the glacial catchment both proglacially and subglacially. These stations form a vital component of the hydropower network and ensure optimal conditions for the running of the power plant. Whilst most hydrological stations, proglacially and subglacially (2 in Figure 2.4) were already fully operational, one station was installed in the proglacial stream (1 in in Figure 2.4), where there had previously been a discharge station before 1997. The previous discharge station was removed when the ice front re-advanced in the 1990's and was only replaced again in May 2012 (Figure 2.4). The subglacial and proglacial lake discharge stations have been operational since around 1993, continuously recording and storing data at hourly intervals. The hydrologcial data used in this thesis are provided by NVE. Data from 2012 and 2013 are presented and discussed along with other time-series data in chapter 5.

Aside from the compartmentalised discharge datasets a limited number of other hydrological experiments were conducted in 2012 and 2013, including dye traces and

one large flushing event (artificial Jökulhlaup experiment). The two are addressed individually below.

Artificial subglacial flood: Jökulhlaup

Jökulhlaup is the Icelandic term given to a large subglacial flood (Björnsson, 2003). These floods are extremely large in water volume and often have a rapid drainage period. The term Jökulhlaup is used here to describe an artificial flushing event at Engabreen, where a large volume of water is reintroduced very rapidly (injected) into the subglacial drainage system.

This experiment was carried out on 23rd September 2013 after months of careful planning. The experiment involves flushing a large volume of water and sediment under the tongue of Engabreen, through an existing Nye-channel at the exit of the flushing tunnel (see Figures 2.4 and 2.3). This experiment is made possible through the flushing of a sedimentation chamber (SC) (see Figure 2.3) which forms an integral part of the hydropower plant operation. The SC is a long thin chamber that has an overdeepening before it leads water into an feeder tunnel that leads to the Storglomvatnet reservoir. The SC accumulates water (and sediments) from all of the subglacial intakes (Figure 2.4. As the water flows into the SC, it is pooled as the speed of the water is slowed down significantly. Subglacial water is typically sediment rich and by reducing the flow speed of the water it is able to deposit most of its load, including some of the finest particles including sands and clay. The SC is a vital component for the successful operation of the hydropower plant, as it prevents any of this sediment entering the turbines and causing large scale damage.
As the SC fills with debris the efficiency of the sediment filtering becomes reduced and as a result, intervention is needed to empty the accumulated sediment. Typically this is done biennially through the back-up and release of stored water in the SC. Once the SC is filled to capacity with water, and begins to overflow out through the flushing tunnel, a hydraulic gate at the deepest point in the SC is opened in order to allow the accumulated water-sediment mixture to be flushed out with the power of the backed up water. This sediment-water mixture is flushed through the gate and out of the flushing tunnel that exits the mountain side in a small channel and enters back under the ice where the small canyon becomes a Nye-Channel at the ice margin (Chapter 4). Once all the sediments have been flushed out of the chamber the hydraulic gate is shut again, allowing water to refill the SC and resume flow to the reservoir.
Surface measurements during the 2013 jökulhlaup are limited to the time-lapse camera velocity only[2]. These measurements are discussed in the context of the effect of water pulses on ice flow in chapter 6. Further limited discussion of a previous jökulhlaup experiment at Engabreen by J.Kohler[3] is also made within chapter 6. This experiment is a useful analogy to pulse meltwater inputs that take place in numerous forms within the glacial context, for example supraglacial lake drainages on the GrIS. The controlled nature of these experiments provide and excellent opportunity to study the response of glacial systems to large, pulse inputs into the subglacial drainage system.

[2]As a result of GPS failure prior to the experiment.

[3]Kohler J. et al, 1998: Effect of a Controlled Discharge Pulse on the Subglacial Drainage System and Ice Flow at Engabreen, Northern Norway. Eos. (Abstract). v. 79(45), p. 274.

Dye Tracing

Dye tracing in a glaciological context is a method used to assess the transport of water through the glacial hydrological system. Typical tracers used in glacial studies include salt, fluorescein and rhodamine. Injection of a known quantity of dye is either done on or at the margin of the glacier where running water is present, whether in a stream, crevasse or moulin. The main goal is to analyse the time taken for dye to reappear in the proglacial stream, and the shape of the dye breakthrough curves (BTC) to infer the type of pathway the water took in order to transport the dye from the site of injection to the site of detection downstream (Hubbard and Glasser, 2005). During 2012 and 2013 a total of 10 rhodamine dye traces were carried out, eight of which were injected from the outflow of the ice marginal lake located on the inner bend of the glacier at approximately 600 m.a.s.l (Figure 2.4). The first injection from this site was carried out on 29th August 2012, in order to confirm that the water re-entered the subglacial drainage network and was routed to the terminus. This was confirmed and subsequently seven more dye traces were injected a month later over the course of 3 days. The final two dye traces were injected in 2013 at the onset and after the artificial Jökulhlaup experiment. The detection method for each of the traces was performed by an automatic fluorometer mounted in the proglacial stream. The BTC and associated metrics provide insights into the efficiency of the subglacial drainage system and are referred to in relation to the hydrological and drainage configuration section in chapter 5.

2.4.4 Load cells

The load cells are vibrating wire pressure sensors that measure the normal stress at the glacier bed. These sensors are mounted in the bedrock underneath 200m of ice in the research shafts in the SSL. They lie flush with the bedrock and any ice, water and debris move over them without interference from the sensor. An example of one of the sensors is shown in Figure 2.7 from two perspectives.

Figure 2.7: *Two perspectives of the load cells the left image shows a plan view of the load cell. Note the striations on the metal surface of the load cell plate. The image right shows a side on view of the load cell with a column of 200m of overlying ice resting on the metal plate.*

The load cell record at the SSL extends back to 1993/1997. A network of up to seven load cells have recorded the subglacial pressure almost continuously at 15 min intervals. It is assumed that the load cells measure ice as well as water pressure at

the base of the glacier (Lappegard et al., 2006; Lefeuvre et al., 2015). These records are extremely useful when analysed with surface data, as they are able to provide an undisturbed measure of the basal pressure during events expressed in the surface data. The data add a basal dimension to the understanding of events observed in the surface velocity and provide insights as to the changing conditions at the base of the glacier. This dataset is presented and discussed in chapter 5 alongside the other hydrology, velocity and meteorological time-series.[4]

2.4.5 Ground Penetrating Radar (GPR)

Currently two datasets of the bed topography exist, one from a GPR on the upper region of western Svartisen (Kohler, 1988) and one from the lower section of Engabreen and the upper icefalls (Kennett et al., 1993). Whilst the bedrock region around the SSL is approximately known from studies mapping the localised bedrock around the research shafts (Lappegard and Kohler, 2005), very little data exists on the lower tongue of Engabreen. Knowledge of the bedrock topography is extremely useful when interpreting water pathways and the the likely associated response of the the drainage system to meltwater forcings. In order to obtain a more detailed bedmap a GPR campaign was run. No winter GPR measurements exist on the lower tongue as it is too dangerous to navigate the surface. At the margin, the steep ice surface slopes and extensive crevassing complicate access to the flatter surface during periods of snow cover in winter. As a result the GPR was attempted in July, using a Malå GPR system. A 50Mhz antenna was used [5]. Due to the timing of the campaign large amounts of meltwater were present, on, in and underneath the glacier. Engabreen is a temperate glacier and thus does not present optimal conditions for GPR, particularly for bed investigations. Unfortunately, as a result of the substantial water content of the glacier no bed data was recorded, as the high water content attenuates the radar signal.

2.4.6 Meteorology

There are two key meteorological datasets used in this thesis; air temperature and precipitation. Two NVE meteorological stations are within the catchment of Svartisen, one at sea level on the shore of the proglacial lake Engabrevatn and the second at 1360 m.a.s.l. on a small nunatak, Skjæret. Both of these stations measure air temperature at hourly intervals, however, neither of these stations measure precipitation. The precipitation used in this study is taken from two local stations, one official station in Reipå [6] (28km away), and one unofficial weather station in Neverdal [7] (15km away). The air temperature is used to assess the onset of melt, in conjunction with the hydrological and velocity data. The temperature and precipitation data help to constrain and interpret the hydrological data and are important variables in identifying key phenomena that take place in glacial catchments. A key example is the spring-event, where the glacier speed increases in relation to the onset of the melt season in response to

[4] The load cell data form the basis of another PhD thesis by a P-M. Lefeuvre working a the SSL and are thus not discussed in great detail as a stand alone dataset.

[5] A lower frequency 25Mhz antenna was intended to be used for the campaign however, unfortunately it was held in customs en route to the field site

[6] Data from the Norwegian Meteorological Institute

[7] This data is available through the following website. http://www.wunderground.com/cgi-bin/findweather/getForecast?query=66.834%2C13.767&sp=IMELYNEV2

meltwater generation and input to the subglacial environment. These relationships are discussed thoroughly in chapter 5.

2.4.7 Geomorphology

Glacial geomorphology is the study of how and what processes shaped the glacial landforms found at and around the margin of former and existing ice masses (Menzies, 2009). The study of these landforms provide a wealth of information about the processes that formed and shaped the landscape. The glacial fore-field is often a chaotic environment, interspersed with distinct evidence for fundamental glacial processes. In this study evidence of fluvioglacial processes and drainage configurations are presented. As stated by Hubbard and Nienow (pp.944 1997) *"Recently-deglaciated bedrock surfaces provide the most readily accessible evidence for the structure of former subglacial drainage systems."* At Engabreen At Engabreen, many large and small scale indicators of ice contact and fluviglacial processes are visible on the recently exposed bedrock. Many of these have well defined origins. These data are presented as series of maps and photographic evidence. They are discussed in detail in chapters 4 and 6 and in the larger context of the structural configuration of the subglacial drainage system at Engabreen and how this influences the surface expression of changes in the hydrology at the base.

2.5 Data availability and overview

Figure 2.8 outlines the availability of key data presented in this chapter. The bold purple areas and the annotated section P1 and J are discussed in detail with in the thesis. As is seen in the figure, the second field campaign provides a large overlap of simultaneous datasets, from all areas of the glacier. Some additional satellite velocity maps and dye traces that fall outside the P1 period are also discussed within their associated sections.

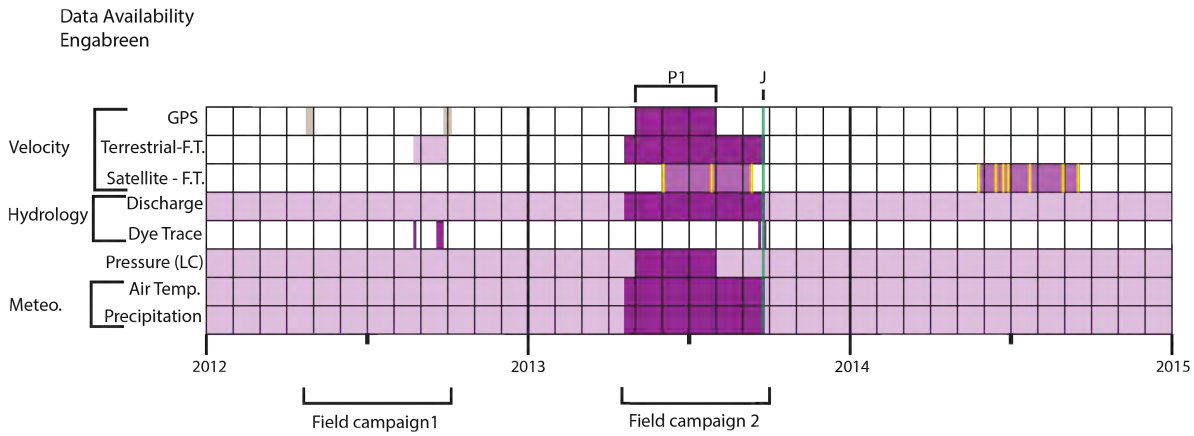

Figure 2.8: *A time-line overview of the data available during the study period. The period of focused discussion is centred around the second field campaign. The notation* ***P1*** *covers the period discussed in chapter 5 and the label* ***J*** *indicates the Jökulhlaup experiment. Yellow bars indicate individual satellite images used to compute the mean velocity fields. Light grey GPS shading in 2012 indicate the two short deployments, where data is unreliable. The light purple periods are not discussed in detail in this thesis and reflect the continuous measurements available at Engabreen and the SSL.*

The data I will focus on in this thesis is based on the data I collected in the field at Engabreen. This includes time-lapse images, GPS, dye tracing, and geomorphological data. These datasets are analysed along with the hydrological, meteorological and subglacial load cell pressure data at Engabreen and the SSL, that are provided by NVE.

Chapter 3

Optical Feature tracking

This chapter contains work presented in two key papers Messerli and Grinsted (2015) and Messerli et al. (2014) developed as part of this thesis. The focus is on optical feature tracking, specifically using the normalised cross correlation method (NCC), with applications of the toolbox developed by Messerli and Grinsted (2015) to time-lapse imagery from Engabreen. A wider study applying the developed toolbox ImGRAFT to large glacier outlets in Greenland is also discussed.

3.1 Introduction to feature tracking

The use of cameras as a means of glaciological monitoring can almost be traced back to the invention of the camera. Its use for glaciological investigation is documented as early as the late 19th century (Pellikka and Rees, 2009). Most of the early glacial observations using cameras were focused on surveying applications such as glacial mapping, however a study by Finsterwalder (1931) was one of the first known studies that measured glacier velocity using terrestrial photogrammetry but it was first around 1970 when an automated time-lapse camera was used to determine ice flow at Unteraargletscher in the Swiss Alps (Flotron, 1973). The data from this study was subsequently used in the ground breaking Iken et al. (1983) study of water storage and sliding of the hard-bedded glacier Unteraargletscher, that paved the way for many glacio-hydrological studies thereafter.

One common theme that runs through all kinds of feature tracking is the simple principle of identifying a feature, texture or pattern in one image and locating the same identified feature,texture or pattern in a subsequent image. At its most basic one is able to estimate displacement of features within image space, i.e. pixels. It is first after some pre and post processing of the images themselves that quantitative estimates of displacement may be obtained. This process may be simple or complex depending on what type of output data is desired.

In this section two forms of optical feature tracking are presented, one from the ground (terrestrial) feature tracking and the other from satellites. Terrestrial feature tracking uses imagery captured from an oblique ground based view of the region of interest, compared to aerial and satellite imagery that provides an almost perfect downward (nadir) view of the region. Rectifying imagery from above is a far easier task than for oblique imagery. In an aerial or satellite image most of the pixels in the image represent the same scale, however this is not true for terrestrial imagery, as

Figure 3.1: *First know automatic time-lapse camera used for measuring ice flow at Unteraargletscher set out by Flotron (1973). Image taken from Flotron (1973)*

pixels that represent the background have a larger spatial scale than the pixels that represent the foreground. In order to account for this change in scale over distances a complex rectification of the imagery is needed.

3.1.1 Challenges

Optical feature tracking presents some additional challenges, these include, cloud in the scene, shadows, background motion and snow cover. Whilst many of these issues are simply unavoidable there are some ways in which to make them manageable.
One of these issues is that of shadowing effects in the image. As discussed in Messerli and Grinsted (2015) shadows can change a feature's appearance significantly depending on illumination angle and direction. This is more problematic in the (high resolution) terrestrial imagery, as subtle changes in lighting can change the way the feature appears from one image to the next. It is less problematic in the 15m-X-15m satellite pixel resolution as many features are averaged within a single pixel, and the high frequency variations of individual crevasses is removed.
The illumination problem discussed in (Messerli and Grinsted, 2015) is more of a challenge on a larger scale, where a large shadow is cast across the glacier from one of the adjacent high mountain peaks. This affects the feature tracking a different way, by introducing a very sharp transition between light and dark across the ice and thus artificially adding an unstable "feature" to the ice surface, resulting in erroneous data. In that case the image can either be removed from the processing, or where large parts of the glacier are unaffected, the data from the shadow regions may be removed from the final dataset. Steep terrain is a problem when feature tracking valley glaciers as the shadows are not only cast on the ice but also on the neighbouring bedrock, thus reducing the area to detect background image motion. Fortunately these issues do not hamper the processing of the rest of the image and are usually a more localised artefact. In most cases useful spatial datasets can be obtained even with the removal of the shadowed area.
In some cases patches of no data are due to a rapidly changing surface in some areas of the glacier. This is caused by melting snow particularly in the early in the spring/sum-

mer where features change their appearance dramatically as during the onset of the melt season. This often leads to a visibly changing surface over only a few days.

3.2 ImGRAFT: Image GeoRectification And Feature Tracking toolbox

This section provides a brief overview of the ImGRAFT toolbox, further details of the tool are presented below in the the recent publication (Messerli and Grinsted, 2015). To date there a few freely available, adaptable packages that can carry out this rectification, and feature track the rectified imagery in one package. As a result of the lack of a complete, adaptable packages available to date we developed a complete tool that processes the imagery and feature tracks the resulting georectified imagery. In the following section 3.2 the development and application of a new image rectification and feature tracking toolbox (ImGRAFT) is presented.

Figure 3.2: *ImGRAFT Logo used on the website*

ImGRAFT is available through the associated website `http://imgraft.glaciology.net/`, where further details about the functions and descriptive demonstration data can be found. The website has been developed alongside the MATLAB based toolbox, in order to provide more up to date user information about any changes and optimisations that are made to the tool. ImGRAFT is a complete georectification and feature tracking tool that is openly available and adaptable to numerous data types and applications. The main toolbox functions and features are as follows:

- Georectification of imagery, particularly designed for terrestrial imagery
- Includes a full distortion model that accounts for poor lens and image quality
- Account for camera motion between image acquisitions
- Feature track sequential imagery (terrestrial, aerial, satellite)
- Easily adaptable source code to for site specific implementation

Geosci. Instrum. Method. Data Syst., 4, 23–34, 2015
www.geosci-instrum-method-data-syst.net/4/23/2015/
doi:10.5194/gi-4-23-2015

Geoscientific Instrumentation Methods and Data Systems
Open Access

Image georectification and feature tracking toolbox: ImGRAFT

A. Messerli[1,2] **and A. Grinsted**[1]

[1]Centre for Ice and Climate, Niels Bohr Institute, University of Copenhagen, Juliane Maries Vej 30, 2100 Copenhagen Ø, Denmark
[2]Section for Glaciers, Snow and Ice, Hydrology Department, Norwegian Water Resources and Energy Directorate, P.O. Box 5091 Majorstua, 0301 Oslo, Norway

Correspondence to: A. Messerli (messerli@nbi.ku.dk)

Received: 31 July 2014 – Published in Geosci. Instrum. Method. Data Syst. Discuss.: 25 August 2014
Revised: 9 January 2015 – Accepted: 20 January 2015 – Published: 11 February 2015

Abstract. The use of time-lapse camera systems is becoming an increasingly popular method for data acquisition. The camera setup is often cost-effective and simple, allowing for a large amount of data to be accumulated over a variety of environments for relatively minimal effort. The acquired data can, with the correct post-processing, result in a wide range of useful quantitative and qualitative information in remote and dangerous areas. The post-processing requires a significant amount of steps to transform images into meaningful data for quantitative analysis, such as velocity fields. To the best of our knowledge at present a complete, openly available package that encompasses georeferencing, georectification and feature tracking of terrestrial, oblique images is still absent. This study presents a complete, yet adaptable, open-source package developed in MATLAB, that addresses and combines each of these post-processing steps into one complete suite in the form of an "Image GeoRectification and Feature Tracking" (ImGRAFT: http://imgraft.glaciology.net) toolbox. The toolbox can also independently produce other useful outputs, such as viewsheds, georectified and orthorectified images. ImGRAFT is primarily focused on terrestrial oblique images, for which there are currently limited post-processing options available. In this study, we illustrate ImGRAFT for glaciological applications on a small outlet glacier Engabreen, Norway.

1 Introduction

The use of terrestrial photography as a means of understanding spatio-temporal landscape evolution and change is not a new concept. It spans a vast range of disciplines including: disaster monitoring (Mulsow et al., 2013); glacier motion (Flotron, 1973; Harrison et al., 1986; Ahn and Box, 2010); mountain ecosystem understanding (Aschenwald et al., 2001); hydrological monitoring (Parajka et al., 2012; Danielson and Sharp, 2013); and snow monitoring (Smith Jr. et al., 2003; Corripio, 2004; Härer et al., 2013). It is a cheap, cost effective, simple method that allows the researcher to obtain a vast array of information about their study site. Today, more and more disciplines are discovering the immense power of terrestrial photography for both qualitative and quantitative applications due to the high repeat imaging capacity. The quantitative aspect relies heavily on the ability of the image to be georectified to a meaningful coordinate system. In order to achieve this, ground control points (GCPs) are needed and a good high resolution digital elevation model (DEM) often makes this process more successful. The conversion from image coordinates to real-world coordinates gives each image pixel a true estimate of the space they represent. In its simplest form, this might be the actual scale each pixel represents in metres. The more complex rectification includes a full registration of the image to an established coordinate system through georeferencing.

Examples of quantitative data are velocity fields of glaciers and other mass movement, such as a landslide or rock glacier (Kääb and Vollmer, 2000; Kääb, 2002; Debella-Gilo and Kääb, 2011). Here we shall focus on velocity measurements however, in addition to velocity, cameras provide other additional supporting information about the field site that is otherwise only obtained from prolonged field campaigns; for example, the exact timing of the first snowfall and at which elevation. This data can support and validate other records from the area, such as precipitation gauges. In some cases

time-lapse imagery has been used to validate seismic data to detect large calving events at large outlet glaciers (Walter et al., 2010).

In this paper we present the new Image GeoRectification and Feature Tracking (ImGRAFT) toolbox. We perform a full georectification of the images using a newly developed processing chain. Once rectified, images are used to produce velocity fields at the glacier test site Engabreen. The ice displacement is determined using a cross-correlation feature tracking algorithm. Previous studies stretching back to the 1970s have also used time-lapse imagery as a means of monitoring glacial flow (e.g. Flotron, 1973; Harrison et al., 1986). These studies used various approaches to achieve the same result of obtaining ice flow estimates by tracking either existing features on the ice such as crevasses (Harrison et al., 1992; Evans, 2000; Ahn and Box, 2010) or specific targets placed on the glacier (Harrison et al., 1986). In our example, the "features" are automatically defined by the software as surface textures and patterns visible on the glacier surface, on which we then run the normalised cross-correlation algorithm. Here we present our method as an open source "toolbox" for georectification and feature tracking terrestrial images. Further full working examples, the source code and additional detailed information can be found in the examples section of the toolbox website at: http://imgraft.glaciology.net/documentation.

2 Motivation

The most successful existing software usually focus on either feature tracking or georectification (Corripio, 2004; Härer et al., 2013). To date the most commonly used publicly available feature tracking software are IMCORR (US National Snow and Ice Data Center (NSIDC), Boulder, CO), COSI-Corr (California Institute of Technology (CalTech), Pasadena, CA) and CIAS (Kääb, 2013). Both IMCORR and COSI-Corr, are optimised for use with aerial and satellite imagery, where the rectification process is fairly straight forward compared to that of an oblique terrestrial image. CIAS can be used for terrestrial imagery, however they still need to be rectified externally from the software.

Photogeoref, developed by Corripio (2004), and the more recent release of PRACTICE (Photo Rectification And ClassificaTIon SoftwarE) Härer et al. (2013), which is based on Photogeoref, focus mainly on the georectification of oblique images. During the testing stages using the aforementioned software we found difficulties with automation due to the use of separate existing georectification and feature tracking tools. Additionally, a workflow was needed that was able to deal with camera motion and lens distortion efficiently. Another concern was that traditional image registration as a preprocessing step can introduce loss of image quality and detail through resampling.

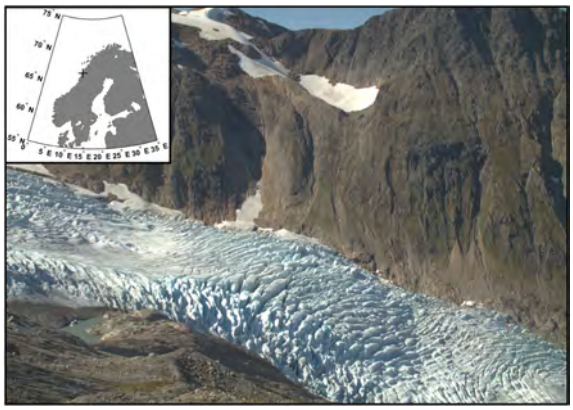

Figure 1. A sample *image* taken by the time-lapse camera located at Engabreen, northern Norway (inset). Note the distinct crevasse features in the main icefall.

As a result we were prompted to develop a new toolbox that met all the requirements, including the georectification and feature tracking processes all to be contained within one MATLAB package. Batch processing of the entire workflow is easily achieved through a case specific custom script, a feature not often available in other image feature tracking tools. The aim of the toolbox is to provide users with flexibility to adapt the code to suite their needs, using the demonstration and documentation online at http://imgraft.glaciology.net/documentation as a basis to structure and implement the toolbox's functions.

3 Field setup and data

The test site for ImGRAFT is located at Engabreen in northern Norway (Fig. 1). Engabreen is a small Arctic valley glacier and outlet of the large Svartisen Ice Cap. Engabreen has a large icefall located at approximately 850 m a.s.l. An icefall is a steep area of the glacier where there is high ice flow and as a result extensional flow, leading to extensive development of large crevasses and unstable ice blocks known as *séracs* (Benn and Evans, 2010). In previous years, attempts have been made to instrument the icefall however, due to the nature of the moderate flow ($> 300\,\mathrm{m\,yr^{-1}}$) and the extensive crevassing the longevity of any instrument in this region is generally short-lived.

Our camera setup in the field consisted of one Canon Rebel T3 (1100D) single-lens reflex camera controlled by a *Harbortronics DigiSnap* intervalometer setup (https://www.harbortronics.com/Products/TimeLapsePackage/). The camera was programmed to take seven pictures per day at 3-hourly intervals at the following times: 05:04; 08:04; 11:04; 14:04; 17:04; 20:04; and 23:04 CEST. During our 6-month monitoring period we experienced a drift in the intervalometer of approximately 5 sec over 6 months. We used a *Sigma*

prime lens with a focal length of 30 mm. Our camera was mounted in a fibreglass, water-tight enclosure on a on a solid metal frame structure that was concreted into the ground. The camera system was powered by an 11.1 V 9000 mAh lithium polymer battery pack and supported by a 5 Watt solar panel. The camera was positioned on the eastern margin of the glacier, at about 770 m elevation on the valley side overlooking an icefall (Fig. 6a). The average height of the surface of the glacier measured was approximately 550 m a.s.l., so the camera was approximately 220 m above the average surface and 120 m above the highest point we measured. The look angle of the camera was approximately 13°.

A key component of ImGRAFT and other georectification processes is the DEM. This is used in the georectification stage and therefore it is beneficial for it to be recent and of high resolution. Fortunately in our case, a high resolution DEM was produced from an airborne laser scan, which took place during the monitoring period on the 25 August 2013. This is extremely useful for georectifying the time-lapse images as both a DEM and at least one of the time-lapse images from the exact same time exist. Therefore, we have an absolute surface that we were able to use to rectify our images. In addition to this, a high resolution (10 cm) orthophoto of the entire area of the laser scan was taken from a camera mounted on board the plane. This combination of the DEM and orthophoto made the selection of additional GCPs easier and we were able to select many visible features in the camera field of view (FOV) that significantly aided the subsequent georectification of our images. We overlaid the orthophoto onto the DEM and picked out the features for our GCPs manually. These features included the entrance to a subterranean tunnel on the western valley side, spray painted boulders, other large distinct boulders and the edges of dominant, persistent snow patches in gulleys. In addition to the rock features, we were also able to use the crevasses as GCPs as a result of the exact overlap of the image and DEM acquisition. A small number of GCPs were measured using a global positioning system (GPS); these included the tunnel and the spray painted boulder.

4 Method

We present the method in separate sections to clearly distinguish between the processes contained within ImGRAFT (Sect. 4.3) and those not. In the first two sections (Sects. 4.1 and 4.2) we describe the image preparation and DEM preparation that are required but not directly contained within the ImGRAFT toolbox. The DEM preparation stage can be written into to the ImGRAFT processing chain, as is shown in the demonstration scripts in the documentation on the ImGRAFT website (http://imgraft.glaciology.net/documentation).

4.1 Image preparation

Firstly we converted all collected images from RAW to tiff format using dcraw (Coffin, 2009). We chose a linear gamma curve in the conversion to preserve the dynamic range of the bright ice. We manually inspected the images to determine if they were suitable for feature tracking purposes or not, and removed all images that were deemed to be unusable. These included images that were taken at night and those where either all or a significant portion of the glacier were obscured by cloud or fog. Images where there appeared to be heavy rainfall were also removed as the raindrops themselves lead to extra distortion as they settle on the camera window. To allow for a better comparison, we also selected image pairs at the same time of day, as the sun illumination was more consistent over the glacier and valley. This also means that the shadowing around large crevasse features is similar between each image (Ahn and Box, 2010). The images that were collected in early spring when snowfall was still regular presented another problem: a lack of rock features for detecting camera motion; a lack of distinct glacier features (as they are covered by snow); and finally a rapidly changing surface. Lastly, the surface features change rapidly from one day to the next, either through new snowfall or as we saw later on, rapid melting.

4.2 DEM preparation

The DEM is a fundamental input in our method (Fig. 3) and needs to be prepared correctly for our purpose. We initially used a 1 m high resolution DEM, however on inspection of the results we identified some complications. The complications arose as large persistent features such as crevasses and *séracs* moved down the glacier over time. As a result it implies that after a day the DEM that encompasses the high resolution crevasses detail no longer represents the ice in the images. This is because the high peaks and low troughs of these crevasses are now downstream. For example, points that correspond to a peak of a crevasse in the image could be a trough in the DEM and vice versa, due to the motion of the glacier. To avoid this problem, we decided to "fill" our crevasses in the DEM, to ensure it corresponds to the visual surface seen by the feature tracking algorithm (templatematch). This removes the large local variability in the glacier surface caused by these crevasses and *séracs* to achieve a smoother surface. A snapshot of our DEM "filling" can be seen in Fig. 2, where the following described surfaces are represented by the three lines.

There are many technical solutions for how you might fill crevasses in the DEM. Generally these methods need the specification of a vertical scale to define what is considered a crevasse and a horizontal scale to define the spatial extent of the crevasses to be bridged. Here, we outline a computationally efficient approach, which uses image filtering techniques. First we smooth the DEM (z) with a Gaussian spa-

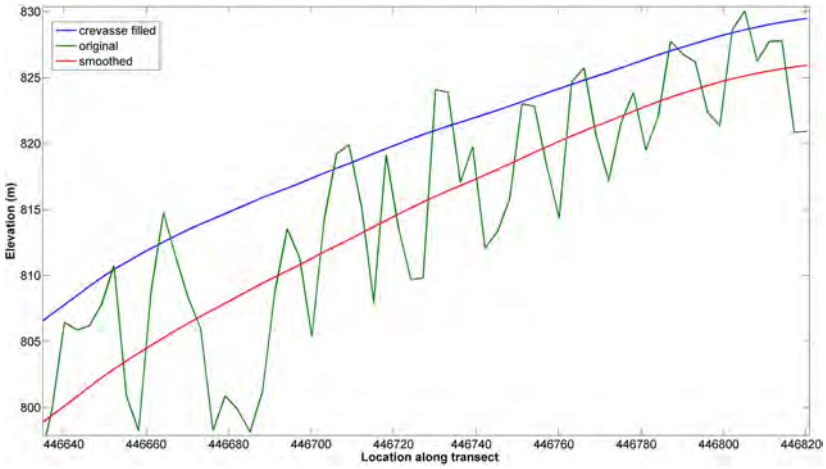

Figure 2. A zoomed-in snapshot of a slice through the DEM. This highlights how the DEM has been "filled". The green line shows the high frequency surface structure from crevasses, which are removed in the final "filled" surface (blue). The red line shows the first stage of the smoothing, which results in a lower surface.

tial filter (S_g), which results in a DEM that lies lower than the original (red line in Fig. 2). The deviation between the smoothed DEM and the original surface (green line in Fig. 2) is passed through a non-linear function (exp) and spatially smoothed with a disk filter (S_d). This strongly weighs positive deviations from the smoothed DEM, i.e. crevasse tops. The final DEM (z_{filled}) is the smoothed DEM plus the upper surface DEM (blue line in Fig. 2):

$$z_{\text{filled}} = a \log\left(S_d\left(\exp\frac{z - S_g(z)}{a}\right)\right) + S_g(z),$$

where a is the weighting constant. We apply a final smoothing (S_g) to reduce the stepped nature of z_{filled}. The characteristic length scale of the smoothing operators has been chosen to bridge the largest crevasses, and the weighting constant a has been chosen to be the same order of magnitude as the standard deviation between z and S_g.

We are fortunate to have obtained a DEM on the 25 August 2013 between 10:20 and 11:13 CEST, and an image was taken on the same day at 11:04 CEST. We are therefore confident that as a result of the simultaneous image and DEM acquisition, our rectification is accurate particularly with regards to the stable rock regions within the image. As we are monitoring a dynamic surface (ice), in all other images the ice surface has changed in relation to the DEM and therefore must have a lowering/raising function applied to it to correct for the glacier surface evolution. This is due to the alteration of the ice surface as a result of melting/snowfall. At Engabreen we experience a significant surface lowering on the order of 10 m on the lower tongue during a single melt season. In this example, we derive the elevation change factor for the ice from direct mass balance measurements taken at the glacier at monthly intervals throughout the operational period of the camera in 2013. In cases where such observations are not possible, then other methods of estimating surface lowering should be investigated. An estimation of the surface elevation change will aid in the correction of the DEM.

4.3 ImGRAFT: processing

Here we present the major steps in the processing chain as illustrated in Fig. 3. All of the specific ImGRAFT terminology is listed and defined in Table 1 and Fig. 3, and is subsequently written in italics in the text. The following sections focus in more detail on the unique ImGRAFT features and provide an overview of the standard processes. Further information about the practical aspects of ImGRAFT along with a full working example can be found on the toolbox website (http://imgraft.glaciology.net/). This includes the link to the source code, documentation and further examples.

4.3.1 Camera motion and *model camera* determination

As for any time-lapse camera setup, minimising movement of the camera is vital. Even though the camera was mounted on a solid structure it is almost impossible to avoid some form of camera motion. This can be due to strong winds, thermal expansion of the camera enclosure or of the mounting platform and human interference, for example when changing SD memory cards. This motion introduces errors and need to be corrected for, as does the distortion around the edge of the *image* as a result of the curvature of the lens. In order to account for any motion and distortion we generate a *model camera* for each corresponding *image*. For clarity, we stress that the *model camera* contains all of the physical camera information from the actual time-lapse camera, plus

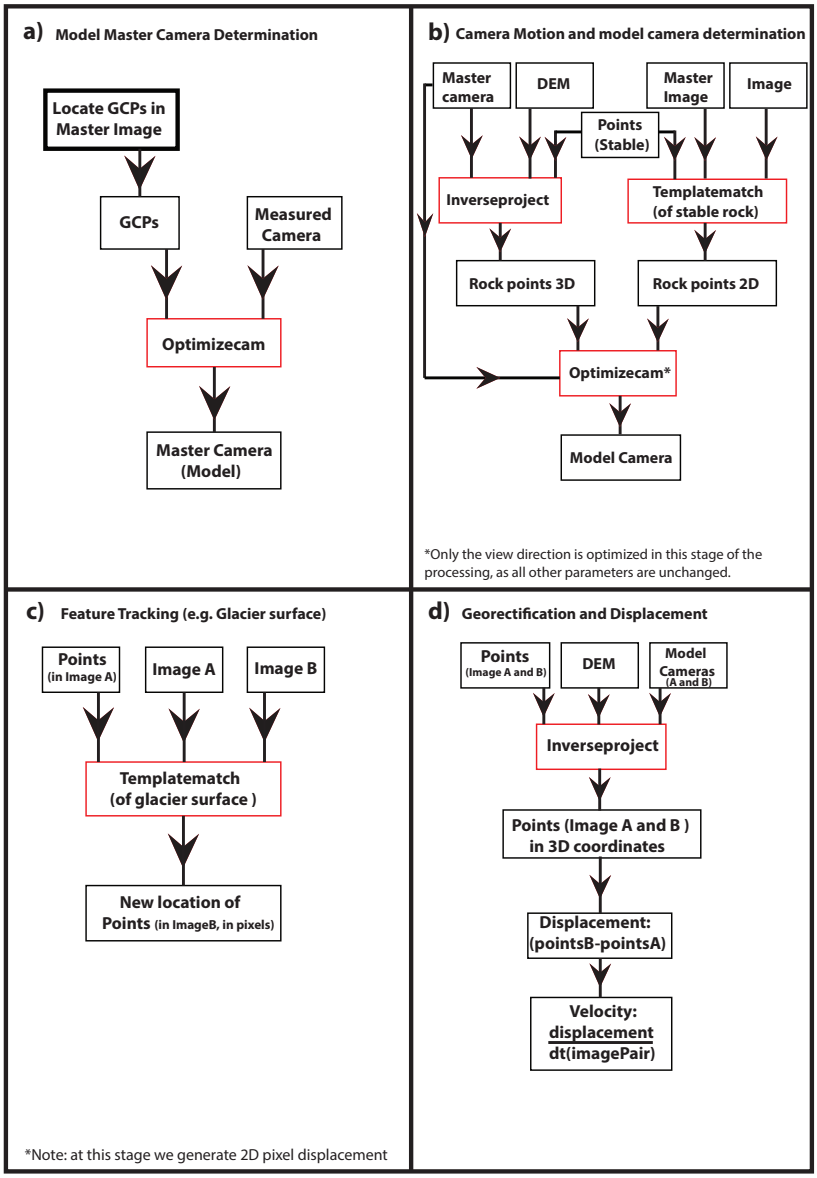

Figure 3. A schematic overview of the key steps in the ImGRAFT processing chain. Boxes outlined in red indicate functions and those in black indicate inputs or outputs.

any optimised camera parameters (e.g. rotations and changes in view direction), that differ from that of the *model master camera*. Each *image* taken from the time-lapse camera has an associated *model camera* containing this updated information. We determine the camera view parameters for a *master image* (see Table 1) from *GCPs* to generate the *model master camera* (Fig. 3a). The view direction, focal lengths, and lens distortion model are optimised to minimise the square projection error of the *GCPs* using a modified Levenberg–Marquardt algorithm (Fletcher, 1971) in the form of *optimizecam*. The *model camera* formulation has a close correspondence to that of OpenCV (Bradski, 2000) which is loosely based on Claus and Fitzgibbon (2005). We reference all other *model cameras* (Fig. 3b) to the *model master camera*. Due to the inclusion of a full distortion model, this opens up the opportunity to use lower quality cameras with higher distortion.

Table 1. Description of key terminology used in the code, flow diagram in Fig. 3 and frequently referred to in the main body of the text. The first column presents the variable or function name, the second column indicates if it is a variable or a function and the third column provides a short description of the associated term.

Name of variable (V) or function (F)	Basic description
Image (V)	A single terrestrial photo taken from the time-lapse camera.
Image pair (V)	Two *images* consisting of *image A* and *image B*. Note that *image A* and *image B* are not fixed.
Model master camera (V)	The camera coordinates and specifications that are measured in the field, optimised within the ImGRAFT processing and relate best to the GCPs.
Master image (V)	Fully rectified terrestrial *image* used to rectify subsequent *images* to. This is the *image* that corresponds to the *master camera*.
Model camera (V)	A set of parameters describing the view for the associated *image*. There is a *model camera* for every *image* in the processing. This *model camera* is an updated camera view direction that includes any motion observed in the *camera*, in terms of yaw, pitch and roll. A full rotational model is applied to fully capture any motion in the *camera* caused by movement of the camera housing, such as from wind. Note that the *model cameras* are optimised camera view directions relative to the *master camera*. These are not physical cameras, just updated view parameters including any camera shift.
GCPs (V)	Ground control points (GCPs) are used to determine the view of the *model master camera/image*. They consist of features that are clearly identifiable in the *images* that have a known coordinate, such as a stable prominent boulder or a static feature such as a tunnel entrance or a distinct mountain peak. Where possible it is an advantage to have *GCPs* spread evenly across the *image*.
Template (V)	The small extract taken from *Image A* that contains the surface textures and features we wish to locate in *Image B* (see Fig. 4 for a schematic example). The *template* is centred around the grid *points* we define. An example of the grid with the associated *points* can be seen in Fig. 5.
Search region (V)	This is a constrained area in *Image B* where the *templatematch* algorithm searches for the best match of the *template*.
Point (V)	Each *point* is defined as a 2-D and 3-D centre coordinates around which the *template* is defined. We choose these points in map coordinates to generate a regular static grid, to ease comparison between velocity fields.
Templatematch (F)	This feature tracking algorithm uses a correlation based matching algorithm such as NCC to find the highest correlation of the *template* from *image A* within the *search region* in *image B*. The coordinate that is registered as the displacement between *image A* and *image B* is the centre of the *template* location that is found to have the highest correlation in *image B*. Note that *templatematch* algorithm is used on both the stable features in the *image* in *templatematch* rock and also on the dynamic features in the *image*, such as the ice surface.
Optimizecam (F)	Function used to minimise the misfit between the 3-D and 2-D coordinates in the *model camera* determination and optimise camera view parameters.
Inverseproject (F)	Inverse projection function that projects the image coordinates to world coordinates (2-D to 3-D).

We determine the *model cameras* of all the other *images* by determining the camera motion relative to the *model master camera/image*. As the physical time-lapse camera is mounted on a solid, stationary platform all relative motion is in the form of rotation. Therefore we only optimise the rotational parameters in Fig. 3b, when generating the subsequent *model cameras*. Typically camera motion is accounted for in a pre-processing step, where all the *images* are co-registered. This can result in compromising the image quality that can occur from cropping, rotating and re-saving. As a result our approach to dealing with camera motion differs, as we account for camera motion in the projection calcu-

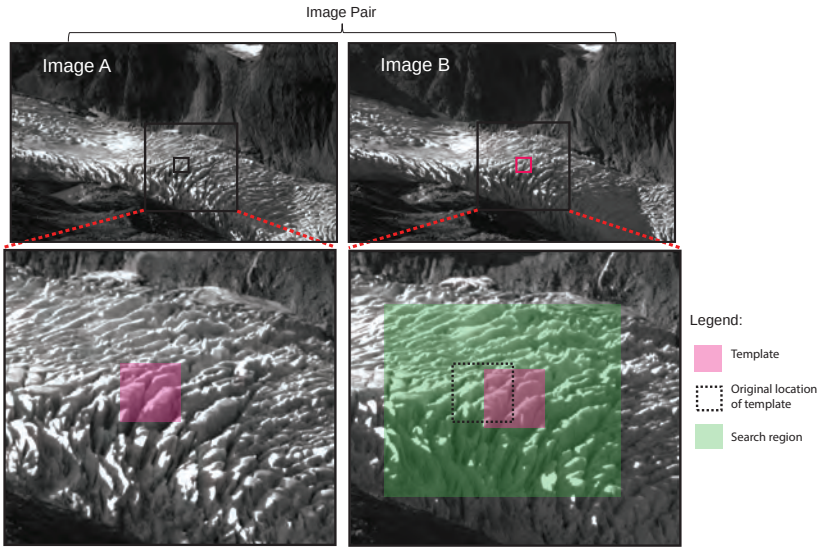

Figure 4. Schematic diagram to show the different components of the *templatematch* process. Note that the *template* and *search region* are not to scale. A unique *template* will be extracted from *image A* for every *point* defined in the grid (see Fig. 5). The user defines the size of both the *template* and the *search region* (Table 1).

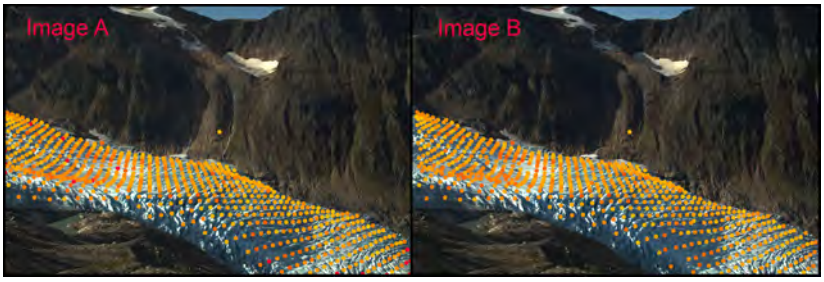

Figure 5. Screen shot of the *templatematch* stage of the processing chain. The regularly spaced grid can be seen in left hand image and the corresponding "tracked" points can be seen in the right hand *image*. The marker colour corresponds to the signal minus the noise, yellow indicating a good match between *image pair*.

lations. Camera motion, as discussed previously, is caused by a variety of uncontrollable factors that subsequently lead to an offset between *image pairs*. The main motion experienced is the rotation about the vertical (yaw), as the camera was mounted on a round pole. However, we experience rotation about all three axes (compass direction/yaw, inclination/pitch, horizon-tilt/roll). We firstly need to determine the offset. This is done by tracking stable rock features on both the near and far valley sides. In order to determine this motion we use the *templatematch* function in ImGRAFT. *Templatematch* uses a standard normalised cross-correlation (NCC) algorithm (Heid and Kääb, 2012), to match the small subset *templates* defined about *points* on a grid in *image A* (see Figs. 4 and 5). The user defines the size of the *template* in order to capture some surface texture and pattern, examples of which can found in Fig. 4. Contrary to some other feature tracking tools, we do not define individual features such as a distinct crevasse or boulder, but rather a small area automatically selected based on the *template* size criteria. We subsequently search for the same texture and pattern contained in the *template* in the second image in the *image pair*, *image B*. In order to reduce the computation time of searching for the best correlation in *image B*, we define a constrained area, the *search region*, within which the *template* is searched for. The *search region* must always be bigger than the *template*, and the location of the *search region* is based around the original location of the selected points. The recorded location of the *template* displacement is defined as the point of highest correlation between the input *template* and the *search region*. We use this NCC based *templatem-*

atch function to both track motion in the bedrock (used to determine camera motion), as well as for determining displacement of the deformational surface, e.g. glacier motion (see Sect. 4.3.2). By running *templatematch* on the stable bedrock we are able to determine the amount and type of motion experienced in the camera. We then use this information to "update" the view direction of the *model camera*. In practice, we project the *master image* pixel coordinates to the new *model camera* and optimise the camera view using *optimizecam*, by minimising the reprojection error (see http://imgraft.glaciology.net/). Instead of correcting the image, we correct the camera orientation based on the offset. Our approach is advantageous since we only save a text file of *model camera* parameters, rather than a large corrected image.

4.3.2 Template matching

This stage of the method refers directly to the *templatematch* function of ImGRAFT, which has been discussed in the previous section in relation to bedrock motion. Here we apply the *tempaltematch* to the moving ice surface (Fig. 3c).

ImGRAFT tracks features between image pairs, *image A* and *image B* (Figs. 3 and 5) by a process called *templatematch* (see Sect. 4.3.1 and Table 1). *Image A* refers to the template image and *image B* refers to the search *image*, which together form an *image pair*. *Image pairs* are any combination of *images* from the data set, where generally *image A* is the first *image* in time and *image B* is the later *image*. The optimal time interval between the *image pairs* varies depending on how much motion is expected and what the resolution the *image* is. In our case, an interval of 1 week is a good balance between expected motion (approximately 5–7 m total), the resolution of the camera and limited change in the appearance of surface texture between the image acquisitions. ImGRAFT uses the NCC algorithm as a measure of template similarity, which generally performs well (Heid and Kääb, 2012) but other measures such as phase correlation and optical flow analysis have been suggested in the literature (Ahn and Box, 2010; Ahn and Howat, 2011; Heid and Kääb, 2012; Vogel et al., 2012). We hope to include more *templatematch* methods in future versions of ImGRAFT.

The NCC method is sensitive to changing light conditions around the feature and to reduce this effect we only choose *image pairs* where illumination is similar, i.e. we only use *image pairs* taken at the same time of day. One way to reduce false matches is by reducing the size of the *search region* and centring it on a prior estimate of the location in the second *image* in the *image pair*, *image B* (Fig. 3). In our case the prior guess is based on the centre coordinate of the *template* in *image A*, reprojected to the view from the *model camera* from *image B*. This prior guess accounts for camera motion, but as mentioned previously, it could be improved with a background ice flow estimate.

We obtain subpixel displacements by bi-cubic intensity interpolation as used in Debella-Gilo and Kääb (2011), followed by local weighing of the NCC peak (3-by-3 pixel) neighbourhood.

It is common to track *points* on a regular grid based on pixel coordinates. However, due to the geometry of the glacier this corresponds to an irregular grid in 3-D space, often characterised by gaps in the velocity field. This is because the grid is not fixed in space but rather image specific as a result of camera motion. Instead we use a static, regular (25 m) geographic grid (Fig. 5) to track our *templates* on the ice, thereby consistently tracking the same coordinate in each *image pair*, rather than tracking a feature through time. This allows for a better comparison between velocity fields from different time periods.

4.3.3 Georectification and displacement

Oblique imagery lacks crucial spatial information needed to extract useful quantitative distance (dimension) information as the *image* is a 2-D representation of a 3-D landscape (Corripio, 2004; Härer et al., 2013). Georectification is the process whereby we assign a 3-D real world coordinate to the corresponding pixel in the 2-D *image* (Fig. 3d). The *model camera* directly allows us to calculate the 2-D pixel coordinates of any 3-D world coordinates. However, we are interested in the 3-D coordinates of features in the *image*, i.e. we want to make an "inverse" projection using *inverseproject*, from 2-D pixel coordinates to 3-D coordinates, constrained to the visible part of the DEM. In principle the *inverseproject* function performs a form of ray tracing to generate the 3-D coordinates of the 2-D *points* using the two *model cameras* from each of the *images* in the *image pairs* and the DEM. In ImGRAFT, we project the visible part of the DEM to 2-D camera view coordinates, and use standard interpolation techniques to obtain 3-D coordinates for any image pixel. The georectification process is carried out on the offset data for all *image pair* combinations in the time-lapse time series. The actual displacement is calculated as the difference between the 3-D *points* between *image A* and *image B*. It is this displacement that is used in the following velocity calculation.

4.3.4 Velocity calculation

The feature tracking returns the pixel coordinates of the feature in the *image pair* (*image A* and *image B*). The corresponding 3-D world coordinates are obtained using the inverse projection of the *model cameras* (Fig. 3d). The velocities can then be calculated from the change in geographic location and dividing the displacement by the time interval between the *images* in the *image pair*.

Having very oblique angles from the camera to the measurement surface can amplify errors along the look vector. In such cases it can be beneficial to only look at the velocity

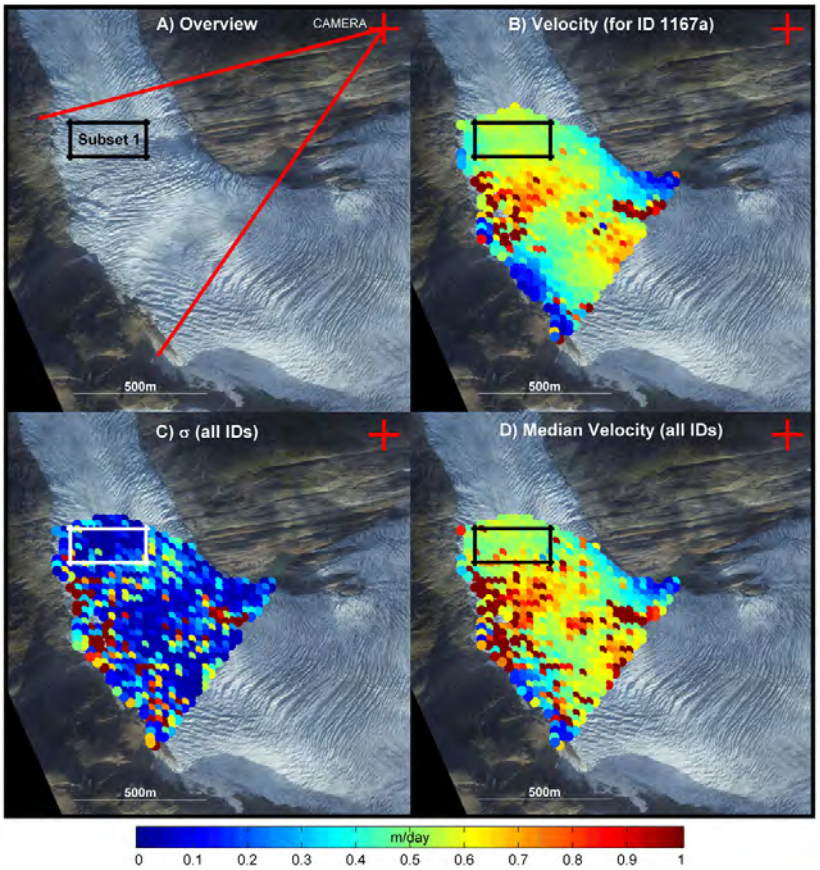

Figure 6. (a) Time-lapse location on the valley side; red lines indicate the viewshed. Subset 1 is the test area used to derive the median displacements presented in Table 2. **(b)** Example of the raw velocity field produced as output from the ImGRAFT toolbox. **(c)** Standard deviation plot of velocity fields produced from all the image pairs in Table 2. **(d)** Median velocity plot for all the image pairs presented in Table 2. Note that we use the median over the mean as it is robust to outliers.

component along the flow direction (i.e. local slope direction or along the centreline). We do not show our data projected in the downslope projection as due to the complex nature of the ice flow in our study site, we risk losing valuable flow information contained within the full velocity component.

In the example presented in the study, we display the unfiltered data *points* in Fig. 6. Some filters can be applied to the velocity fields, including correlation coefficient (CC) thresholds and signal to noise ratio (SNR) threshold. However, we experienced that this removed more positive matches than mismatches, therefore we decided to carry out our calculations on unfiltered data. It is possible to test varying CC and SNR filter thresholds, for example a strict CC threshold set at 0.9, where any matched *points* with a correlation peak below 0.9 would be removed, thereby leaving only the matches with the highest correlation according to the NCC algorithm used in the *templatematch* (Fig. 3d).

5 Quality control

Subsets of the velocity field were extracted from regions of slow, high and medium flow. The slow flow regions around the margins was one obvious quality control area where one expects the highest drag from the valley sides. We assume that small errors will propagate to areas furthest away from the camera, and therefore we begin our quality control checks here. We inspect the velocity fields to identify the velocity profile across the glacier. If the margin areas indicate high velocities, similar to those in the centre of the glacier, it is indicative of a potential error in our processing chain of that *image pair*; for example, if one of the *model camera* view direction parameters is incorrect. In order to correct for this, the processing highlighted in the second processing stage in (Fig. 3b) must be re-run to reproduce the offset between stable features. This can then be used to recalculate the *model camera*. If this does not solve the anomalous velocity pattern

Table 2. *Image pair* IDs and parameters used in the error calculation based on subset 1, including the median velocity for that *image pair*.

Image pair ID	Date *image A*	Date *image B*	Time	Interval	Median velocity ($m\,day^{-1}$)
1151x	17 Jul 2013	22 Jul 2013	11:04	5 days	0.54 ± 0.03
1252y	17 Jul 2013	22 Jul 2013	14:04	5 days	0.49 ± 0.03
1167x	17 Jul 2013	24 Jul 2013	11:04	7 days	0.53 ± 0.02
1268y	17 Jul 2013	24 Jul 2013	14:04	7 days	0.51 ± 0.02
1175x	17 Jul 2013	25 Jul 2013	11:04	8 days	0.54 ± 0.02
1276y	17 Jul 2013	25 Jul 2013	14:04	8 days	0.52 ± 0.02
1183x	17 Jul 2013	26 Jul 2013	11:04	9 days	0.53 ± 0.02
1284y	17 Jul 2013	26 Jul 2013	14:04	9 days	0.53 ± 0.02
1191x	17 Jul 2013	27 Jul 2013	11:04	10 days	0.54 ± 0.02
1292y	17 Jul 2013	27 Jul 2013	14:04	10 days	0.52 ± 0.02
					Mean: 0.53 Range: 0.05

then there may be a problem with the *image* itself. Light fog and rain can cause problems in the feature tracking of the features in the *image* leading to mismatches. If this problem persists after re-running the processing, the velocity field is removed.

Error estimation

There are multiple sources of errors that propagate through the processing chain and end up in the final 3-D positions and velocity estimates. Errors in the *GCPs* will result in errors in the *model master camera* and consequently all other *model cameras* referenced to it. Uncertainties in the *templatematch* of the stable rock features will propagate to the *model cameras*. Uncertainties in the pixel coordinates of features, *model cameras*, and the DEM will as a result propagate through the inverse projections to the estimate of the 3-D position. All of these uncertainties can be accounted for by Monte Carlo sampling of the uncertainties provided the uncertainties in the GCPs, DEM, and the uncertainty of the feature tracking. This can be incorporated into ImGRAFT processing chain, and an example is given in the frequently asked question section of the ImGRAFT website (http://imgraft.glaciology.net/documentation). A related, more approximate method is to use an error budget approach. In our case we have a near perfect DEM and a strongly constrained viewing geometry, and the errors in our estimates are dominated by errors in feature tracking, and a simpler more empirical approach can be used. In our Engabreen example, we estimate the uncertainty from the sample variance between independent estimates of the velocity. We expect this estimate to be greater than the actual uncertainty as it also includes the variance due to real velocity variations between samples. When we estimate the error variance, it is therefore desirable to choose a set of independent velocity samples with little velocity variability. This is accomplished by choosing independent *image pairs* with a high degree of temporal overlap. Ideally all the samples used in the calculation should span an equal temporal range, however here we estimate the error from *image pairs* spanning 5 to 10 days (Table 2). A more in-depth analysis of the actual error estimates is presented in the results (Sect. 6). Error estimation is not directly incorporated into the toolbox, instead we present our case specific method outlined above as a suggestion for similar cases. Error estimations for other studies should be addressed on a case-by-case basis and the most appropriate method of error estimation should be applied. As ImGRAFT is open source, it allows users to incorporate the most appropriate error estimation method for their data set.

6 Results

ImGRAFT produces consistent velocity fields over the mid icefall section of Engabreen. They match the expected flow pattern of a small alpine glacier, for which we expect slow flow at the margins where there is highest friction along the valley walls and fastest flow in the centre of the glacier. ImGRAFT is able to capture the specific velocity pattern at Engabreen, which include the extensional and compressional flow as the ice flows in, through and out of the icefalls. The icefalls can be clearly seen on the *image* in Fig. 6a, where there are large crevasse fields indicate the icefalls. The uppermost icefall ends as the camera viewshed begins, the flow then enters an overdeepening in the upper-centre of the viewshed, before finally entering the lower icefall in the centre of the viewshed before ending in a compressional zone at the base of the icefall. Subset 1 in Fig. 6 is located at the base of the lower icefall. The high flow can be separated into two distinct areas; firstly the edge of the upper icefall flowing into an overdeepening, and secondly the ice flowing out of the overdeepening into the lower icefall as demonstrated

by the yellow/orange areas in Fig. 6b. In these areas the ice experiences extensional flow and in the examples in Fig. 6 the glacier achieved speeds of between 60 and 80 cm day^{-1}, which contrasts to the compressional flow experienced in the overdeepening and the base of the icefall where speeds are typically around 50 cm day^{-1} (see Table 2).

The velocity fields produced using ImGRAFT match well with the velocity pattern observed in two SAR velocity fields (Unpublished data, Schellenberger, 2014) covering the same area. Similar magnitudes of velocity averaging around 50 cm day^{-1} in the same viewshed area are observed. As well as comparing to the SAR maps, we also improve the existing surface velocity estimates from Engabreen (Jackson et al., 2005). We significantly improve the temporal coverage due to the high number of images acquired each day. We achieve a dense velocity field at Engabreen, albeit over a smaller area than Jackson et al. (2005). The Jackson et al. (2005) study uses IMCORR software, to feature track two orthorectified aerial images from 2002. They found that the central part of the glacier was moving slower than the margins. Our results and preliminary SAR data indicate that this is likely an artefact of the processing due to the long time interval between image acquisitions (> than 20 days). This long interval between images results in features deforming beyond recognition and are thus no longer feasibly trackable.

We estimate the associated error in the velocities in Table 2, following the approach outlined in Sect. 5. We take the standard deviation of all the velocity estimates presented in Table 2, which results in a conservative estimate of the uncertainty for the *image pair* spanning the longest time interval (ID: 1191x and 1292y). We assume that the error in the displacement is constant and the error in the velocity fields scales directly with the time interval, which we use to estimate the uncertainty for the shorter time intervals. Table 2 summarises all of the *image pairs* used in the error analysis. All *image pair* IDs that have the suffix x consist of pairs taken at 11:04 CEST, and all IDs that have the suffix y are *image pairs* taken at 14:04 CEST. These periods are chosen as they both have high quality *images* available with similar lighting both at 11:04 and at 14:04 CEST. We selected a small area (black box, Fig. 6) for more detailed analysis. This area was chosen as it appears not to be affected substantially by changes in illumination. Therefore, we attribute any existing error in this region to the *templatematch* function. This is indicated by the low standard deviation of velocity estimates here (Fig. 6c). Here we compare the offset time period velocity calculations for all *image pairs* presented in Fig. 2. Figure 6d is the median plot for all the ten time periods together. The final column in Table 2 shows the overall spread in medians between all the time periods. When we only compare the same hourly periods in Table 2, then the range is lower at only 5 cm day^{-1}. This is our simple error estimation of the velocity calculation from our feature tracking processing chain. The average velocity for the whole feature tracked area is approximately 60 cm day^{-1} therefore our error estimate of 5 cm day^{-1} equates to a rough error estimate of ± 8 % error. This error estimate is based on unfiltered data where known mismatched *points* are included. It is expected that the error will reduce if known mismatches are removed through filtering as mentioned in the methods section.

Further results using ImGRAFT to produce velocity fields over Greenland can be found in the following study (Messerli et al, 2014).

7 Conclusions

We present a flexible, open source Image GeoRectification And Feature Tracking toolbox (ImGRAFT), We apply it to our test case, Engabreen, an outlet glacier in Arctic Norway. ImGRAFT incorporates all the processing steps needed to transform monoscopic, terrestrial, oblique images into a velocity field. ImGRAFT assimilates the rectification of the images and subsequent feature tracking into one toolbox. These features are advantageous, as current existing software tend to address only one of these processes, and thereby require numerous software to complete the entire processing. Furthermore, the source code is freely available and adaptable, allowing the user to tailor the toolbox to meet their specific processing needs, whilst all being contained within the MATLAB environment. Additional benefits are the inclusion of a full distortion model, which opens up the possibility to use images taken on lower quality cameras with lower quality lenses. This significantly increases the diversity of the toolbox as it accommodates a wide range of image sources and possibilities for feature tracking. We offer suggestions of how to prepare the images and DEM correctly for input to ImGRAFT and additionally provide a comprehensive online documentation (http://imgraft.glaciology.net/) and demonstrations. We provide some guidelines for error assessment within the context of our Engabreen example, in which we propose an empirical approach for error assessment that incorporates the accumulated errors throughout the processing chain. Our continuously updated online documentation offers users further pre/post-processing tips and other example cases. Our aim is to allow for further algorithm development and improvement through our own efforts and those within the user community. ImGRAFT provides a flexible, adaptable tool to process large volumes of imagery with a high degree of automation, in order to obtain quantitative data in the form of displacement. It produces consistent, velocity fields that require minimal post-processing and filtering. ImGRAFT has been developed with a focus on glaciological applications, and in this paper we only consider terrestrial based imagery. However, it has also been tested on a variety of satellite data, with encouraging results (e.g. using Landsat-8, Messerli et al, 2014). Applications to other mass movement environments is achievable with slight modifications of the processing chain.

Acknowledgements. This publication is contribution number 46 of the Nordic Centre of Excellence, SVALI (Stability and Variations of Arctic Land Ice), funded by the Nordic Top-level Research Initiative (TRI). Additional funds came from the Centre for Ice and Climate (CIC), the Scottish Arctic Club and the Anglo-Danish Society. DEM and orthophoto data of Engabreen was provided by the Norwegian Water Resources and Energy Directorate (NVE). The authors would like to thank NVE, especially M. Jackson, for logistical and financial support with fieldwork. We would also like to thank L. Mackay, P.-M. Lefeuvre and H. Sevestre for their support in the field and T. Schellenberger for providing SAR velocity data used in the preliminary analysis, but not presented here. We also thank A. Kääb for useful discussions in the earlier versions of this study, and thanks to N. Karlsson and H. Pillar for reading and offering suggestions on draft versions. Finally we thank the two anonymous reviewers for their comments, which helped to improve the paper.

Edited by: L. Eppelbaum

References

Ahn, Y. and Box, J. E.: Instruments and Methods Glacier velocities from time-lapse photos: technique development and first results from the Extreme Ice Survey (EIS) in Greenland, J. Glaciol., 56, 723–734, 2010.

Ahn, Y. and Howat, I. M.: Efficient Automated Glacier Surface Velocity Measurement From Repeat Images Using Multi-Image/Multichip and Null Exclusion Feature Tracking, IEEE T. Geosci. Remote, 49, 2838–2846, 2011.

Aschenwald, J., Leichter, K., Tasser, E., and Tappeiner, U.: Spatio-temporal landscape analysis in mountainous terrain by means of small format photography: a methodological approach, IEEE T. Geosci. Remote, 39, 885–893, 2001.

Benn, D. I. and Evans, D. J. A.: Glaciers and Glaciation, 2nd Edn., Hodder Arnold Publication, Hodder Education, London, 2010.

Bradski, G.: OpenCV Library, Dr. Dobb's J. Softw. Tool., 25, 122–125, 2000.

Claus, D. and Fitzgibbon, A. W.: A rational function lens distortion model for general cameras, in: Proceedings of the IEEE conference on Computer Vision and Pattern Recognition, 213–219, 2005.

Coffin, D.: Decoding raw digital photos in Linux, http://www.cybercom.net/~dcoffin/dcraw/ (last access: 29 July 2014), 2009.

Corripio, J. G.: Snow surface albedo estimation using terrestrial photography, Int. J. Remote Sens., 25, 5705–5729, 2004.

Danielson, B. and Sharp, M.: Development and application of a time-lapse photograph analysis method to investigate the link between tidewater glacier flow variations and supraglacial lake drainage events, J. Glaciol., 59, 287–302, 2013.

Debella-Gilo, M. and Kääb, A.: Sub-pixel precision image matching for measuring surface displacements on mass movements using normalized cross-correlation, Remote Sens. Environ., 115, 130–142, 2011.

Evans, A. N.: Glacier surface motion computation from digital image sequences, IEEE T. Geosci. Remote, 38, 1064–1072, 2000.

Fletcher, R.: Modified Marquardt subroutine for non-linear least squares, Tech. Rep. AERE-R-6799, Atomic Energy Research Establishment, Harwell, England, 971.

Flotron, A.: Photogrammetirsche Messungen von Gletscherbewegunen mit automatischer Kamera, Schweiz. Z. Vermess. Photogramm. Kult. Tech., 71, 1–73, 1973.

Härer, S., Bernhardt, M., Corripio, J. G., and Schulz, K.: PRACTISE – Photo Rectification And ClassificaTIon SoftwarE (V.1.0), Geosci. Model Dev., 6, 837–848, doi:10.5194/gmd-6-837-2013, 2013.

Harrison, W. D., Raymond, C. F., and MacKeith, P.: Short period motion events on Variegated Glacier as observed by automatic photography and seismic methods, Ann. Glaciol., 8, 82–89, 1986.

Harrision, W. D., Echelmeyer, K. A., Cosgrover, D. M., and Raymond, C. F.: The determination of glacier speed by time-lapse photography under unfavorable conditions, J. Glaciol., 38, 257–265, 1992.

Heid, T. and Kääb, A.: Evaluation of existing image matching methods for deriving glacier surface displacements globally from optical satellite imagery, Remote Sens. Environ., 118, 339–355, 2012.

Jackson, M., Brown, I. A., and Elvehøy, H.: Velocity measurements on Engabreen, Norway, Ann. Glaciol., 42, 29–34, 2005.

Kääb, A.: Monitoring high-mountain terrain deformation from repeated air- and spaceborne optical data: examples using digital aerial imagery and ASTER data, ISPRS J. Photogramm. Remote Sens., 57, 39–52, 2002.

Kääb, A.: Image correlation software CIAS, http://www.mn.uio.no/icemass (last access: 09 January 2015), 2013.

Kääb, A. and Vollmer, M.: Surface geometry, thickness changes and flow fields on creeping mountain permafrost: automatic extraction by digital image analysis, Permafrost Periglac. Process., 11, 315–326, 2000.

Messerli, A., Karlsson, N. B., and Grinsted, A.: Brief Communication: 2014 velocity and flux for five major Greenland outlet glaciers using ImGRAFT and Landsat-8, The Cryosphere Discuss., 8, 6235–6250, doi:10.5194/tcd-8-6235-2014, 2014.

Muslow, C., Koschitzki, R., and Maas, H.-G.: Photogrammetric Monitoring of Glacier Margin Lakes, ISPRS Archives J. Photogramm. Remote Sens. Spatial Inf. Sci., 1, 1–6, 2013.

Parajka, J., Haas, P., Kirnbauer, R., Jansa, J., and Blöschl, G.: Potential of time-lapse photography of snow for hydrological purposes at the small catchment scale, Hydrol. Process., 26, 3327–3337, 2012.

Smith Jr., K. L., Baldwin, R. J., Glatts, R. C., Chereskin, T. K., Ruhl, H., and Lagun, V.: Weather, ice, and snow conditions at Deception Island, Antarctica: long time-series photographic monitoring, Deep Sea-Res. Pt. II, 50, 1649–1664, 2003.

Vogel, C., Bauder, A., and Schindler, K.: Optical Flow for Glacier Motion Estimation, ISPRS Annals J. Photogramm. Remote Sens., 1, 359–364, 2012.

Walter, F., O'Neel, S., McNamara, D., Pfeffer, W. T., Bassis, J. N., and Fricker, H. A.: Iceberg calving during transition from grounded to floating ice: Columbia Glacier, Alaska, Geophys. Res. Lett., 10, L15501, doi:10.1029/2010GL043201, 2010.

3.3 Optical Feature Tracking at Engabreen

Two sets of results from ImGRAFT are presented for Engabreen. Firstly results from the terrestrial camera are further expanded from Messerli and Grinsted (2015) and secondly results from satellite feature tracking at Engabreen are shown.

3.3.1 Terrestrial Feature Tracking

To follow on from the results presented in Messerli and Grinsted (2015) a longer time series of velocity fields are presented that capture seasonal variations in speed at Engabreen during 2013. A short series of velocity fields (Figure 3.3) demonstrate the ability of ImGRAFT to document velocity variability throughout the year over a large spatial area. A more detailed application of this data is presented in Chapter 5, where the velocity data in the form of a graphical time-series is analysed alongside numerous other geophysical datasets.

The data in the time-series in Figure 3.3 span from late-May to mid-September.The velocity fields present average velocity between the image dates in the image pair. Most of the velocity maps in the figure are averaged over approximately 5 days. This time interval is an optimal time-window over which to produce consistent velocity maps with few erroneous matches. The data presented in Figure 3.3 has had a minimal amount of filtering applied, similar to that discussed in (Messerli and Grinsted, 2015). This has removed a certain number of mismatched features, but not all. The data are presented in orthorectified form for better comparison.

General flow patterns at Engabreen are captured in the velocity fields, with clear horizontal velocity gradients, where there is higher flow in the central part of the glacier and slower flow at the margins. Flow speeds of up to 1 $m\ d^{-1}$ are recorded, appearing in the lower ice fall. The upper icefall terminates as it enters an overdeepening in the centre of the velocity maps and slows down, before flowing out over a riegl and into the second lower icefall. The slow flow areas around the margins reflect the higher lateral drag from the valley sides. From the six images in the time-series a clear seasonal slowdown is captured. The flow in the lower icefall drops from around 0.8 $m\ d^{-1}$ in late-May to around 0.5 $m\ d^{-1}$. During the late melt season the flow pattern appears to be more homogeneous than in spring and early summer. The details of this time-series with relation to changes in the hydrology at Engabreen are discussed in chapter 5.

3.3.2 Satellite Feature Tracking

In order to extend the spatial coverage of the terrestrial velocity maps (Figure 2.8), velocity fields for Engabreen were generated for 2013 and 2014 (Figures 3.4 and 3.5) using Landsat-8 imagery available from the U.S. Geological Survey (`http://landsat.usgs.gov/`). The data used is the Level 1 Terrain corrected (L1T) panchromatic Landsat band, which has the highest Landsat spatial resolution of 15m. This product is topographically and geometrically corrected using a DEM and GCP's, the quality of which determine the accuracy of the L1T product (`http://landsat.usgs.gov/`).
At Engabreen where the average surface velocity is around 0.5 md^{-1}, there is an additional aspect to be taken into consideration, particularly when using such relatively coarse satellite imagery. Even though ImGRAFT is able to achieve sub-pixel displacement, the interval between two Landsat images needs to be considerably higher than

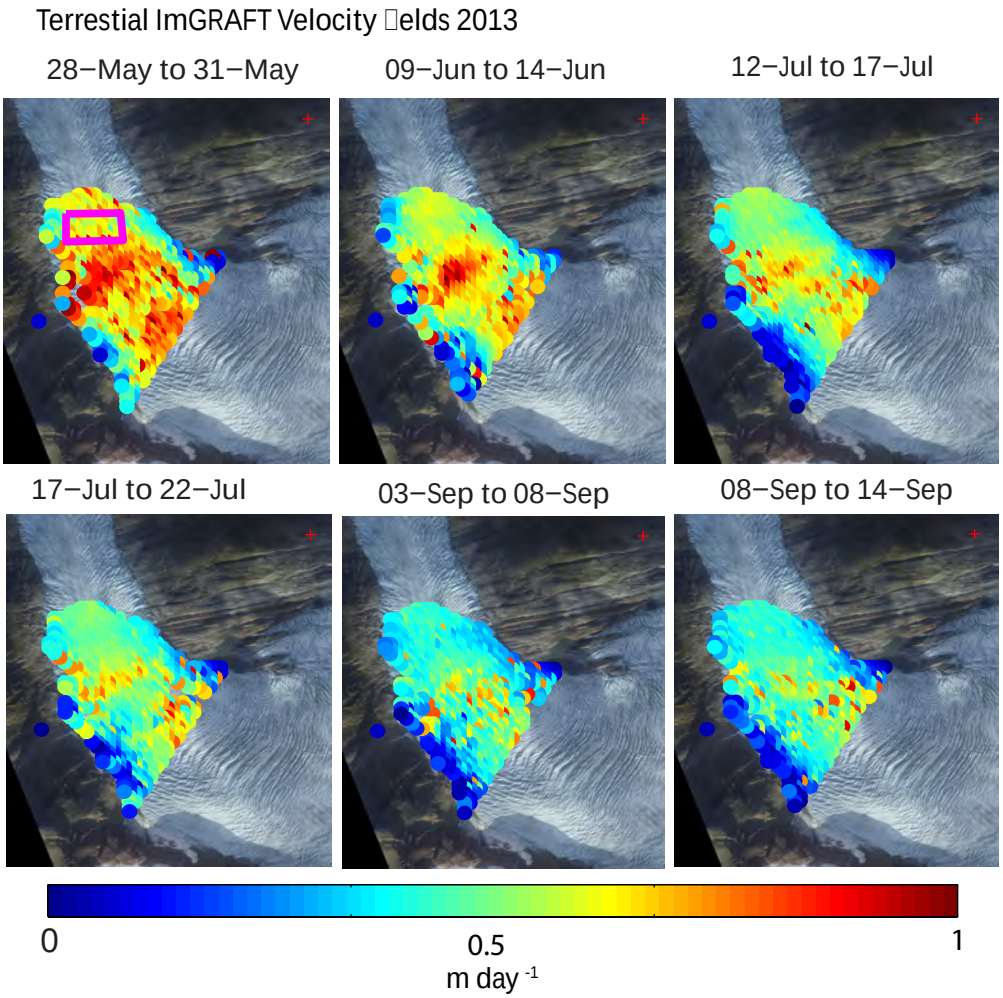

Figure 3.3: *A series of consecutive velocity fields produced from the terrestrial time-lapse imagery using ImGRAFT. These velocity fields are used to produce the velocity time-series shown in chapter 5. Subset 1 is indicated by the magenta box, the median estimates used in Chapter 5 are calculated within this box from each velocity field. The data are displayed in orthorectified form. The red cross indicated the location of the camera.*

that of say the terrestrial imagery, which can resolve displacement over only a few days at Engabreen. Over the 26 day Landsat interval in the first image pair, less than one pixel of motion is expected. Irrespective of this slow flow a good overview of ice flow in the summer is achieved in 2013.

In 2013, Landsat-8 scenes were available that overlap both spatially and temporally with the terrestrial velocity fields and the GPS data on the tongue of Engabreen (see also Chapter 5 for GPS data). Thus, the datasets can be used for validation during that period. Unfortunately, there are only three usable cloud free images in 2013 and therefore there are only two satellite velocity fields that cover the same period as the terrestrial imagery. The time-span covered by the 2013 images ranges from the 1st June 2013 to the 12th September 2013. The spatial coverage in 2013 mean velocity map is patchy due to lack of data in some areas of the glacier. In 2013 the interval between the first two images was 26 days during which snow cover had changed dra-

matically, particularly at higher elevations. The second image pair had a interval of 48 days, during which the surface had undergone yet further alterations. Shadowing also reduces the tracking area as the dark shadows cannot be tracked, in the case of Engabreen there is a persistent shadow in the upper southern margin boundary as it lies nested at the foot of a large steep cliff face. Nevertheless, good spatial coverage was achieved with the two individual velocity maps. The overall flow structure is captured, with high flow experienced in the two prominent icefalls, where a narrow band of slower flow at the bend separates the two high flow areas.

As presented in section 3.3.1 using the terrestrial imagery similar magnitudes of velocity are captured in both the terrestrial and satellite data in 2013. The pattern of flow through the overdeepening and into the lower ice fall is very similar between the two datasets, where the higher flow speeds are visible in the two ice falls, around $0.6md^{-1}$ in both cases. The mean velocity on the tongue at the same location of the GPS locations (see Figure 2.4), is only marginally higher ($0.01md^{-1}$) than the mean recorded at the GPS' spanning the same period. Further discussion of the GPS velocities and the terrestrial time-lapse velocities are made in chapter 5.

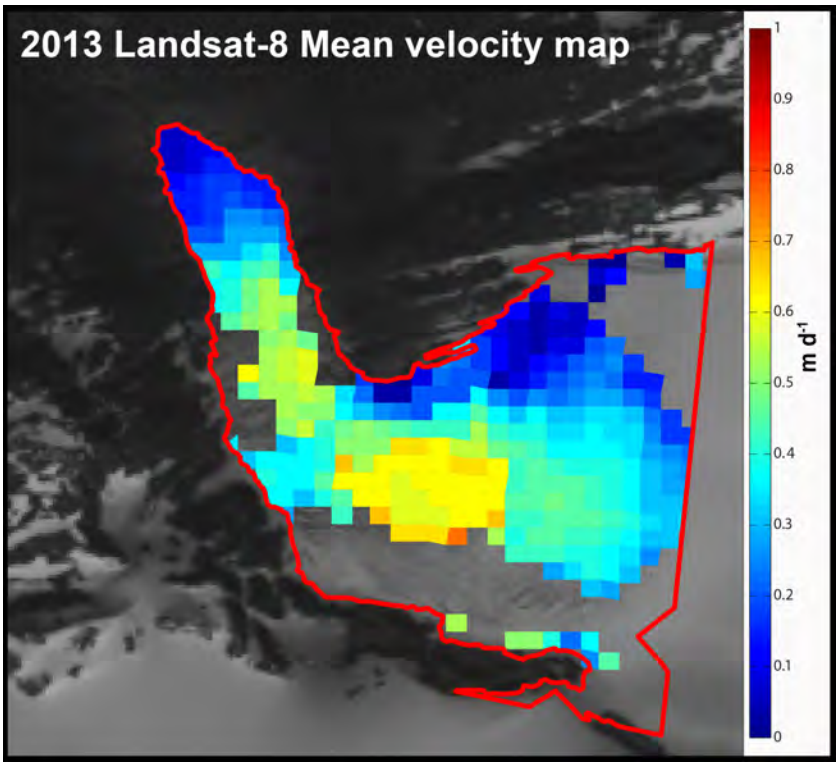

Figure 3.4: *Mean velocity 2013 field produced from Landsat-8 using ImGRAFT.*

In 2014, there were more usable Landsat-8 images, and a total of nineteen image pair combinations could be feature tracked with ImGRAFT. Of the nineteen velocity maps the five best were stacked to form the mean velocity maps in Figure 3.5. The five individual time-slice velocity maps had the best spatial and temporal coverage and the least number of mismatches. The data range covered by the mean velocity map is from the 28 May 2014 to the 15 September 2013. The available imagery in 2014 was also much more evenly distributed than in 2013, which lead to a more representative mean

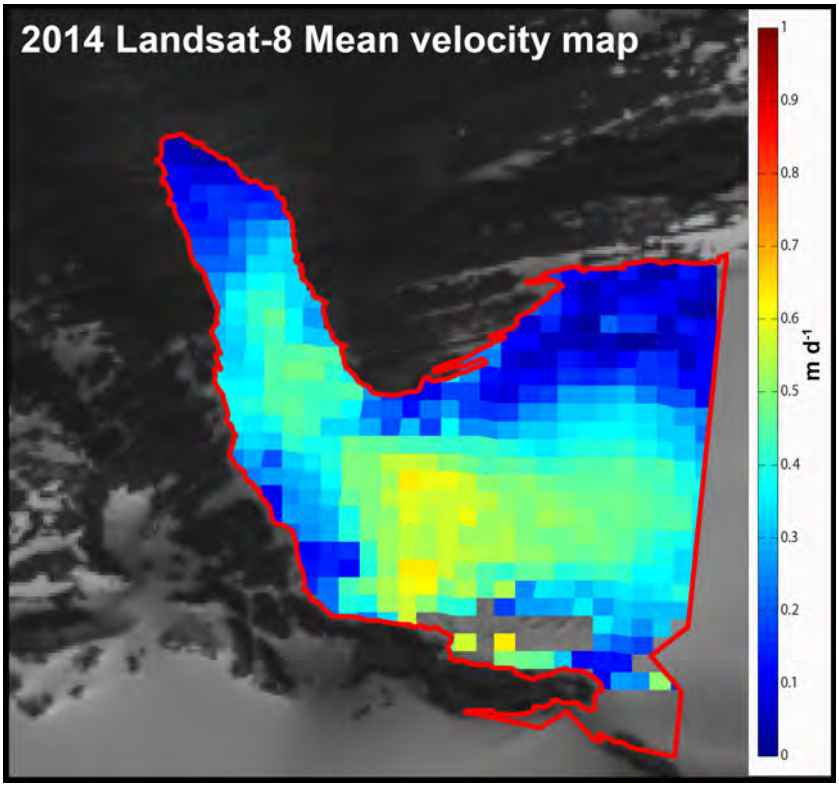

Figure 3.5: *Mean velocity 2014 field produced from Landsat-8 using ImGRAFT.*

summer velocity map that in 2013. This results in a generally lower velocity map, the difference between the two figures is clear(3.4 and 3.5). The 2014 map shows slower velocities than in 2013.
The denser coverage of data also allowed for a better comparison with the terrestrial data, albeit from the previous year. The slow marginal areas are evident in both sets of velocity data.

3.4 Other ImGRAFT examples

3.4.1 Greenland

To further test ImGRAFT on satellite data, the toolbox was applied on well studied large, fast flowing outlet glaciers in Greenland, where a wealth of velocity maps already exist and therefore allow for a better validation of the technique. The results of which are presented in the following paper (Messerli et al., 2014) (section 3.4.1).

This paper presents the first intensive study applying ImGRAFT to Greenlandic glaciers using Landsat-8 panchromatic band data. The paper provides velocity maps of five major Greenlandic outlet glaciers; Helheim Glacier, Kangerdlugssuaq Glacier, Nioghalvfjerdsbræ, Petermann Glacier and Jakobshavn Isbræ. Using ImGRAFT velocity estimates in conjunction with other existing datasets of ice thickness, ice flux estimates for each glacier are estimated at locally defined flux gates. The paper demonstrates the ability of optical image feature tracking to compliment interferometric synthetic aperture radar (InSAR) produced velocity fields, such as those produced by Joughin et al. (2010).

The following manuscript is currently in review for The Cryosphere.

The Cryosphere Discuss., 8, 6235–6250, 2014
www.the-cryosphere-discuss.net/8/6235/2014/
doi:10.5194/tcd-8-6235-2014

The Cryosphere Discussions
Open Access

Brief Communication: 2014 velocity and flux for five major Greenland outlet glaciers using ImGRAFT and Landsat-8

A. Messerli[1,2], **N. B. Karlsson**[1], **and A. Grinsted**[1]

[1]Centre for Ice and Climate, Niels Bohr Institute, University of Copenhagen, Juliane Maries Vej 30, 2100 Copenhagen Ø, Denmark
[2]Section for Glaciers, Snow and Ice, Hydrology Department, Norwegian Water Resources and Energy Directorate, P.O. Box 5091 Majorstua, 0301 Oslo, Norway

Received: 1 October 2014 – Accepted: 10 December 2014 – Published: 20 December 2014

Correspondence to: A. Messerli (messerli@nbi.ku.dk)

Published by Copernicus Publications on behalf of the European Geosciences Union.

Abstract

This study presents average velocity fields, mass flux estimates and central flowline profiles for five major Greenland outlet glaciers; Jakobshavn Isbræ, Nioghalvfjerdsbræ, Kangerdlugssuaq, Helheim and Petermann glaciers, spanning the period (August) 2013–(September) 2014. The results are produced by the feature tracking toolbox, ImGRAFT using Landsat-8, panchromatic data. The resulting velocity fields agree with the findings of existing studies. Furthermore, our results show an unprecedented speed of over 50 m day^{-1} at Jakobshavn Isbræ as it continues to retreat. All the processed data will be freely available for download at http://imgraft.glaciology.net.

1 Introduction

The Greenland Ice Sheet is currently losing mass at an accelerating rate (Rignot et al., 2011), and a significant part of this mass loss can be attributed to increased surface velocities leading to increasing discharge from outlet glaciers. The changes in ice flow velocity have been observed by satellite for the past two decades and display large spatial and temporal variations especially for marine-terminating glaciers (Moon et al., 2012). The processes controlling the variations are not completely understood, but are probably a combination of a warming atmosphere leading to increased surface melt (Andersen et al., 2010), increasing submarine melt rates (e.g. Holland et al., 2008), and changes in conditions at the terminus triggering thinning and acceleration (Nick et al., 2009).

About 20 % (by area Bevan et al., 2012) of the ice-sheet is drained by five glaciers (cf. map Fig. 1); Jakobshavn Isbræ, Nioghalvfjerdsbræ (also referred to as 79 North Glacier), Kangerdlugssuaq, Helheim and Petermann glaciers. Jakobshavn Isbræ has exhibited increasing acceleration and thinning in recent years (Joughin et al., 2012, 2014), leading to a contribution to global sea level rise of 1 mm during 2000–2011 (Howat et al., 2011). Smaller fluctuations in surface velocity have been observed since

Discussion Paper | Discussion Paper | Discussion Paper | Discussion Paper |

the 1990s showing seasonal variations with speedup in summer and slowdown in winter (Joughin et al., 2012). In contrast both Helheim and Kangerdlugssuaq were relatively stable until dramatic speedups occurred in 2002 (Helheim) and 2004 (Kangerdlugssuaq) followed by recent deceleration and apparent stability (Bevan et al., 2012). For Helheim the associated mass loss was off-set by an increase accumulation, while for Kangerdlugssuaq the lost mass corresponds to seven years of surface mass balance (Howat et al., 2011). On the other hand, the northern glaciers in this study appear to be influenced by different climatic conditions. Petermann experienced a large calving event in 2010 but in spite of this the ice-flow speeds have remained relatively stable or only slightly increasing (Bevan et al., 2012). Until recently Nioghalvfjerdsbræ exhibited the same stability with few variations in surface velocity (Bevan et al., 2012) or margin position (Joughin et al., 2010b). However, a recent study has shown that thinning and speedup are now also taking place in northeast Greenland (Khan et al., 2014). In short, there is an increasing need to continuously monitor the velocity of outlet glaciers on varying temporal scales if we are to predict their future contribution to global sea level rise.

In this study we use the newly developed ImGRAFT toolbox (Messerli and Grinsted, 2014) to retrieve surface velocities of Jakobshavn Isbræ, Kangerdlugssuaq, Helheim, Petermann, and Nioghalvfjerdsbræ. ImGRAFT is a feature tracking toolbox and is based on the Matlab programming suite (for more details see Messerli and Grinsted, 2014). We use LandSat 8 imagery from 2013 and 2014 to calculate surface velocities during the year from August 2013 to September 2014. Our results further demonstrate the capability of ImGRAFT to produce velocity maps over a variety of glaciers moving at different speeds. The fact that ImGRAFT is easy to use and freely available from the ImGRAFT website makes it suitable for other studies in need of updated surface velocity data on different temporal scales. The toolbox and the datasets presented here are available on the ImGRAFT website http://imgraft.glaciology.net.

2 Data and method

This study explores the new Landsat 8 data acquired over Greenland since 2013. The highest resolution Landsat-8 band is used in this study; Panchromatic band-8, which has a surface resolution of 15 m.

The initial data selection criteria is based on the quality and coverage of the individual images. This stage of the processing is carried out through manual inspection of each individual scene. Cloud cover poses a challenge when working with optical imagery and can in some cases lead to data gaps if there are no suitable cloud-free images. Here, clouds in the scene are accepted as long as they do not directly obscure the region of interest. Whilst it is possible to use images with different viewing geometries, the resulting shift between the images needs to be corrected. We find that the best results are produced from images that have the same viewing geometry.

The velocity field is produced using feature tracking, whereby features such as crevasses and crevasse fields are tracked through time in sequences of image pairs. In order to track the features a minimum of two images is required. The first image is the template image where features are identified and second image is known as the search image. The search image is scanned, within a defined search window to find the best match of those features from the template image. In this study we apply the ImGRAFT toolbox by Messerli and Grinsted (2014). Although ImGRAFT was originally developed for terrestrial, oblique imagery this study demonstrates its versatility by adapting it to satellite imagery. ImGRAFT has a suit of algorithms in its toolbox, however, only the template matching algorithm is necessary here, because the satellite images are already available in GeoTIFF (Georeferenced Tagged Image File Format) format as a part of the L1T product from the USGS (United States Geological Survey) Earth Explorer database (http://earthexplorer.usgs.gov/).

In this study we experimented with an adapted template match algorithm at Jakobshavn Isbræ that incorporates a pre-guess location based on existing velocity data from the regions, for example SAR velocity data from the MEaSUREs project (Joughin

et al., 2010a). The pre-guess helps to define the location of the search window. Not only does this speed up the feature tracking process but also it minimises the risk of mismatching features.

Once the feature tracking of all the images is complete the velocity fields are stacked to produce a mean velocity field. Only velocity fields with large spatial coverage are used to produce the mean velocity estimate and each velocity field is weighted according to the time period that it covers. If there is an overlap in time, the weighting is reduced for each overlapping period. The conservative error estimate for each displacement map is 2 pixels (30 m) or less. I.e. the error on any velocity field with a time interval greater than 15 days results in less than 2 m day^{-1} error in the velocity. This error is estimated by running the template matching algorithm on the bedrock flanking the glaciers and fjord. The velocity maps are then manually inspected for any detectable motion on the static rock features, as this provides an indication of the error in the displacement on the ice, due to the uncertainties in the georeferenced L1T products. In cases where there is a large displacement on static features, the scene pairs are discarded from the processing.

In addition to the velocity estimates and centreline flow profiles (hereafter referred to as flow profiles) we also produce mass flux estimates from ice flow through fixed flux gates (Fig. 1). We use thickness data for each of the five glaciers obtained from the CReSIS (Center for Remote Sensing of Ice Sheets) (https://data.cresis.ku.edu/data/grids/) website. The horizontal ice flow estimate used in the flux calculations is based on the mean velocity field calculated for each glacier, presented in Fig. 1. We assume a constant horizontal velocity with depth when estimating the flux, and define the flux gates as close as possible to the estimated grounding line. We estimate the grounding line position using a simple method outlined in Enderlin and Howat (2013), where we define the location as the point where the ice starts to float according to the CReSIS bed and ice thickness data. This method is used to estimate the grounding line location shown in Figs. 1 and 2, for Helheim and Kangerdlugssuaq. For Petermann and Nigoghalvfjerdsbræ, we use existing published grounding line locations (Rignot

et al., 1997; Rignot and Steffen, 2008). Unfortunately due to the unprecedented retreat of Jakobshavn Isbræ, it is not possible to locate the grounding line with much certainty. We therefore estimate the position from Fig. 3 in Joughin et al. (2014) which shows the frontal seasonal evolution in relation to the bed topography. They also conclude that as of the end of 2013 that Jakobshavn Isbræ has retreated to a local topographic high, we interpret this as a possible grounding line location, especially as they stress that there is a very small floating tongue.

As discussed above, it is unavoidable to have gaps in the time-series of velocity fields and as a result the mean is influenced more by times where we have observations. This is partly compensated by weighting the mean, as explained above. However, to estimate the potential seasonal bias in the flux we adopt the following scheme: at all glaciers except one (Petermann) our observations composing the mean are primarily spring/summer (fast) velocities. Therefore we can make an estimate of the seasonal bias in the flux by filling missing time-periods with our minimum velocity data for each glacier. For Petermann where we mostly have winter (slow) velocities comprising the mean we fill the missing time-periods with our maximum velocity. We use this method because according to observations (Moon et al., 2014; Joughin et al., 2014) we most likely capture both the maximum and minimum flow speeds at all glaciers in the study. Once the data is filled we recompute the mean velocity field, and rerun the flux calculation. We report the seasonal bias as the difference between the original flux and this new estimate (Table 1). In all cases except one (Jakobshavn Isbræ) the bias small (Table 1). We attribute the notable flux bias at Jakobshavn Isbræ to the large (40 + %) range in seasonal velocities experienced at the glacier (Joughin et al., 2014; Moon et al., 2014), compared to the relatively low seasonality at the other glaciers in the study.

3 Results and discussion

The velocity fields and flow profiles for the five glaciers are presented in Figs. 1 and 2 respectively. The velocities in the upper catchments for each glacier are very slow, on the order of a few metres per day. As a result longer time intervals between images generate the best results in these slow moving regions. These results give us confidence that ImGRAFT is able to track features over long (> 3 months) time spans, even over winter. The velocity fields presented are a weighted mean of individual velocity fields covering a long time frame from August 2013 (where possible) to September 2014. The velocity time periods are listed in the centreline flow profiles for each glacier in Fig. 2. A full list of all the images used in the study can be found in the Supplement.

The velocity fields and flow profiles display variations spatially and temporally. One interesting feature identified at Jakobshavn Isbræ and clearly visible in the flow profiles (Fig. 2), is the high range of speeds at the terminus compared to all other glaciers in the study. A range of 20 m day^{-1} 4 km upstream of the calving front is clearly visible between two velocity fields one and a half months apart. This rapid change in speed matches the observations of a recent study by Joughin et al. (2014). In our case the averaging periods were 21 and 16 days respectively, therefore no significant bias from a longer observational time interval is expected. For the latter period from 3–19 July at 4 km from the calving front the speed is 19 m day^{-1} above average, whereas the period 9 May–1 June is 2 m day^{-1} below the average at this distance. A recent study by Joughin et al. (2014) presents velocity fields from using TerraSAR-X data for years 2009 to 2013, documenting the rapid retreat of Jakobshavn Isbræ. The authors report the highest known recorded speed of any Greenlandic glacier, approximately 47 m day^{-1} in 2012, and suggest that the recent retreat of the grounding line into a deep (∼ 1300 m) trough is the cause of these high velocities. Our data indicate yet a further speed up of Jakobshavn Isbræ in July 2014 with measured speeds peak-

ing at 52 m day^{-1}. This was manually verified using a simple triangulation of selected features near the terminus, where the high speeds were measured.

Other glaciers investigated here do not exhibit the same range of speeds at the terminus as Jakobshavn Isbræ. Although Helheim and Kangerdlugssuaq glaciers both exhibit some variability at the calving front, neither consistently show such large ranges in speeds. It has been suggested this may be due to the ice mélange that is present for a large part of the year in the Sermilik fjord (Andresen et al., 2011) and Kangerdlugssuag fjord (Sundal et al., 2013). In the case of Petermann and Nioghalvfjerdsbræ the ranges are even smaller, this is most likely a result of the buttressing effect from their ice shelves (Joughin et al., 2010b). All the glaciers presented in this study including Jakobshavn Isbræ (beyond 15 km upstream of the calving front) display only slight seasonal variations.

At Kangerdlugssuaq there is a sharp change in speed of 6 m day^{-1} over a short distance of only 1.5 km, 12 km upstream of the calving front. The start of this transition zone coincides directly with the narrowing of the outlet where the ice from the large catchment is forced into the fjord. This narrowing can be clearly seen on the velocity map in Fig. 1 and in the sharp transition in the flow profile in Fig. 2. Helheim exhibits a similar effect of funnelling ice into the narrow outlet, it is visible as a step change in speed (Fig. 2). This effect is most likely enhanced at Helheim due to the confluence of the two large tributaries merging at 10 km (Fig. 1) from the calving front as they flow into the outlet.

Both Petermann and Nioghalvfjerdsbræ exhibit similar characteristics. They are the widest two glaciers in the study (> 20 km wide) and both terminate in small ice shelves (Joughin et al., 2010b; Münchow et al., 2014). A noticeable observation at Petermann is the distinct separation between the main trunk and the northern marginal slower flow which has been described in Münchow et al. (2014). The large tributary that flows into the main glacier forms a slower flowing part of the glacier tongue. Petermann and Nioghalvfjerdsbræ display highest speeds not at the terminus but at approximately 45 and 70 km from the calving front respectively. The peak in velocity in both cases coin-

cides well with the location of the grounding line where the ice is no longer supported by the bed (Morlighem et al., 2014; Münchow et al., 2014). These glaciers are grounded in troughs that lie below sea level, suggesting that the outlets could increase their flux significantly in a future warming climate (Morlighem et al., 2014).

The flux estimates are presented in Table 1. Throughout, our flux estimates are in accordance with existing estimates, slight discrepancies are ascribed to slight differences in the time frame of data used, method and associated errors, as well as other individual factors such as the exact location of the flux gate. The current flux at the grounding line for Jakobshavn Isbræ is estimated to be approximately 30 $km^3 yr^{-1}$. This matches well with existing estimates by Howat et al. (2011), although Joughin et al. (2014) suggest that a tenfold increase in this estimate in the future is plausible. Helheim and Kangerdlugssuaq experienced their highest recorded fluxes in 2006 and 2005, respectively (Howat et al., 2011). Since then the flux has decreased which is also mirrored in the decline in speed near the terminus of both glaciers (Bevan et al., 2012). It took Helheim less than two years to return to pre-speed up flux (Howat et al., 2011; Bevan et al., 2012), and our results also support that ice flux values have returned to that of pre-speed up estimates. In contrast it has taken Kangerdlugssuaq nearly a decade to return to pre-speed up flux following the speed-up event, but we now find similar flux values to pre-speed up estimates. Although the range in flux was slightly higher at Kangerdlugssuaq compared to Helheim the variations were on the same order of magnitude, thus highlighting the different response times of each glacier. The flux estimates for both Petermann and Nioghalvfjerdsbræ match existing results from studies by Münchow et al. (2014) and Rignot et al. (2001). It is conceivable that the ice fluxes for Petermann and Nioghalvfjerdsbræ are likely to increase if thinning continues, allowing the grounding line to retreat in land. This is also a likely scenario for Jakobshavn Isbræ which lies in a deep trough 1300 m below sea level (Joughin et al., 2014).

4 Conclusions

This study provides the latest 2014 velocity maps and flux estimates for five major Greenland outlet glaciers, and presents the first extensive results using the ImGRAFT feature tracking toolbox on satellite imagery. Our results match those of previous studies covering similar time-frames, locations and scales. A significant finding of this study is that Jakobshavn Isbræ shows little sign of slowing down, with speeds exceeding 50 $m\,day^{-1}$ registered during July 2014, further increasing the previous upper limit recorded in 2012 (Joughin et al., 2014). Both Helheim and Kangerdlugssuaq have now returned to pre-speed up ice fluxes, following a peak in ice flux in 2006 and 2005 respectively. In the north we note little variability in speeds at Petermann and Nigohalvfjerdsbræ, however these two glaciers are also currently supported at their terminus by small ice shelves. Recent studies that have resolved the bed topography in detail have exposed two deep and long troughs extending far into the interior of the ice sheet at both these glaciers (Morlighem et al., 2014). This highlights the need for close monitoring of these outlets as they harbour a large potential for future GrIS mass loss.

The Supplement related to this article is available online at doi:10.5194/tcd-8-6235-2014-supplement.

Acknowledgements. This publication is contribution number 49 of the Nordic Centre of Excellence SVALI, Stability and Variations of Arctic Land Ice, funded by the Nordic Top-level Research Initiative (TRI). N. B. Karlsson is supported by European Research Council grant No. 246815 Water Under the Ice. The Centre for Ice and Climate is funded by the Danish National Research Foundation.

References

Andersen, M. L., Larsen, T. B., Nettles, M., Elosegui, P., van As, D., Hamilton, G. S., Stearns, L. A., Davis, J. L., Ahlstrøm, A. P., de Juan, J., Ekström, G., Stenseng, L., Khan, S. A., Forsberg, R., and Dahl-Jensen, D.: Spatial and temporal melt variability at Helheim Glacier, East Greenland, and its effect on ice dynamics, J. Geophys. Res., 115, F04041, doi:10.1029/2010JF001760, 2010. 6236

Andresen, C. S., Straneo, F., Ribergaard, M. H., Bjørk, A. A., Andersen, T. J., Kuijpers, A., Nørgaard-Pedersen, N., Kjær, K. H., Schjøth, F., Weckström, K., and Ahlstrøm, A. P.: Rapid response of Helheim Glacier in Greenland to climate variability over the past century, Nat. Geosci., 5, 37–41, doi:10.1038/ngeo1349, 2011. 6242

Bevan, S. L., Luckman, A. J., and Murray, T.: Glacier dynamics over the last quarter of a century at Helheim, Kangerdlugssuaq and 14 other major Greenland outlet glaciers, The Cryosphere, 6, 923–937, doi:10.5194/tc-6-923-2012, 2012. 6236, 6237, 6243, 6248

Enderlin, E. M. and Howat, I. M.: Submarine melt rate estimates for floating termini of Greenland outlet glaciers (2000–2010), J. Glaciol., 59, 67–75, doi:10.3189/2013JoG12J049, 2013. 6239

Holland, D. M., Thomas, R. H., de Young, B., Ribergaard, M. H., and Lyberth, B.: Acceleration of Jakobshavn Isbræ triggered by warm subsurface ocean waters, Nat. Geosci., 1, 659–664, doi:10.1038/ngeo316, 2008. 6236

Howat, I. M., Ahn, Y., Joughin, I., van den Broeke, M. R., Lenaerts, J. T. M., and Smith, B.: Mass balance of Greenland's three largest outlet glaciers, 2000–2010, Geophys. Res. Lett., 38, L12501, doi:10.1029/2011GL047565, 2011. 6236, 6237, 6243

Joughin, I., Smith, B., Howat, I., and Scambos, T.: MEaSUREs Greenland Ice Velocity: Selected Glacier Site Velocity Maps from InSAR, Tech. rep., National Snow and Ice Data Center, Digital media, Boulder, Colorado, USA, doi:10.5067/MEASURES/CRYOSPHERE/nsidc-0481.001, 2010a. 6238

Joughin, I., Smith, B. E., Howat, I. M., Scambos, T., and Moon, T.: Greenland flow variability from ice-sheet-wide velocity mapping, J. Glaciol., 56, 415–430, doi:10.3189/002214310792447734, 2010b. 6237, 6242, 6250

Joughin, I., Smith, B. E., Howat, I. M., Floricioiu, D., Alley, R. B., Truffer, M., and Fahnestock, M.: Seasonal to decadal scale variations in the surface velocity of Jakobshavn Isbræ, Greenland: observation and model-based analysis, J. Geophys. Res., 117, F02030, doi:10.1029/2011JF002110, 2012. 6236, 6237

Joughin, I., Smith, B. E., Shean, D. E., and Floricioiu, D.: Brief Communication: Further summer speedup of Jakobshavn Isbræ, The Cryosphere, 8, 209–214, doi:10.5194/tc-8-209-2014, 2014. 6236, 6240, 6241, 6243, 6244

Khan, S. A., Kjær, K. H., Bevis, M., Bamber, J. L., Wahr, J., Kjeldsen, K. K., Bjørk, A. A., Korsgaard, N. J., Stearns, L. A., van den Broeke, M. R., Liu, L., Larsen, N. K., and Muresan, I. S.: Sustained mass loss of the northeast Greenland ice sheet triggered by regional warming, Nat. Clim. Change, 4, 292–299, doi:10.1038/nclimate2161, 2014. 6237

Messerli, A. and Grinsted, A.: Image GeoRectification And Feature Tracking toolbox: ImGRAFT, Geosci. Instrum. Method. Data Syst. Discuss., 4, 491–513, doi:10.5194/gid-4-491-2014, 2014. 6237, 6238

Moon, T., Joughin, I., Smith, B., and Howat, I.: 21st-century evolution of Greenland outlet glacier velocities, Science, 336, 576–578, doi:10.1126/science.1219985, 2012. 6236

Moon, T., Joughin, I., Smith, B., van den Broeke, M. R., van de Berg, W. J., Noël, B., and Usher, M.: Distinct patterns of seasonal Greenland glacier velocity, Geophys. Res. Lett., 41, 7209–7216, doi:10.1002/2014GL061836, 2014. 6240

Morlighem, M., Rignot, E., Mouginot, J., Seroussi, H., and Larour, E.: Deeply incised submarine glacial valleys beneath the Greenland ice sheet, Nat. Geosci., 7, 418–422, doi:10.1038/ngeo2167, 2014. 6243, 6244

Münchow, A., Padman, L., and Fricker, H. A.: Interannual changes of the floating ice shelf of Petermann Gletscher, North Greenland, from 2000 to 2012, J. Glaciol., 60, 489–499, doi:10.3189/2014JoG13J135, 2014. 6242, 6243

Nick, F. M., Vieli, A., Howat, I. M., and Joughin, I.: Large-scale changes in Greenland outlet glacier dynamics triggered at the terminus, Nat. Geosci., 2, 110–114, doi:10.1038/ngeo394, 2009. 6236

Rignot, E. J. and Steffen, K.: Channelized bottom melting and stability of floating ice shelves, Geophys. Res. Lett., 35, L02503, doi:10.1029/2007GL031765, 2008. 6240

Rignot, E. J., Gogineni, S. P., Krabill, W. B., and Ekholm, S.: North and northeast Greenland ice discharge from satellite radar interferometry, Science, 276, 934–937, doi:10.1126/science.276.5314.934, 1997. 6239

Rignot, E. J., Gogineni, S., Joughin, I., and Krabill, W.: Contribution to the glaciology of northern Greenland from satellite radar interferometry, J. Geophys. Res., 106, 34007–34019, doi:10.1029/2001JD900071, 2001. 6243

Rignot, E. J., Mouginot, J., and Scheuchl, B.: Ice flow of the Antarctic ice sheet, Science, 333, 1427–1430, doi:10.1126/science.1208336, 2011. 6236

Sundal, A. V., Shepherd, A., Van Den Broeke, M., Van Angelen, J., Gourmelen, N., and Park, J.: Controls on short-term variations in Greenland glacier dynamics, J. Glaciol., 59, 883–892, doi:10.3189/2013JoG13J019, 2013. 6242

Table 1. Flux estimates for each of the glaciers from the mean velocity fields (see Fig. 1 for flux gate location). A conservative estimate of the seasonal bias in the flux is listed in the "bias" column in the table. A positive/negative bias indicates an over/under estimation of the flux. The dominant source of error in the flux gate values arise from the uncertainty in the thickness profile along the gate which we estimate to be on the order of 15 %.The drainage area is in percent of the entire GrIS area based on Bevan et al. (2012) estimates.

Glacier Name	Flux Estimate ($km^3\,yr^{-1}$)	Bias ($km^3\,yr^{-1}$)	No. of days covered by obs.	Drainage area (%)
Petermann	7.3	+0.28	303	4.2
Nioghalvfjerdsbræ	10.0	−1.36	126	3.8
Kangerdlugssuaq	17.42	−0.07	217	2.9
Helheim	26.78	+0.56	176	3.0
Jakobshavn Isbræ	29.8	+6	199	5.1

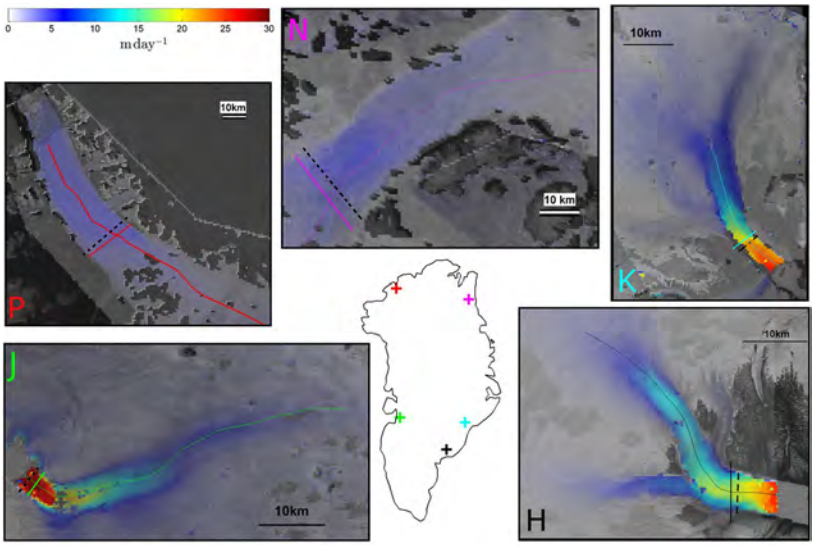

Figure 1. Mean velocity fields for each of the glaciers presented in this study: J = Jakobshavn Isbræ, P = Petermann, N = Nioghalvfjerdsbræ, K = Kangerdlugssuaq and H = Helheim. The dates of the individual velocity fields used to compose this average are listed in the supplementary material. The approximate grounding line location for each glacier is marked as a black dashed line on each velocity field.

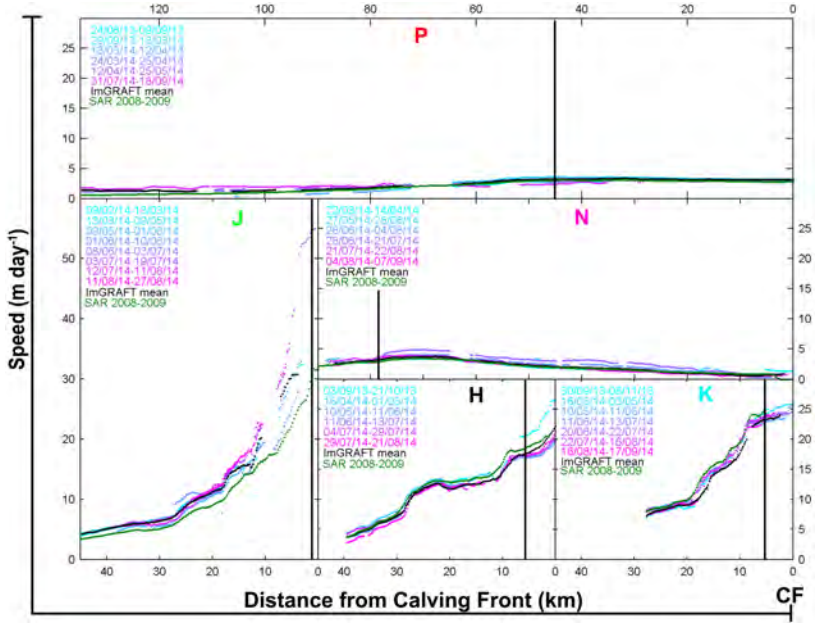

Figure 2. Centreline flowline profiles for each glacier for the range of dates listed. The ImGRAFT mean (black dots) is comprised of the velocity fields for the dates listed, however in the case of Jakobshavn, Kangerdlugssuaq and Helheim additional velocity fields are also used to estimate the mean. The SAR velocities for 2008–2009 (green dots) are from Joughin et al. (2010b). The black vertical bars represent each estimated grounding line location. Note the different *y* axis for Jakobshavn Isbræ.

Chapter 4

Geomorphological evidence at Engabreen

This chapter presents a large of variety of geomorphological data and observations that provide direct evidence of former and contemporary subglacial drainage configurations under Engabreen. Particular attention is given to erosional and depositional fluvioglacial landforms. The collated geomorphological observations, are used to identify and explain the causality between drainage mechanisms and surface velocity, that are observed in chapter 5.
In the following sections three main lines of evidence are presented that reveal the drainage configuration both past and present from both an overview and detailed perspective. The observations are presented in three main figures (4.1, 4.2 and 4.3). The large overview figures present the lower basin of Engabreen where freshly exposed bedrock reveal distinct glacio-hydrological features that provide direct evidence for various drainage mechanisms and associated ice-bedrock, ice-water processes. It should be noted, that the majority of the interpretation is concentrated on the lower (past the bend) catchment of Engabreen as there is evidence for a slightly different hydrological network in the upper region of Engabreen and around the SSL.

4.1 Introduction to geomorphology

As stated by numerous studies, recently deglaciated margins provide some of the most compelling evidence for the likely structure of the former and current drainage configurations and understanding the nature of the bed beneath hard-bedded glacier is especially important in understanding the process of basal sliding in relation to hydrological conditions (Iken et al., 1995). Large bodies of literature that aim to asses and understand the drainage of water beneath a glacier do so using model simulations and indirect observations to quantify and theorise the flow of water and the complex dynamical interaction between the water, local topography and the overlying ice. In doing so they are forced to use a number of simplification of the systems. This is not to say that simulations do not significantly assist our explanations of these deeply complex systems, but rather that they cannot and do not replace the need for continued observations, using a suite of interdisciplinary methods to do so. This thesis and indeed this chapter, aims to highlight the usefulness and importance of a diverse multi-method approach.

Nye-channels

Nye-Channels are channels that are incised down into the bedrock, unlike R-channels that are incised upwards into the ice (Benn and Evans, 2010). These channels form part of a drainage system that is often referred to as a channelised system. Channelised drainage as its name suggests is efficient at routing water at the base of the ice. Two key sites display a dense network of formerly active Nye-channels; the most famous of which is Glacier de Tsanfleuron, Switzerland (Sharp et al., 1989, 1990; Hubbard et al., 1998) and secondly Blackfoot Glacier Montana, USA (Walder and Hallet, 1979). Both of the aforementioned examples are glaciers underlain by a karst, limestone hard bed. In both these examples the flow of subglacial water has exploited lines of weakness in the bedrock and eroded its own pathways into the bedrock, which in-turn promotes seasonal meltwater to be routed in these existing channels, further erodes and incising deeper into the bedrock through the turbulent flow of water. At Tsanfleuron both channels and "orifices" are referred to as Nye-channels. Generally their preferred alignment at Tsanfleuron is sub-parallel.

Cavities

Cavities generally tend to form in the lee side of obstacles and undulations in the bed, and are often linked by channel like structures called orifices (Kamb, 1987; Cohen et al., 1968; Fowler, 1987). Cavities provide a space in which water can exist both as an isolated body or water or in connection through orifices (or as described above Nye-channels) to the main drainage system. The presence of a cavity system also been linked to unique glacial phenomenons such as glacial surges (Kamb, 1987; Sharp et al., 1989; Walder and Hallet, 1979). As with any drainage type, one of the most interesting and studied relationships is the that of drainage configuration and associated ice flow variations. The cavity or linked-cavity system is generally thought to dominate drainage and storage of water during the winter months, where it forms a spatially distributed and inefficient drainage system, that develops as a direct result of an almost complete cessation of meltwater input to the base.

Calcite deposits

Calcite is carbonate precipitate that often has a light grey colour and is predominantly found in association with bedrock bumps and cavities. Calcite is considered a key indicator of the regelation process. Regelation is the process by which ice can flow over and around bedrock perturbations, where high pressure on the upstream, stoss side of the pump decrease the pressure melting point and allows for a thin film of water to develop between the ice and the bedrock. As the water flows over (or around) the bedrock bump to the relatively low pressure lee side of the bump downstream, the pressure drops, increases the melting point and the water freezes again (Hubbard et al., 1998; Ng and Hallet, 2002). At this point where the water film refreezes a layer of calcite may be deposited on the area just beyond the crest of the bedrock bump, as a result of calcite saturation in the water film (Yde et al., 2012). These calcite deposits often display a streamline, fluted appearance which is aligned with the dominant flow direction of the ice (Ng and Hallet, 2002). This characteristic highlights that the thin water film is extremely thin (micro-meter scale) and is a process where the ice is in close contact with the bed (Hubbard et al., 1998; Ng and Hallet, 2002). It is

particularly common at sites where the glacier has a hard bed and the bedrock has a considerable limestone content (Sharp et al., 1990; Hubbard et al., 1998). Calcite deposits have been extensively studied at Glacier de Tsanfleuron, Switzerland (Sharp et al., 1989, 1990; Hubbard et al., 1998) and at Blackfoot Glacier, U.S.A. (Walder and Hallet, 1979). Calcite deposits can also form in cavities where that is a refreezing process or CO^2 degassing mechanism occur on $CaCO_3$ rich subglacial water (Ng and Hallet, 2002; Hubbard et al., 1998). The deposition of calcite in the base of cavities can be an indication of stagnant water, for example isolated cavities during the winter, where $CaCO_3$ rich waters freeze in the cavity and the calcite precipitates out of solution to form a layer of calcite. These deposits in base of depressions often do not bare the markings of the former ice flow direction as they are not an indication of an intimate ice contact process unlike regelation based calcite deposits.

4.2 Observations at Engabreen

The geomorphological data from Engabreen is presented in two forms; a series of themed geomorphological maps, and photographic evidence of the discussed features. The following list provides a short overview of the contents of each other three key figures. Each of the figures are referred to continuously throughout the chapter, in which the text directly relates to features highlighted in the figures. The first two figures provide a broad, annotated overview from LiDAR data from 2013 and high resolution satellite imagery[1] from 2013 and 2001, to provide an aerial perspective of the exposed bedrock. The third and final figure presents detailed imagery of the key features located and identified with a unique id in the previous two figures.

- The first Figure 4.1 is a large overview map that highlights a dense, extensive network of Nye-channels in the bedrock which are discussed in detail. The figure is annotated with id's of most of the features presented in Figures 4.2 and 4.3
- The second Figure 4.2 presents two perspectives of the former 2001 and the current exposed bedrock, using an overlay. This allows potential former drainage pathways to be "seen" through the overlay (A). Hydrological pathways are discussed in relation to clearly visibly flowing water in 2001 and 2013. Note that this figure is split over two pages into part A overlay and part B.
- The third Figure 4.3, is a series of close up images taken from the ground. Each of these images refers to a defined feature annotated with a unique id in the previous two Figures.

[1] Imagery from Norge i bilder, available from http://www.norgeibilder.no/

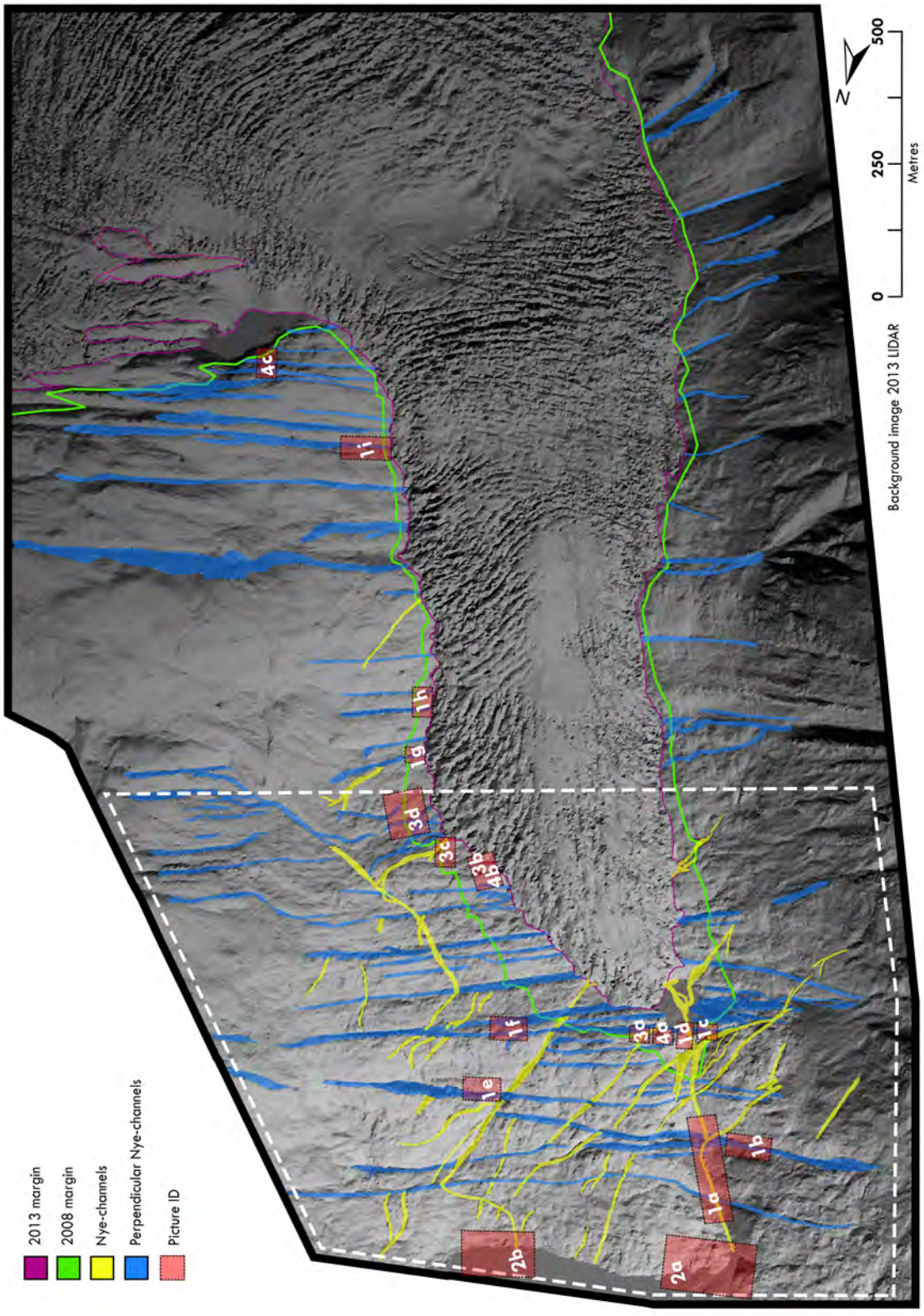

Figure 4.1: *An overview map of the geomorphological features at Engabreen. Key features include Nye-channels and locations of small scale features such as cavities and calcite deposits. The white dashed line indicates the area in focus in Figure 4.2. See insert for a larger version of the figure.*

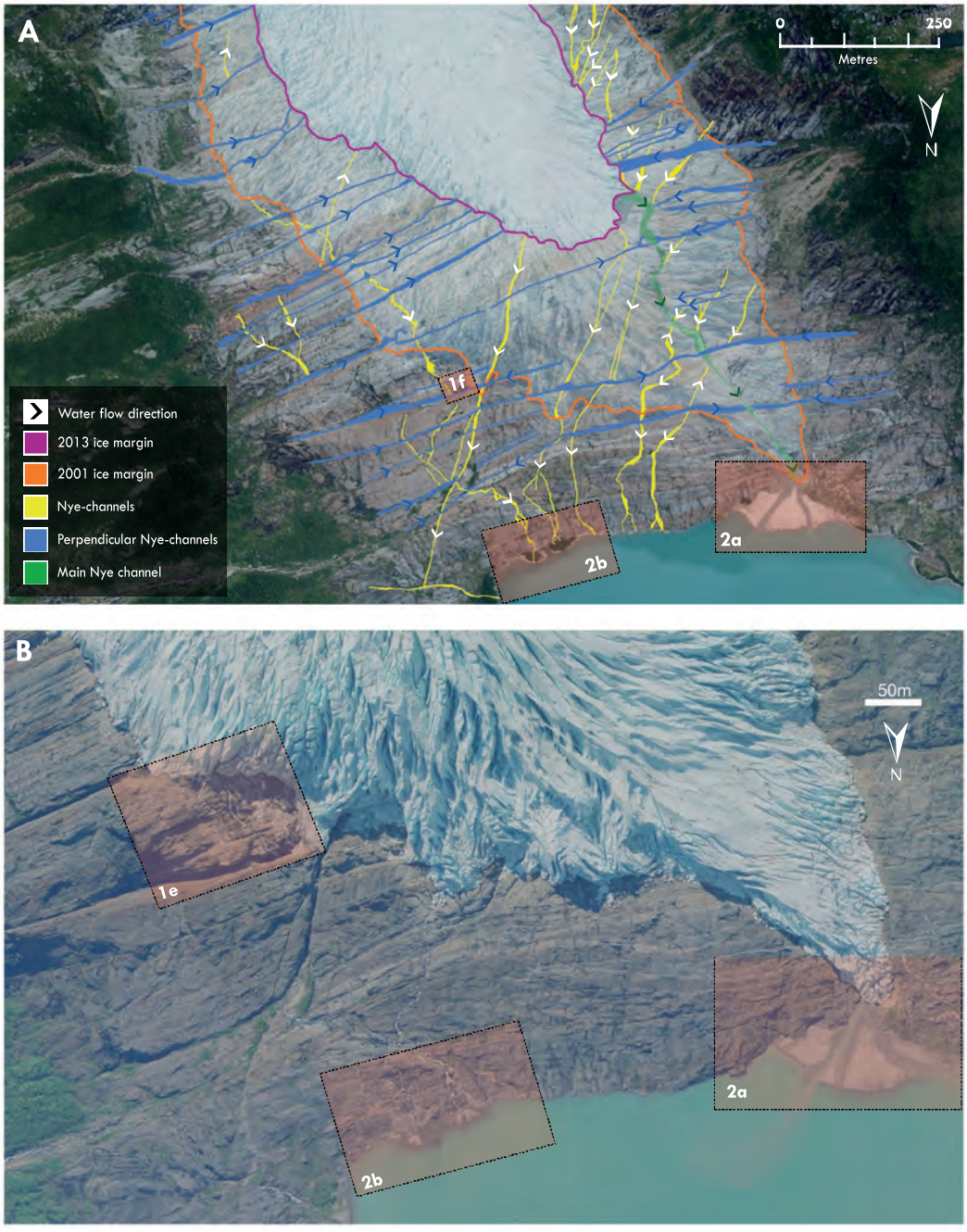

Figure 4.2. *A, is an overlay of the former 2001 ice extend on a background image from 2013, in order to "view" the former subglacial draining system. B, shows the ice extend in 2001, where additional proglacial streams are visible. Note the waterflow over the bedrock in 1e, which is captured by the large Nye-channel. The two smaller deltas in 2b, appear active in 2001, with no vegetation growth.*

Figure 4.2: *A, is an overlay of the former 2001 ice extent on an image from 2013, in order to "view" the former subglacial drainage system. B, shows the ice extent in 2001, where additional proglacial streams are visible. Note the water flow over the bedrock in 1e, which is captured by the large Nye-channel. The two smaller deltas (2b) appear active in 2001, with no vegetation growth. See insert for a larger version of the figure.*

Nye-Channels: active and relic

1a

1a

The deeply incised former subglacial channel. The is now the channel of the proglacial river Engabreelv. Note the deeply incised Nye channel. It is anticipated that a similar centralised channel exists under the lower tongue of Engabreen today.

1b

1c

Examples of perpendicular feeder Nye-channels that route water into the proglacial Nye-channel. These features are abundant and large (note person for scale in 1c). These would have previously funnelled water under the ice from the margins, where it joined the subglacial drainage network.

Nye-Channels: active and relic

1d

A very deeply incised channel at the head of the proglacial river. The height of the waterfall is over 5m.

1e

A clear steep area of the bedrock that is likely to drain water through the visible cavity-like structures into the deep perpendicular Nye-channel. This water could then be transported back under the ice and into the subglacial drainage network. An example of this process taking place in 2001 is visible in plot B Figure 5.2.

1f

1g

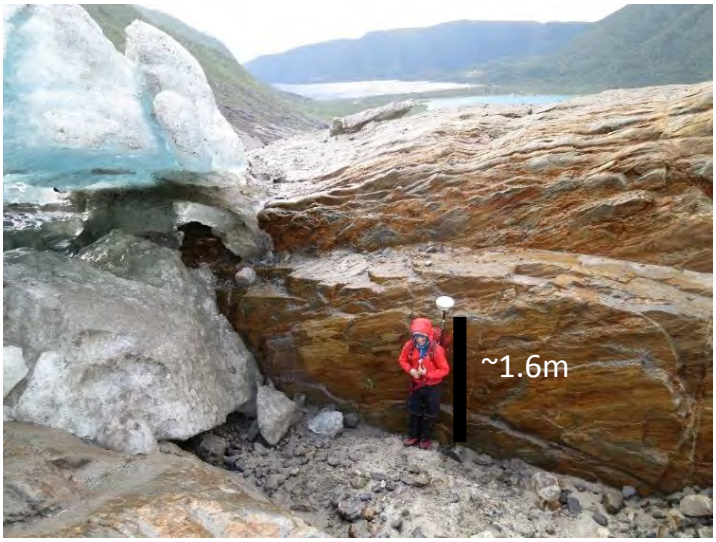

Two examples of perpendicular deep and wide Nye-channels. Both of these example indicate stream beds with rounded clasts and sediments in the base of the channels. Example 1g, is still active today during the snow melt season and high rain events.

Nye Channels: active and relic

1h

1h

Two clearly active smaller perpendicular, feeder Nye-channels currently routing small streams from the valley sides under the current glacial margin. The capacity of these streams increases significantly during high precipitation events .

1i

Nye channel through which the artificial Jökulhlaup is flushed. This perspective shows the clear perpendicular alignment of the channel. Ice flow is from left to right. Most water is now extracted from this channel further upstream, however a small stream still remains.

1i

The view of the entrance to the same Nye-channel as in the image to the left. This image was taken shortly after the 2013 flushing. The height of the entrance to the channel is approximately 5 to 7 metres at in the centre. Photo: P-M. Lefeuvre

Deltas: active and relic

2a in 2001

Dominant delta is very active in 2001 with no signs of vegetation. Low ice front suggests some meltwater overflow on bedrock onto delta.

2a in 2013

Similar high streamflow and activity. Ice margin retreated and some small vegetation has grown where the meltwater overflow on the bedrock has ceased.

2b in 2001

Dominant delta active in 2001. No vegetation visible and high streamflow into lake.

2b in 2013

Significant changes in the appearance of the deltas. Somewhat reduced streamflow and extensive growth of vegetation. The vegetation growth is indicative of a reduction in hydrological activity at the deltas.

Cavities

3a

A scalloped cavity in the lee of a large bed undulation. The arrow indicated former ice flow direction.

3b

A large cavity on the margin of Engabreen, where the ice flows over a steep bedrock. Note the person for scale (red circle).

3b

Evidence for fluvial processes can be seen including scalloping and channel erosion in the bedrock, indicating former water pathways.

3b

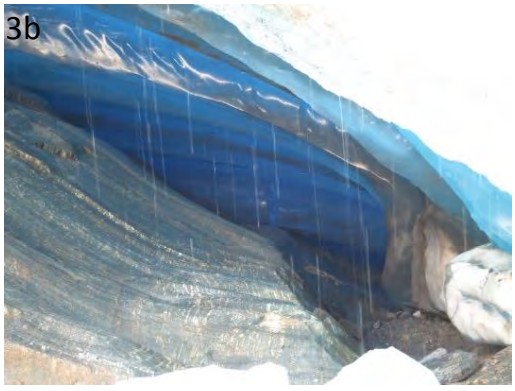

A closer look inside the cavity, with indications of fluvially enhanced flowpathways. Note the stress bridging of the ice downstream of the cavity.

3c

A former subglacial cavity exposed and now water filled, surrounded by glacially scoured bedrock. Note the very little amount of till present.

3d

Examples of glacially scoured and striated bedrock incised with fluvially eroded channels and cavities. Again very little amounts of till are visible on the bedrock.

Calcite precipitates

4a

4a

4a

4a

Calcite deposits near the terminus. Note the flutes which have formed aligned with the dominant flow direction, also visible in the striations on the bedrock bump. The arrow indicate flow direction of the ice. All these images are of the lee side of the bedrock bumps.

4a

An more unusual calcite deposit at the terminus of Engabreen where the calcite has been deposited on the top and sides of the bed rock bump. This image was taken perpendicular to the bedrock bump with clear signs of glacial and fluvioglacial erosion.

Calcite precipitates

4b

The thickest calcite deposit found near the large cavity (3b). It appears to have formed on a different rock type compared to all the other calcite examples. Its light colour and more chalky texture is suggestive of a high carbonate content.

4c

4c

Other calcite deposits found by the ice marginal lake in the bend of Engabreen. These deposits have a less streamlined orientation and are found in a range of localised environments, including small hollows as the image on the right indicates.

As can be seen in the figures in this chapter, the bed at Engabreen is far from a uniform flat surface. Instead there is a complex, spatially heterogeneous, mix of flat and undulating zones at a range of scales, many of which are a direct result of the geology at Engabreen. This section presents numerous lines of evidence for a dense Nye-channel network, cavities and calcite deposits at Engabreen

Figure 4.1, highlights the dominant Nye-channel alignment, which is perpendicular (blue channels) to the direction of ice flow, with the exception of the main centralised channel (exposed in proglacial channel) and some exploited lines of weakness in the geology (yellow lines). The Nye-channels at Engabreen have a very clearly geologically controlled geometry where there are distinct cross-cutting channels. The are a number of observations to suggest that these channels extend under the current ice and connect to visible channels on the other side of the glacier.

Additional image overlays in Figure 4.2 show the former ice extent in 2001 which covered these directly, Nye-channels that captured water flowing from the glacier (id 1) and local streams confined to perpendicular exposed channels. The corresponding image id's in Figure 4.3 provide and estimate of the size of the channels and their overall capacity to accumulate and drain water. These channels have and do route water directly from the marginal area into what is hypothesised to be a major, centralised Nye-channel. Clear evidence for this is seen in the overlay figure where the former drainage pathway is highlighted.

The 2001 margin as annotated in Figure 4.2 provides yet further indications of a dominant centralised subglacial channel, where the largest visible discharge appears to be from the channel producing the largest glaciofluvial delta (id 2a). During 2001 it water is visibly flowing from both the main and subsidiary channels as the proglacial meltwater pathways suggest. The water exists the glacier and flows along the bedrock before entering a large exposed perpendicular Nye-channel (id 1e) and flows into a sub-parallel prominent Nye-channel that routes the water to to proglacial lake. It is proposed that this drainage pathway was similar to the current proglacial channel. Evidence for this is seen in the shift in observed activity in each channel terminus between 2001 and 2013.

Both images in Figure 4.2 show varying levels of activity. In 2001 the smaller proglacial delta and the large dominant delta are active, however since 2001 significant amounts of vegetation have grown on the two smaller deltas (id 2b), unlike the dominant delta. This indicates that as the glacier retreats the dominance of the central flow pathway appears to increase. The channel which now exists as a deeply incised canyon provides firm evidence for a geologically controlled and glaciologically enhanced drainage network. This is particularly true in this lower region of the glacier from the sharp corner to the lake (see annotation on Figure 4.1). The hypothesis proposed in this thesis is, that the lateral, perpendicular feeder Nye-channels (id 1d,1c) funnel water into a central Nye-channel, similar to the one that is now exposed at the terminus. The main proglacial Nye-channel provides the foremost evidence for, as indicated in Figure 4.2 and the associated id (1a) 4.3, the bulk water routing under Engabreen in the past. Id's 1h,i, and 1a,b, which show both active and relic feeder Nye-channels that suggest water is being routed into the glacier subglacial drainage system from the margins, where is joins the main subglacial drainage pathway and re-emerges through the

centralised channel at the terminus. The hydropotential map in (Figure 5.8) further supports this hypothesis of a main centralised channel, where hydropotential-gradient is an indication of the flow direction of the water.

An undulating bed is often indicative of the presence of cavities, and together form an important aspect of the drainage configuration at many glaciers. There are numerous locations (id 3) around the margin of Engabreen that appear to be a dense network of linked cavities. In some places the cavities are extremely large as the one found at the current ice margin (id 3b). This large cavity has a similar shape to the step nature cavities by (Kamb, 1987). Whilst this is an extreme example it also reflects back to the Nye-channel evidence that has the potential in places to provide an extensive orifice network linking multiple cavity locations together. The bedrock at Engabreen displays both small undulating cavities (id 3c,d) and large step-like cavity networks, where meltwater erosional features such as scalloping are clearly observed (id 3a,b). Discontinuous striations over depressions offer yet further evidence for a spatially extensive network of cavities. Ice looses contact with the bed when flowing over the depression and this any abrasion ceases until contact is made with the bed at the next bedrock high. Today many of the exposed isolated cavities remain water filled after rain events (id 3c) that provide an overview of their location.

Previous studies at Engabreen have provided evidence for a linked-cavity system around the SSL (Lappegard and Kohler, 2005; Lappegard et al., 2006). They used pump tests in boreholes to assess the connectivity between different boreholes using pressure transducers. During the winter many of the boreholes and load cells connected in response to the artificial pressurisation of an individual borehole. They found, that during the winter months a high pressure, low discharge drainage system dominated and conversely during summer experiments a channelised low pressure system dominated. This is consistent with the observations and evidence presented in chapter (5).

Other features visible on the bedrock, indicate intricate, process-based features. For example, the calcite deposits at Engabreen are a clear indication of the regelation process. Id(4a,b,c) provide clear examples of calcite deposits, with a streamline appearance. The calcite deposits found near the terminus of Engabreen (id 4a) are often accompanied by striations in the bedrock. The calcite deposits shown in id 4a are on the order of a few centimetres in width and tens of centimetres in length and run along the lee side of the crest. One example of calcite deposits on the vertical edge of a bedrock bump can be seen in id 4a. The calcite deposits are an indication of a thin water film existing at the bed of Engabreen. Lappegard et al. (2006) also presented observations that confirm the presence of a thin water film at the base of Engabreen from the correlation between loadcells. The geomorphological evidence presented here confirms the findings by Lappegard et al. (2006). One interesting observation is that the local geology at Engabreen is not limestone based, but rather gneiss. Therefore, there is a limited supply of carbonate with which to form the calcite deposits. The limited supply of carbonate, is reflected in the limited number of calcite observations.

4.3 Summary

The bedrock at Engabreen provides extensive evidence for numerous, distinct landforms. Many of these indicate the former flowpath of subglacial meltwater. The most unique feature at Engabreen is extensive network of cross-cutting Nye-channels. It is evident that they both capture and deliver large volumes of water into the subglacial drainage system. The retreating margin has revealed a large number of structures since 2001, that suggest they are also a contemporary facet of the subglacial environment. These include a dense cavity network that ranges in size from a few tens of centimetre many metres. The comprehensive geomorphological evidence presented in this chapter provides a complete structural overview of the subglacial drainage. This knowledge of the drainage configuration facilitates the interpretation of dynamic responses to changes in the input of subglacial meltwater observed in the time-series analysis in chapter 5. A complete discussion of the influence of these geomorphological features on the dynamics at Engabreen are presented in chapter 6.

Chapter 5

Hydrology and Dynamics at Engabreen

This chapter focuses on the assessment of two major components of the work carried out at Engabreen; the hydrological network and the surface velocity measurements.

5.1 Background and Motivation

Aside from the Engabreen and the SSL literature, a vast catalogue of glacio-hydrological literature exists (e.g., Hubbard and Nienow, 1997; Nienow et al., 1998), that has strived to reveal the effect of meltwater on ice flow. Much of this literature focuses on the glacier Haut glacier d'Arolla in the swiss Alps, where numerous studies exist (Mair et al., 2001, 2003; Nienow et al., 1998). Another glacier in the Swiss Alps, glacier d'Tsanfleuron was also a site of detailed investigations due to its well preserved and accessible previously active karst subglacial drainage system (Sharp et al., 1989, 1990; Hubbard et al., 1998). In recent years the focus has been on the larger ice mass of Greenland and how this will affect the draw-down of the inland ice to the margin and eventually the flux into the ocean Zwally et al. (2002); Bartholomew et al. (2010); Cowton et al. (2013); Das et al. (2008)

The hydrological monitoring network is very well maintained at Engabreen as a result of the importance for the functional operation of the Svartisen hydropower plant. As mentioned in chapter 2, numerous subglacial and proglacial discharge stations exist at Engabreen, with a long time-series of data. However, the same cannot be said for the surface measurements, which are often far and few between with short, isolated measurement campaigns, often providing only a few days of point measurements (Christianson, 2012). Looking back into the limited surface velocity literature and reports almost no continued time series of surface velocity measurements exists, with the exception of (Kohler, 1998). One aim of this thesis was to obtain a longer time-series that would improve on the existing surface measurements and offer a practical solution for achieving a long-term surface velocity record in the future.
The aim of the longer surface velocity time-series was in order to complement the long-term subglacial and discharge datasets, with the aim of investigating the complex interaction between the hydrological network and ice flow at Engabreen. Particular emphasis is placed upon short-term speed-up events (i.e. spring speed-up events and rainfall/melt events). The unique combination of the SSL and the surface measure-

ments offers an ideal site to study the interaction of water and ice flow from two perspectives; the surface and the subglacial environment. Currently a far larger body of work exists from the laboratory (Lappegard and Kohler, 2005; Lappegard et al., 2006; Cohen et al., 2000; Iverson et al., 2007) to name a few. The most recent of studies at the SSL (Lefeuvre et al., 2015) investigates the long time-series of subglacial pressure data. In order to complement the subglacial measurements, a spring/summer surface campaign was carried out (outlined in Chapter 2). The campaigns were focused on the spring/summer season to in order to capture the spring speed-up event and further short-term speed-up events throughout the warmer summer months. In this chapter collated evidence from the datasets presented in chapter 2 are synthesised and analysed in the context of the observed interactions between the hydrological network and ice flow at Engabreen.

5.1.1 Spring-events

Firstly an overall description is provided of how a typical spring-event appears within the time-series datasets at an Alpine style glacier. Spring-events often occur at the beginning of the melt season, and are a phenomenon that are often observed on valley glaciers (Iken et al., 1983; Mair et al., 2003). They are generally observed as an increase in surface velocity in response to the initial connection of surface melt and the bed during the onset of the melt season (Iken et al., 1983; Mair et al., 2001). The characteristics of a spring-event, as observed in meteorological, velocity and discharge datasets show rapid increases in most of these components. Figure 5.1 is a schematic of a typical spring-event expressed in the key aforementioned variables.

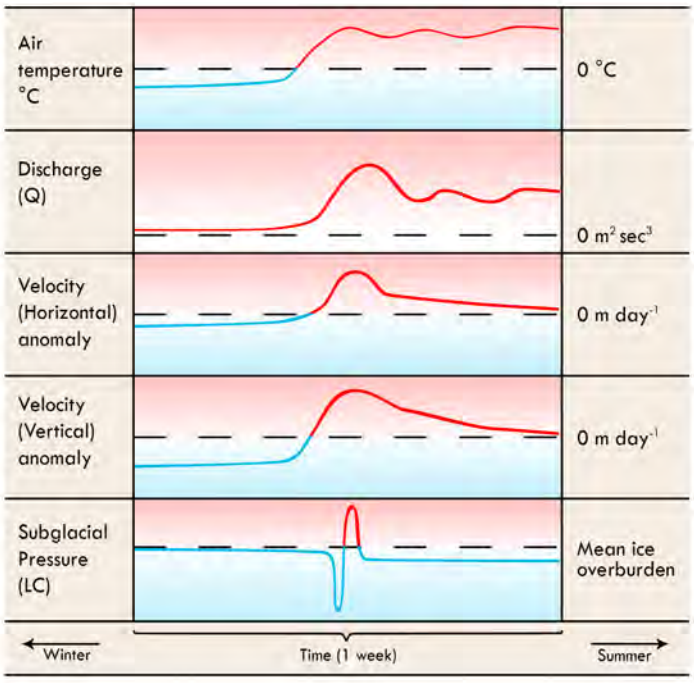

Figure 5.1: *A schematic of a typical spring-event as observed in a variety of time-series data*

Typically the onset of a spring-event can be driven by two forcings; an increase in air temperature to above melting point or, in association with an intense rainfall

event (Mair et al., 2003). In the following example we address a typical temperature induced spring-event. In the days prior to the observation of a spring-event, the local air temperature is likely to exceed $0°C$ for a prolonged time, which in turn initiates the melting process. At this stage the glacier is snow covered and thus the resultant increased melt rate will begin to melt the winter snowpack. The meltwater will percolate through the remaining snowpack, where it eventually reaches the firn layer. Finally the meltwater will reach glacier ice where it can be routed through the ice column to the base of the glacier, and enters the subglacial drainage system. During this process, there is likely to be a lag between the peak in the discharge in response to increasing air temperatures, as the transport of surface melt through snowpack and firn layer can be slow, compared to times where there is no snow on the glacier surface.
The expression of the spring-event becomes apparent in the discharge and the ice velocity after the connection between the surface metlwater and the sublacial environment has been made. The initial routing of water from the surface to the base of the glacier, marks the activation of the subglacial drainage system after the winter, where little or no meltwater has reached the bed. During the first connection the subglacial drainage system is typically in an inefficient configuration that is not yet developed to accommodate the sudden influx of water. This therefore can be interpreted as a flooding or overwhelming of the subglacial drainage system. Iken et al. (1983) attributed the initial spring-event to the pressurisation and storage of water in the winter linked-cavity system, that led to an uplift of the ice surface in response to the over pressurisation of the water at the glacier bed. In response to this, the drainage configuration must reorganise in order to route the inflowing water through the system to the terminus, and in doing so reducing the water pressure. Throughout this reorganisation phase numerous positive and negative feedbacks operate that may both enhance or reduce basal sliding (Hoffman and Price, 2014). One such feedback is the increased sliding and increased cavitation feedback that is positive and negative feedback. Increased sliding, opens more cavity space at the bed of the glacier, which in turn reduces subglacial water pressure and reduces sliding. A small positive feedback is also expected as a result of increased frictional heat production due to higher sliding rates. This in turn increases the softness of the ice and associated creep closure rates, thus allowing for a more rapid closure of the cavities. This increases water pressure that re-initiates the loop. It has been noted that the negative feedback of increased cavitation is the dominant feedback (Hoffman and Price, 2014).

The expression in the horizontal surface velocities, tends to be punctuated by an increase in velocity, where the peak coincides with a rapid pulse increase in discharge at the proglacial stream (Flowers and Clarke, 2002; Mair et al., 2003). There also tends to be a shift in pre-event and post-event background discharge, associated with the passing of a spring-event, where the post-event baseflow in the proglacial stream is elevated compared to that of pre-event base-flow.

Vertical velocities also typically display a characteristic response to the spring-event that sees a sudden uplift of the ice surface up to 0.5m. This has been linked to a direct reflection of the effective pressure (N) conditions at the bed, where effective pressure is mean ice overburden pressure (P_i) minus water pressure (P_w) (Equation 5.1.1). The increase in the subglacial water pressure that exceeds that of the local ice overburden pressure (Iken et al., 1983; Zwally et al., 2002), thereby leading to hydraulic jacking of the ice in response as a result of low effective pressure (Equation 5.1.1).

$$N = P_i - P_w \tag{5.1}$$

The increased uplift is indicative of the decoupling of the ice-bed interface. It should be noted that whilst this presents a characteristic spring-event, the timing and magnitude of the event in the data will vary from site to site. The responses that are measured at the surface for example are highly variable depending on the local conditions, and vary slightly from glacier to glacier. This is a result of the individual drainage configurations that vary between glaciers, i.e. hardbed, or soft unconsolidated bed. The onset of the melt season at valley glaciers may also be punctuated by numerous spring-events, with similar but varying characteristics, in response to different forcing, for example rain events or high melt events (Mair et al., 2003).

5.2 Time-series analysis

In this section we focus in the longest time-series of data collected in 2013 (as outlined in chapter 2). These include GPS data, discharge data, load cell (pressure) data and various meteorological parameters, particularly air temperature. The collection methods are outlined in Chapter 2.
The datasets displayed in Figure 5.2 provide an overview of the focus data of the entire 2013 period. The focus time-period (P1- pink shaded areas in time-series data graphs) is the most complete time series that includes numerous overlapping datasets over a longer time-period from May until the end of July. P1 is split into two key sub-focus time-periods: P1a, and P1b. P1a covers the spring-event and the month of May, the second sub-period, P1b covers the latter end of the GPS time-series which falls in July. The detailed analysis in the following subsections is limited to the periods of available surface velocity data, in particular GPS data. The analysis of the GPS data consists of the two most complete time-series provided by the two Javad GPS, (JB and JL, see overview Figure 2.4). All the time-series data is collated and presented to extract information on the coupling of the hydrological system and the overlying ice. Like any natural system a number of factors influence the response of each component in relation to varying forcings and conditions throughout the melt season. The results in this chapter elucidate key areas for further discussion in relation to the geomorphological evidence described in Chapter 4.

In order to better understand any causal relationships within the datasets, a measure of the relation between each time-series is calculated using wavelet coherence. Following this, a presentation of the datasets are made from the outlined focus periods.

Figure 5.2 shows the entire time series of air temperature and three key discharge stations, two of which are proglacial and one subglacial station. Clear seasonal cycles can be seen in many of the time-series in Figure 5.2, particularly, as expected, in all the discharge data and air temperature. Higher temperatures in spring and summer are visible at both stations, at sea level and at over 1000 m.a.s.l. This is reflected in the variations in discharge at all the gauging stations. The converse response is visible

in the shorter GPS time-series. Where as warmer temperatures and higher discharges persist throughout the summer period, GPS velocities show a gradual seasonal decline, to well below background levels (horizontal, dotted blue lines in subplot 4 of Figure 5.2). Some trends are observed in the precipitation data at both sites, although a clear seasonality is less apparent. However, a period of larger precipitation events is apparent in late autumn, and their frequency remains high during late autumn and winter. Some larger winter and early spring precipitation events are also visible with increased winter temperatures exceeding 0^oC. These large events stand out in the discharge measurements at all the sites. A spring example of one of these events is discussed briefly in section 5.3.1

The fact that discharge increases prior to event P1a indicate other possible spring-events. One particular interesting melt event that could have triggered a spring-event appears late winter at the end of February 2013, where an anomalously warm period was experienced that clearly led to some snow melt. The steep rising limb of the peak in the proglacial lake discharge during this time, suggests that a very early spring-event is conceivable in 2013. This however, is not a common event but in a warming climate it may become more frequent, where winter temperatures at Engabreen exceed 0° for extend periods of time. Further longterm investigation is needed to assess if this is likely to cause an overall increase or decrease of the subsequent annual mean glacier velocities. The reorganisation of the subglacial hydrological system may be initiated earlier as the length of the melt season increases, both at the beginning and the end. The lengthening of the melt season and in this context, the early onset of spring-event activity, could lead to both a positive and negative feedback on ice flow Sundal et al. (2009). However, in the absence of surface GPS data during these other potential spring-event periods at Engabreen in 2013, no detailed discussion of these will be made with respect to changes in ice flow.

No direct measurement of water pressure from boreholes were made at Engabreen in 2013. Nevertheless, based on similar studies(Iken and Bindschadler, 1986; Mair et al., 2003), we assume that the surface expression reflects pulses of high water pressure at the bed of the glacier. The load cell time-series (Figure 5.7) at the SSL record the basal pressure around the SSL and their signal shows clear pressure events, where the subglacial pressure exceeds that of mean local ice overburden pressure. Often these disturbances are in relation to water pulses. We interpret this as an indirect measure of the "pressure" in the subglacial drainage system (Lefeuvre et al., 2015; Lappegard and Kohler, 2005; Lappegard et al., 2006). Using this as an indicator for disturbances in the subglacial system we observe how this event is expressed in the other geophysical time-series of discharge and velocity in the following section.

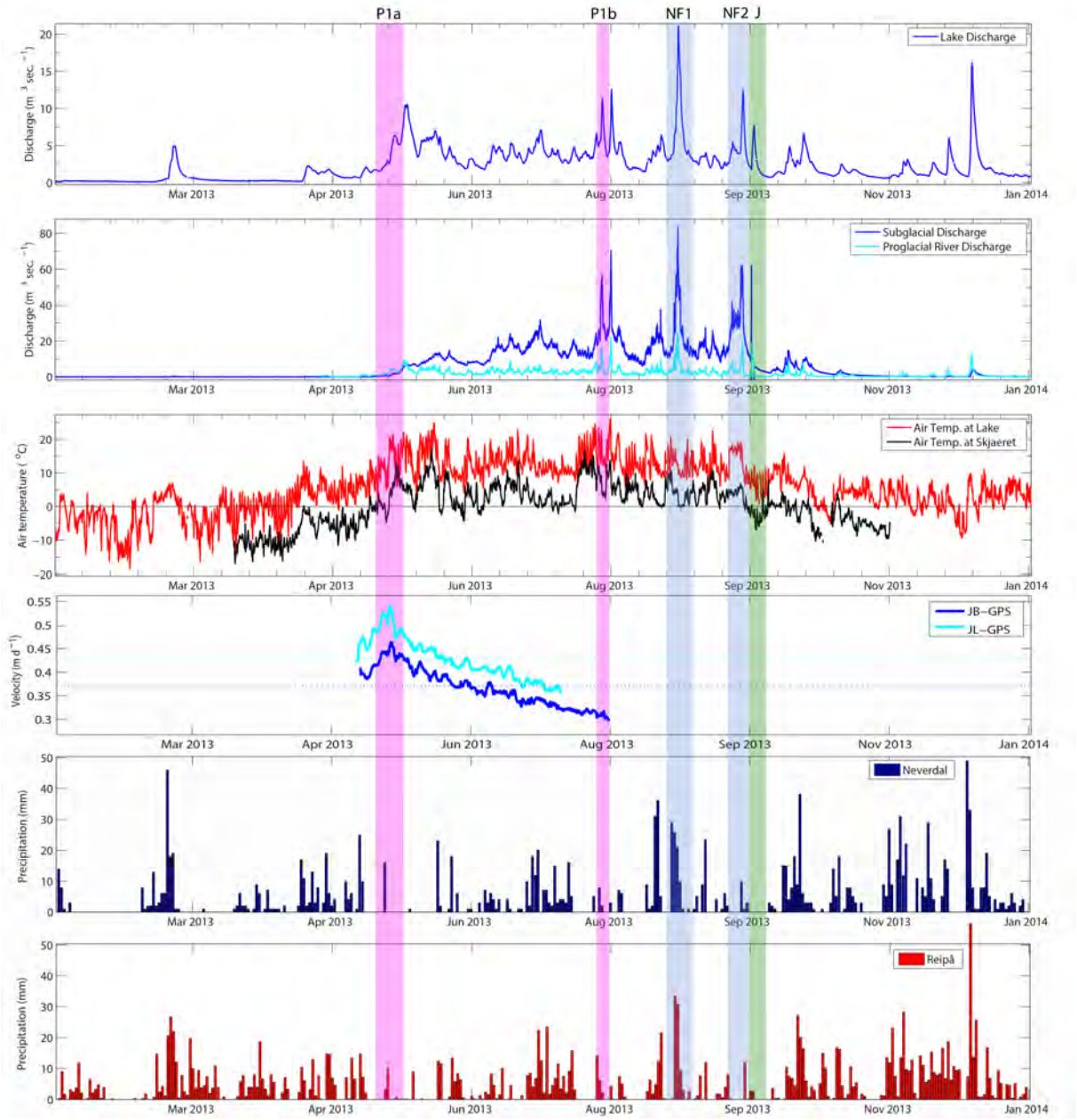

Figure 5.2: *The time-series of all the discharge data used in this section, two from proglacial stations Engabreelv and Engabrevatn, and one subglacial discharge station from the SSL, along with air temperature time-series of two meteorological stations Skjæret at 1360m.a.s.l. and proglacial lake at 8m.a.s.l. The GPS data for the two continuous records from JB and JL are shown in subplot 4. The two precipitation time-series are from Neverdal (12km from Engabreen) and Reipå (20km from Engabreen). The blue and green shaded areas are NF-Natural Flood, J- Jöokulhlaup.*

5.2.1 Wavelet coherence of time-series

Before analysing the results of each P1 event individually, an overview of the relationship between the time-series variables presented in Figure 5.2. One particularly useful metric for assessing the relationship between two series is the wavelet coherence (WTC) (Grinsted et al., 2004). WTC is a normalized measure of similarity and can be interpreted as localized correlation in time-frequency space. WTC can only be pos-

itive values in the range zero to one, unlike traditional correlation coefficients. Both strong anti-correlation and strong correlation will return values close to one. The relative lag/phase relationship is determined by the complex angle from the cross wavelet transform (XWT) of the two time series (Grinsted et al., 2004). In the WTC plots shown in the following (e.g. Figure 5.3) the relative phase angle is shown as arrows with in-phase pointing right and anti-phase pointing left. WTC allows us to assess the relationship between the variables and at which wavelengths these relationships are expressed. Most importantly this allows us to understand the connection, if at all present, between variables.

The following plot (Figure 5.3) offers insights into how two time-series share a similar signal and over which periods, e.g. daily or weekly. As the plot contains the time variable, they are an extremely useful method for assessing changes in connection between variables for example over a melt season , and provide indications for periods where any existing connection is lost, for example during a weather event such as a storm. The coherence plots enable us to assess whether or not it is likely that a signal is genuine or is a result of noise in the dataset. There are a number of benefits using WTC, particularly to when trying to extract signals from datasets where there are low signal-to-noise ratio (Grinsted et al., 2004). In comparison to other standard correlation tests, e.g. simple correlation coefficient of two time-series, the WTC plots provide the user with indications of which wavelengths or periods are likely to generate a reliable signal. A simple correlation coefficient can be misleading and biased based on the users averaging window for example and does not provide the user with the same information about temporal aspects of relationship between the two time-series. The WTC plots can help to identify periods within the data where a breakdown in the relationship arises from an additional forcing, and thus warrant further investigation to identify possible causes.

Discharge and air temperature is an example of where we expect to find a relatively strong relationship (Figure 5.3). The correlation coefficient between proglacial discharge and air temperature between May 2013 and August 2013 is 0.63, indicating a positive correlation during the period. In WTC plot in Figure 5.3 there is coherence at a 1 day wavelength, this is somewhat expected as air temperature drives melt, which in turn is expressed in the proglacial discharge time-series. The WTC also shows coherence at longer wavelengths on the order of a week or so, again which is expected where there are extended periods of high temperatures and high melt. This relationship is stronger in the spring and early summer where high melt is easier to generate, for example through the melt of the snowpack in comparison to the melt of solid glacial ice. Additionally this may be a result of a larger melt catchment during early spring as the immediate area around the glacier and the valleys sides are also covered by snow. During the spring this snow cover melts exposing solid rock, the associated snow melt makes its way into the proglacial river.

At all wavelengths in Figure 5.3, the arrow is pointing slightly upward, which is indicative of the second variable (air temperature) leading the first (discharge). In this case the air temperature leads discharge, as expected. On the 1 day periods there are clear coherent patches and incoherent patches. The incoherent times are as a result of a breakdown in the relationship. These could for example, indicate periods where there are clear weather events such as intense rainfall. One such event takes place between

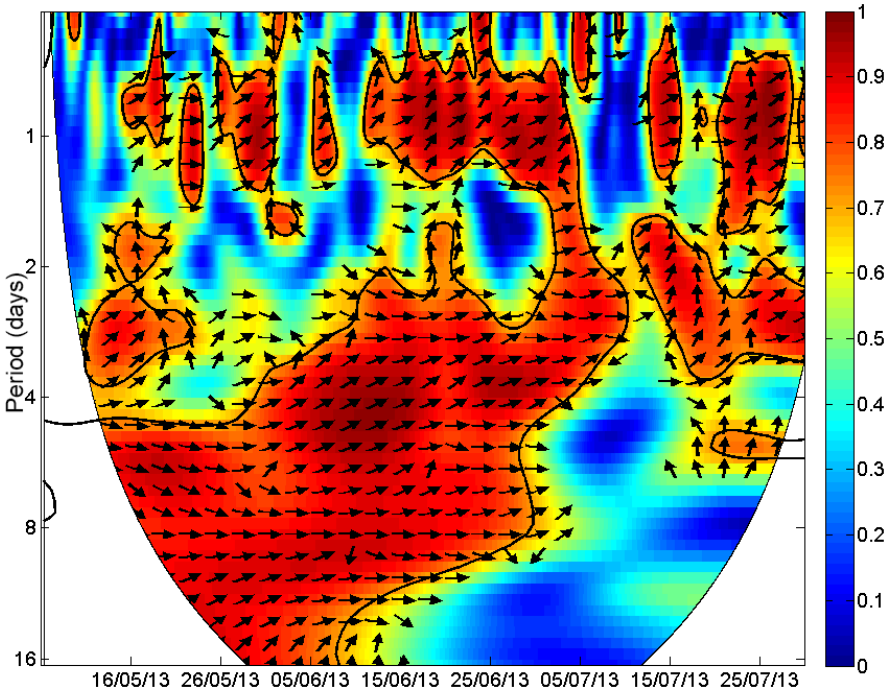

Figure 5.3: *WTC plot of Proglacial discharge and air temperature. These two datasets indicate a close relationship as is expected, as air temperature drives melt.*

the 7th and 15th of July 2013, where there is a complete breakdown of the relationship between air temperature and proglacial discharge, after assessing the time series data there appears to be a significant increase in proglacial discharge and a drop in average air temperature from approximate 13^oC in the weeks leading up to approximately 10^oC during the loss of power in the WTC. At this time a period of high rainfall is recorded at a site nearby where daily precipitation exceeds 25 mm on more than one occasion during the breakdown in coherence in the WTC plot. This breakdown in the coherence between air temperature and discharge, during the July event, indicates it is most likely a rainfall not melt driven event.

Our final WTC plots demonstrate the relationship between the GPS velocity from JB and air temperature in plot A, and GPS velocity from JB and proglacial discharge in plot B in Figure 5.4. Both A (velocity and air temperature) and B (discharge and velocity) show a similar pattern of coherence, which as noted earlier is due to the relatively strong causal relationship between air temperature and melt. These plots in Figure 5.4 show the coherence between the surface velocities from the GPS and meltwater input. Sections 5.3.2 discuss this relationship in more detail in relation to the time-series plots.

Both plots A and B (Figure 5.4) show strong coherence at weekly period during the month of May 2013. As is expected in plot A during the month of May air temperature leads the GPS velocity slightly, this is intuitive where first the temperature must rise for a period of time to allow melt to occur and subsequently for the melt to reach the base of the glacier, where it has the potential to influence basal sliding. At the beginning of June to the end of June the period over which the coherence is strongest shifts to slightly longer wavelengths approximately 8 to 9 days.

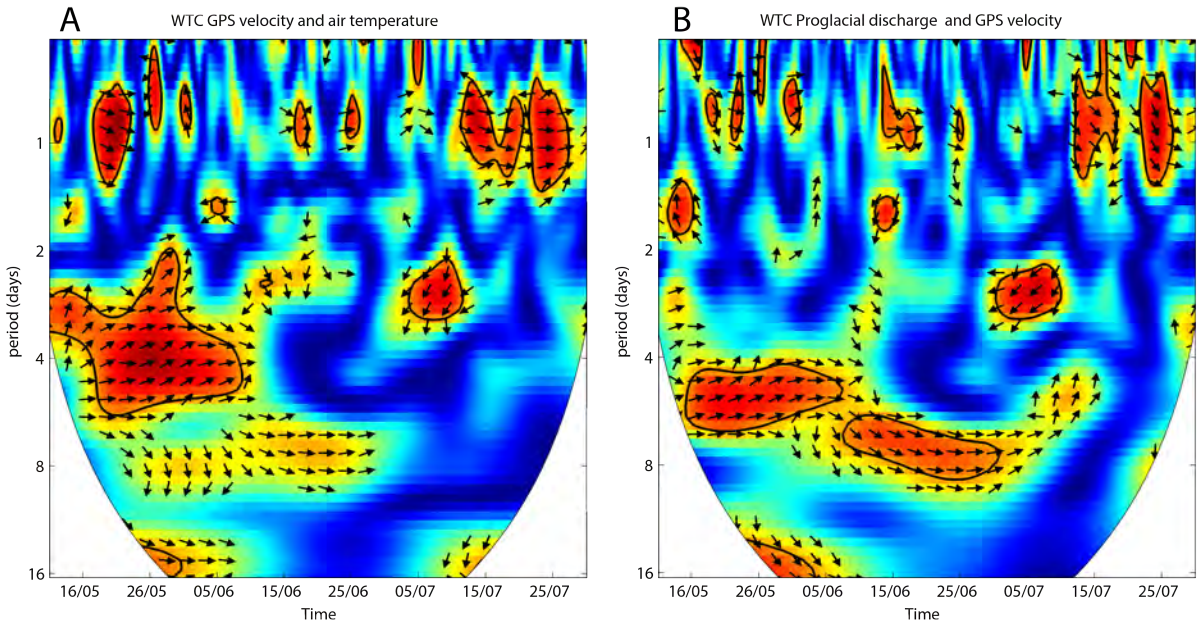

Figure 5.4: *Plot A is the WTC plot of air temperature and GPS velocity measured at JB. Plot B is the WTC plot of proglacial discharge and GPS velocity measured at JB. These two datasets indicate a mixed relationship with varying coherence over a variety of wavelengths. The overall pattern of coherence is similar between the two plots. This is somewhat expected as seen in the WTC plot of air temperature and proglacial discharge in Figure 5.3, which shows how air temperature drives melt.*

The strongest power is in plot B, however this is also observed in plot A albeit at a much lower power, however as it falls outside the 5% significance contour it is not as clear as in plot B. Other more discrete signals are observed at much shorter daily periods in both A and B. The timing of which is similar in both plots in Figure 5.4. During the spring-event (P1a), which is discussed in detail in section 5.3.2 there appears to be a strong coherent signal in plot A and a shorter signal with strong power in plot B, these findings are consistent with the pattern of velocity seen in Figure 5.2. Overall it appears that the coherence at longer wavelengths of a approximately a week is lost and any remaining coherence is expressed at daily wavelengths. Physically this could be due to a shift in the dominant weather patterns, or the removal of the snow pack for example.

5.3 Results

This section focuses on the time-period P1,(pink shaded areas in, Figure 5.2), where we explore the relationship between the datasets during the spring and early summer months in 2013.

5.3.1 Onset of the meltseason

The P1a spring-event is clearly visible in four datasets at Engabreen and are highlighted in Figure 5.2. As mentioned it is likely that other similar spring-event style events took place in the time leading up to the P1a time period. A short period of warm weather and excessive melt occurred in mid-April(prior to P1a), whilst fieldwork was being

carried out at Engabreen, this led to a complete saturation of the snow pack which can be seen in the photos in Figure 5.5.

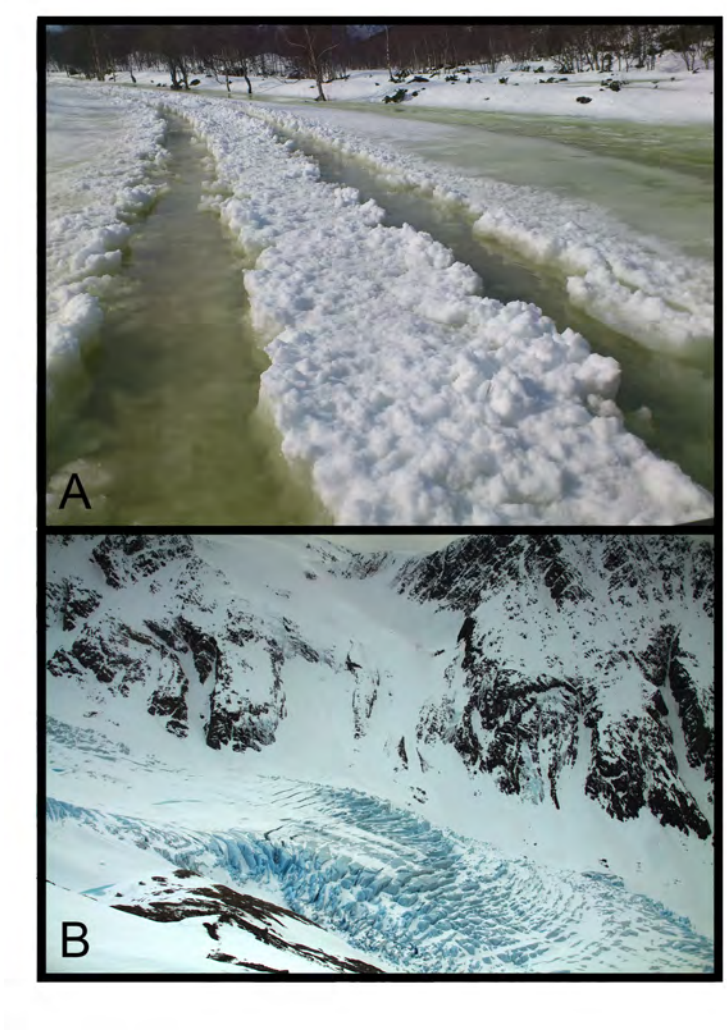

Figure 5.5: *Complete saturation of the snowpack at sea level as an indication of intense melting during mid-April. A, shows the saturated snowpack at sea level and B, shows indications of melt at over 500m.a.s.l with the development of two melt ponds, one on the ice and one at the ice margin in the lower left corner. The same features zoomed in are seen in fig. 5.6.*

Much of the snow cover on the lower part of Engabreen had already melted at this point allowing for a much shorter delay in transporting water from the surface to the bed as the dampening effect of snow cover was removed. However, directly after this melt event temperatures dropped and snowfall covered the lower tongue of Engabreen with a layer of snow. Unfortunately, no record of meltwater in the proglacial stream is available at this time, nevertheless the proglacial lake sensor did record a very sudden rise in discharge during the short intense melt event. This suggests that most likely stream flow also increased in the proglacial stream. Further evidence from the time-lapse camera (Figure 5.6) shows that significant areas of bare ice surface were exposed in mind April (17th April 2013) at elevations over 600m.a.s.l. After inspection of subglacial discharge during this period, a very small peak in discharge occurs at this time with an increase of approximately 0.1 $m\ sec^{-1}$. According to Christianson (2012) this may be enough to affect sliding. A small disturbance is also noted in the load cells

at this time.

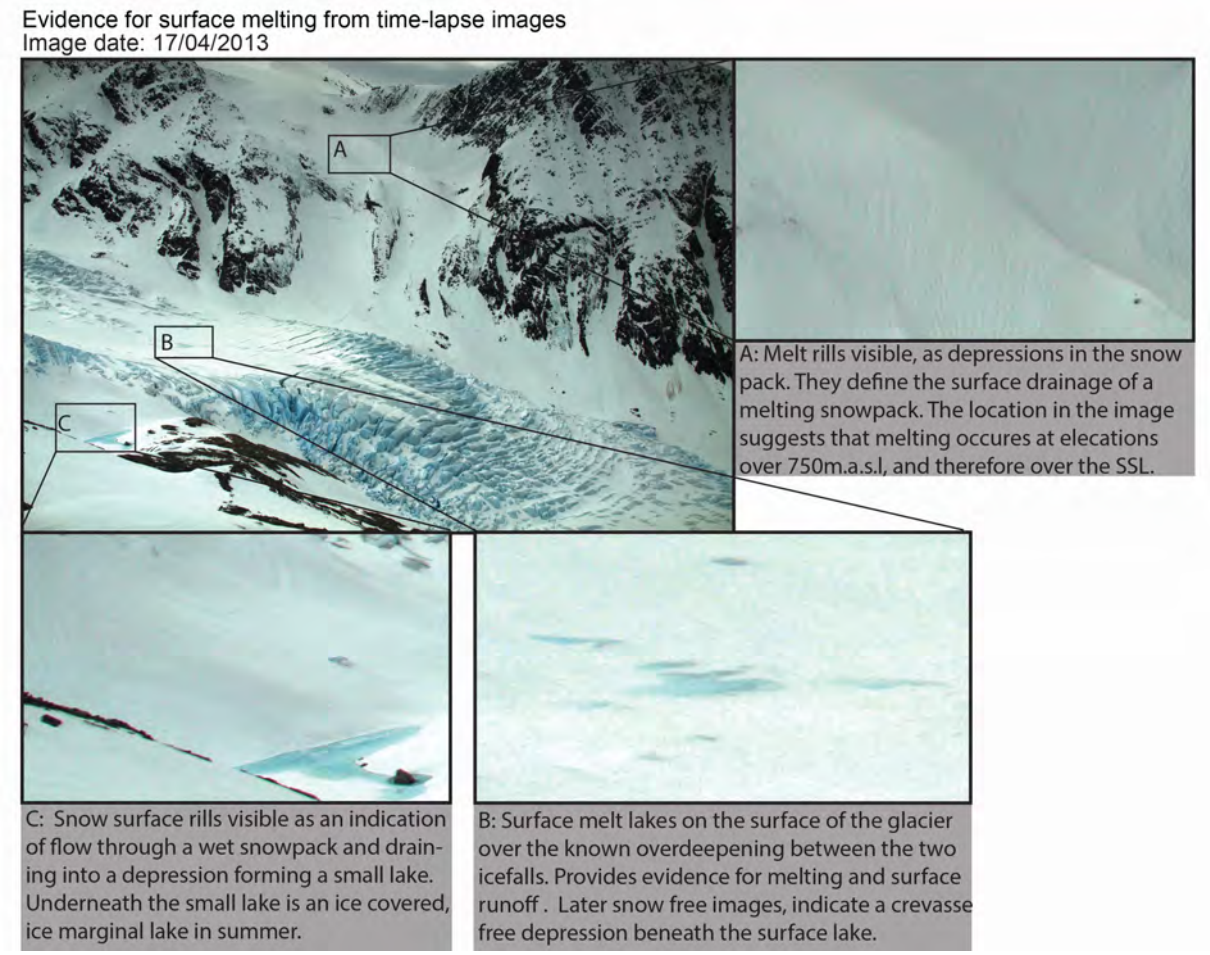

Figure 5.6: *Zoom snapshots from a time-lapse image in April that show evidence of surface melt processes, including melt gullies at the snow surface and surface melt lakes, on and off the ice. The same features are seen in fig. 5.5*

.

5.3.2 Spring-event P1a

This section focuses the observed relationships between discharge, surface velocity and subglacial pressure in Figure 5.7. The individual plots in the figure show the discharge in the pro- and subglacial environment and how the surface velocity and subglacial pressure (measured using the load cells) respond to this seasonal hydrological forcing. The discharge gradually increases during the period in Figure 5.7, and is punctuated by one very rapid increase in discharge on the 16th May. The discharge gradually increases to a peak on the 21st May before subsiding. The GPS velocity follows the general trend of the discharge data however, it reaches its maximum shortly after the rapid rise in discharge on the 16th May, and gradually decreases thereafter. The load cells do not have a typical seasonal cycle, and instead are characterised by series of pressure fluctuations that appear to respond to changes in the two other time-series.

As noted by Mair et al. (2003) the background stream discharge following a spring-event is generally higher than the background flow before the spring event. This is

the case in all the discharge measurements at Engabreen during the P1a spring-event. According to the discharge time-series from the proglacial stream it appears that the P1a event marks the onset of the uninterrupted meltseason in 2013, where complete shut down of the subglacial hydrological system is unlikely as discharge and air temperatures do not drop to zero until mid-September. The P1a spring-event appears at a time where there has been several weeks of increasing air temperatures prior to that of the spring-event. Further inspection of the time-lapse images during the period shortly before and during the spring-event P1a provide evidence of clear skies and lots of sunshine. During this time the snowpack melts quickly, this has a two fold impact on the routing of the meltwater. Firstly, the diminishing snow pack reduces the storage capacity of meltwater at the surface and therefore reduces the delay between melt generation and routing to subglacial drainage system. Secondly, the reduced snow cover exposes crevasses and more direct routes for the water to reach the bed. The increasing air temperatures at the site facilitated the melting of a large proportion of the snow pack on the tongue. Interestingly, the subglacial discharge measurements taken at approximately 700 m.a.s.l. under ≈200m thick ice, also indicate activation of the subglacial drainage system at the same time as the lower tongue. Evidence of melt above 650m.a.s.l. similar to that shown in Figure 5.6 is visible in time-lapse images during the spring-event. This suggests that the P1a event affected a larger portion of the glacier bed compared to that of the previous melt events event during which negligible (0.1 $m^3 sec^{-1}$) increase in subglacial discharge was observed in the time-series at the SSL.

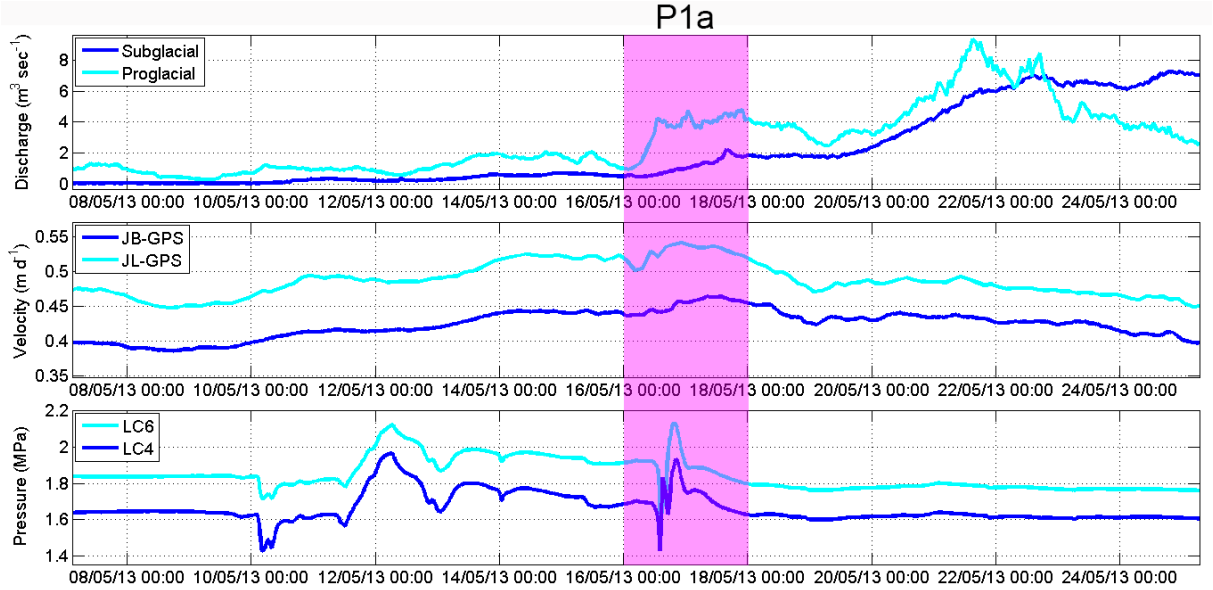

Figure 5.7: *Zoom in of the P1a spring-event, highlighted in the previous overview time-series plot in Figure 5.2 as seen in the two discharge stations, two GPS and two load-cells.*

The horizontal GPS velocity closely follows the changes in varying proglacial discharge from the onset of the recording period on the 6th May 2013 until the first significant peak in proglacial discharge on the 16th of May to the 17th May 2013, following a steep rise in discharge from approximately 1 $m^3 sec^{-1}$ to just over 4 $m^3 sec^{-1}$. The termination pressure drop and rise in LC4 and LC6 corresponds directly with an intermittent sharp peak in the subglacial discharge on the 17th of May. The horizontal velocity decreases quickly following the peak to a plateau around 43 $cm\ d^{-1}$, despite

a second much higher peak (9.4 m^3sec^{-1} proglacial and 9.4 m^3sec^{-1} subglacial) in proglacial discharge on the 21st May 2013 over double the previous peak.

This is also confirmed by load cells (referred to individually as LC4 and LC6 hereafter) installed at the SSL, where a highly variable, multi-day event is recorded in the LC4 and LC6 at the onset of the increase in discharge at the subglacial discharge stations on the 10th May 2013 (Figure 5.7). The event captured in both load cells coincides directly with the sudden increase in the discharge and peak in surface velocity. This multi-day event spanning from the 10th May to the termination on the 19th May 2013, displays a rather chaotic signal in the load cells. However, the termination of the event is similar to other pressure events later in the melt season, which are generally punctuated by a distinct signal that first appears as a drop in pressure followed by an instantaneous rise, that peaks above the background pressure. The background pressure is most likely an indication of approximate local ice overburden pressure. The chaotic load cell signal during the P1a event is interpreted as the activation phase of the subglacial drainage system. During this time the pressure generally remains high, with slight drops that remain above local background pressure. The relatively high pressure during this event with slight drops in pressure, could be indicative of the increased cavitation caused by the initiation of sliding, the short drop in pressure could indicate the growth phase of the cavity which causes a localised low pressure that is immediately flooded with the higher pressure meltwater. The reflection of this in LC4 and LC6 is attributed to according to Lappegard et al. (2006) the presence of a thin water film. The special location of LC4 and LC6 suggests that the high degree of connection between them is only conceivable as a result of a thin water film transferring the same pressure signals (Lappegard and Kohler, 2005; Lefeuvre et al., 2015). Further evidence for a thin water film existing at the base of Engabreen is presented in section 4.

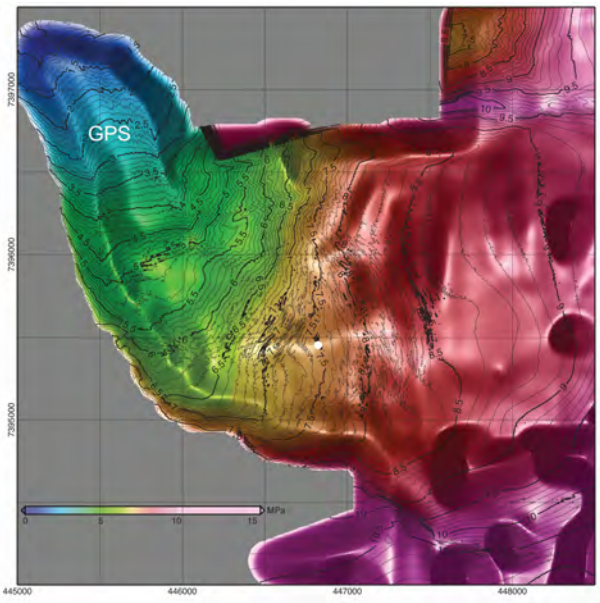

Figure 5.8: *Map of hydropotential at Engabreen, (Figure from Christianson (2012)). Note that the GPS appear to be positioned over the location of the proposed channel.*

The lack of response measured in both the JB and JL GPS' suggests a decrease in subglacial pressure and an indication that the subglacial drainage system is likely

to have undergone a reorganisation over the whole lower glacier. This large-scale reorganisation results in a more efficient evacuation of increasing meltwater through the subglacial drainage network. It is inferred that the changes in the subglacial drainage system were not localised to just the region around the SSL and the load cells. The response recorded by the GPS on the lower tongue (Christianson, 2012) (Figure 5.8) is indicative of a transition between a more distributed inefficient drainage configuration to one that is more efficient and channelised.

5.3.3 Discharge event P1b

This section focuses on a large discharge event at the end of the GPS monitoring period at the end of July. Only one of the GPS', JB was still running at this time and the interpretation is therefore limited to JB velocity data. Figure 5.9 shows a zoom in on the days around the event. This event is a prominent feature of the 2013 melt season, and appears as a string signal in the discharge, and is measured at all the stations. The P1b event appears in the time-series as a consistently high temperature period prior to the discharge event, however the "peakiness" of the discharge curve would suggest an additional sudden source of water. The most obvious of which would be from large precipitation event. However, on inspection of the two precipitation datasets not one single large event stands out. Another source could be from the release of a large volume of stored water within the glacial system. Observations presented in section 5.3.4 offer an insight into the conditions at Engabreen during the P1b period, that assist in the determination of the most likely source of additional water.

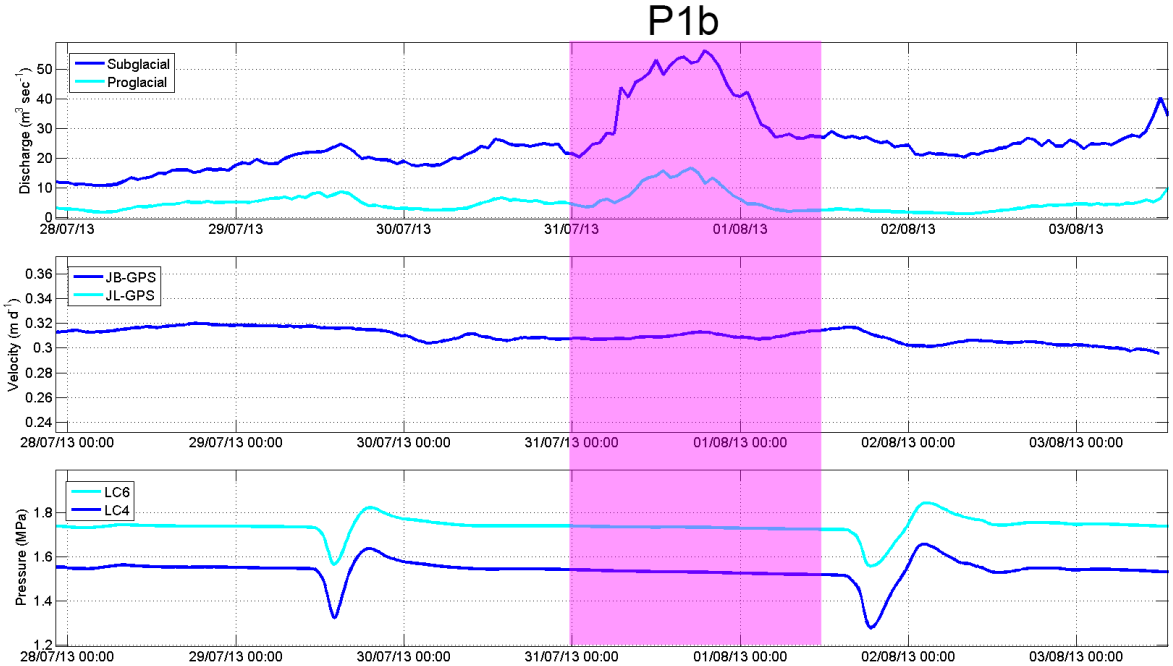

Figure 5.9: *A zoomed in plot of the P1b event. Note that there is only JB GPS data during this period.*

The peak in proglacial discharge exceeds all other peaks in the previous three months since the spring-event (P1a) and reaches a maximum discharge of over 15 $m^3\ sec^{-1}$, and is double the peak in the previous week. The subglacial discharge records a peak

in discharge of over 55 $m^3\ sec^{-1}$, compared to the previous weekly average around 15 $m^3\ sec^{-1}$. The peak in the discharge at both proglacial and subglacial stations is extremely sudden, yet no marked response is detected in the GPS. As discussed in the introduction, the relationship between hydrology and ice flow is complex and this case highlights a situation where it might be expected that the glacier velocity would respond to subglacial forcing, as large volumes of water are routed through the subglacial drainage system, and the discharge curve has a steep gradient. It is therefore somewhat surprising that the large and rapid influx of water has no apparent effect on ice flow. Additionally, the load cell data do not indicate any significant activity directly over the pulse period. Instead they both show a drop-rise-drop signal shortly before and after the discharge event.
The overall slowdown of glaciers during the melt season is very well documented both on valley glacier scales and major outlets of the GrIS (Iken et al., 1983; Sundal et al., 2009). This is usually attributed to the increasing efficiency of the subglacial drainage system. However, during these peak discharge events, and even at periods of highly variable diurnal discharge pulses the drainage system is periodically overloaded resulting in an intermittent increase in surface velocity. This is because the drainage system, again if generally R-channel based, is in constant evolution between the process of melting of the channel walls to keep the channels open and the opposing force of creep closure of the channels due to the ice overburden pressure. This balance on the channel walls is what determines the size of the channels and whether they are expanding or contracting in diameter. Schoof (2010) offers a careful overview of this process that discusses this fine balance of channel enlargement and the balance between expanding and contracting channels. Many studies on alpine glaciers document diurnal and periodic speed-up events on glaciers in the Alps, (Iken and Bindschadler, 1986; Nienow et al., 2005). However, even during periods of strong diurnal discharge pulsing no diurnal signal is observed in the GPS at Engabreen below the lower icefall, at least not during the 2013 season. Possible reasons for the lack of response to the P1b rain enhanced melt event, and the apparent lack of diurnal surface velocity in response to large diurnal meltwater fluxes are discussed in the context of an overall discussion of the hydrological structure of Engabreen in Chapter 6.
The numerous recent studies emphasise that it is not necessarily the volume of water but rather the rate at which the water is routed to the subglacial drainage system (Das et al., 2008; Schoof, 2010; Bartholomew et al., 2010). The rate at which water is input to the subglacial drainage system has the effect of overloading the existing drainage system and increasing water pressure. As a result the drainage system evolves to accommodate the water often in the form of enhancing melt of the surrounding ice through the dissipation of heat from the turbulent flow of water in the channel, if the channels are of R-type.

5.3.4 Results: P1 from time-lapse camera

Velocity

As discussed in detail in chapter 3 the time-lapse and ImGRAFT velocity product is a useful combination which provides velocity estimates over a large spatial area. Here we present a time-series of median-velocities (Figure 5.10) as taken from a small subset (indicated as subset 1 Figure 5.11) of a series of velocity fields that span the entire P1 period (see Chapter 3 for complete velocity maps). Even though images were chosen

with similar snow and lighting conditions there was still a large amount of variability in areas where snow melt was significant between image acquisitions. As a result, subset 1 was chosen based on evidence that in this region the features are very persistent throughout the year and are also visible with a somewhat changing snowcover. Subset 1 lies within the lower section of the lower icefall, just as it enters a compression zone.

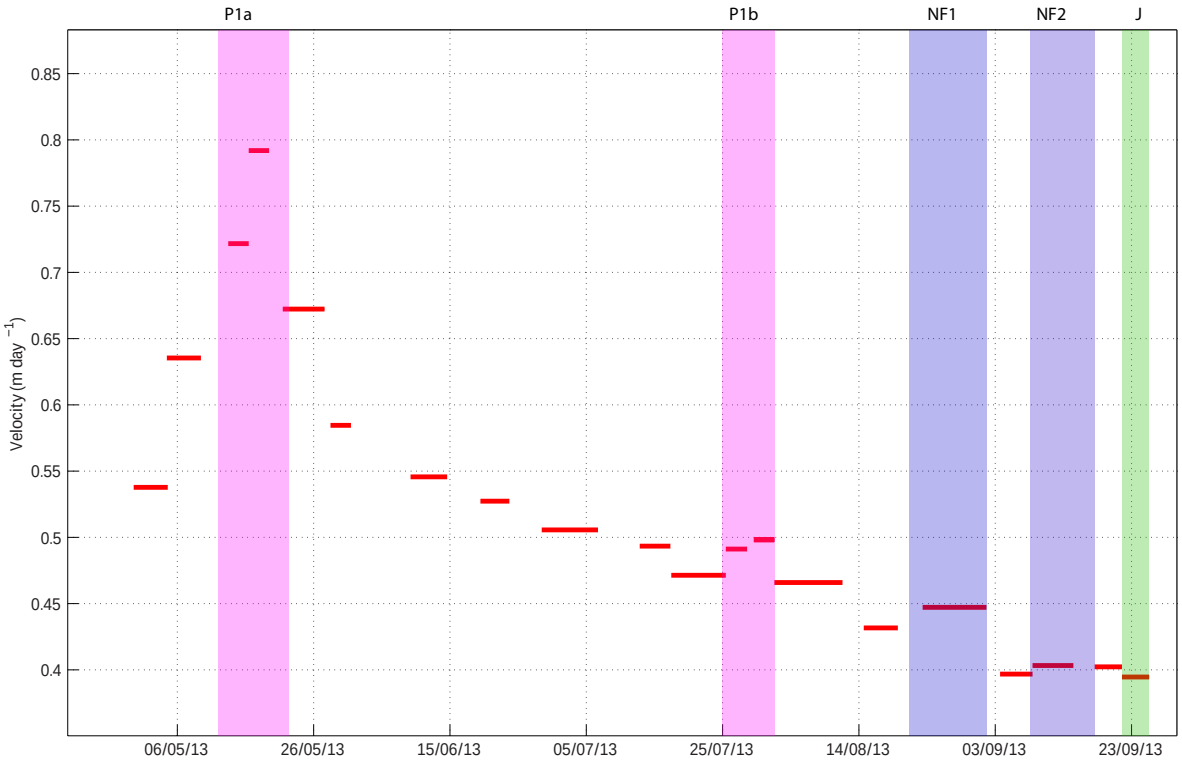

Figure 5.10: *Median velocity during 2013 as extracted from subset 1 from velocity fields produced using ImGRAFT. The length of each individual line indicates the time period between the two images in the image pair. The pink shaded areas are the two P1 events, the NF1 and NF" natural floods are the same as shown in Figure 5.2, the J is the j*ˆ*okulhlaup event.*

The median calculated from the velocity estimates in subset 1 are shown in Figure 5.10, a clear peak is observed in the median velocities during the P1a spring-event. This directly coincides with the observed peak in GPS velocity as discussed in section 5.3.2. Median velocities in the lower section of the lower ice fall peak at just below 0.8 $m\ d^{-1}$. This is almost double what is observed in the two GPS', JB and JL. This is expected as the flow speeds recorded in icefalls are generally higher. In these regions with steep slopes the driving stress is increased compared to ice flowing at shallower gradients. The ice fall is a distinct region of extensional flow, punctuated by large crevasses and séracs. It is is also anticipated that the peak velocities in the subset 1 area were likely to be higher than those presented in Figure 5.10 as these velocities are averaged over a few days.

It should be noted that the median is used instead of the mean as the calculation is performed on unfiltered data, where known mismatches can and do remain. Therefore, by using the median any false-matches have little effect on the result.
Additionally, as demonstrated in Figure 5.11 the data provides a much larger spatial coverage than the point data provided by the GPS, and whilst the frequency of

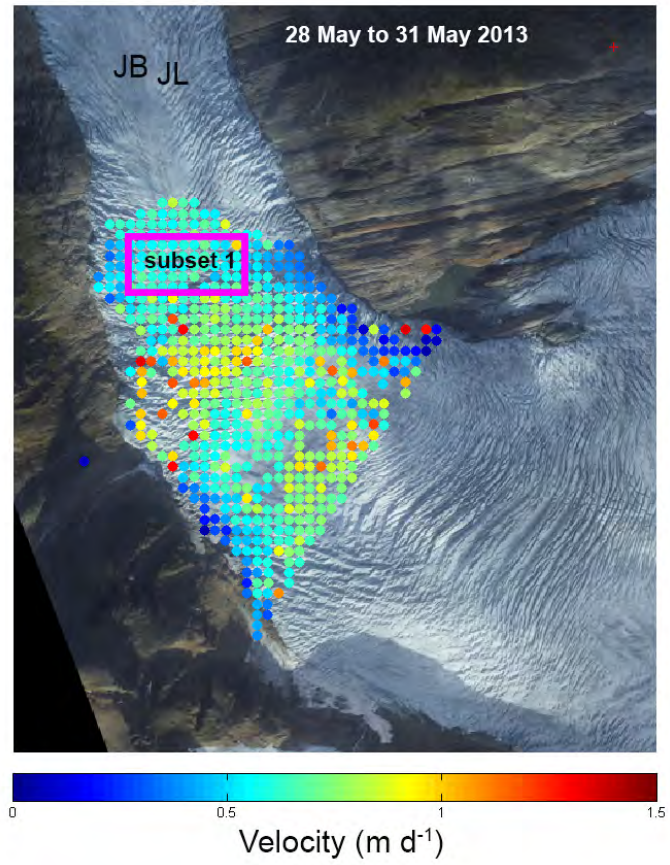

Figure 5.11: *Example velocity field in May 2013. The magenta box indicates subset 1 from which the median velocities are extracted. JB and JL indicate the rough position of the two GPS'.*

measurements of velocity from the time-lapse are much fewer than that of the GPS' fundamental velocity phenomena such as the spring-event can be clearly observed.

Visual Observations

The time-lapse data can also be used to somewhat visibly verify other contradicting datasets. For example in the absence of a local precipitation gauge at Engabreen, two nearby precipitation datasets are used, Reipå and Neverdal, both of which are over 10km away from Engabreen. The general trend appears to be similar between the two stations. However, individual rain events, and in particular the magnitudes of events are extremely variable. This is a clear indication of the highly localised precipitation in the maritime region, that is dominated by high mountains and fjord systems. In these instances where there is a mismatch between the two sites it is useful to refer to the time-lapse imagery to assess whether or not there was an indication of rain as demonstrated in the P1b event where it appears from the meteorological data to be a primarily melt driven event enhanced by periods of precipitation at Engabreen.

The images in Figure 5.12 clearly show change in the discharge of small streams on the opposing valley side. This is an indication of rain, as it appears in unison with cloudy weather and the ground appears wet in the images. The observation of changes in stream activity on the valley side assists in the interpretation of the hydro-meteorological datasets, and help to determine the cause of the increase in discharge

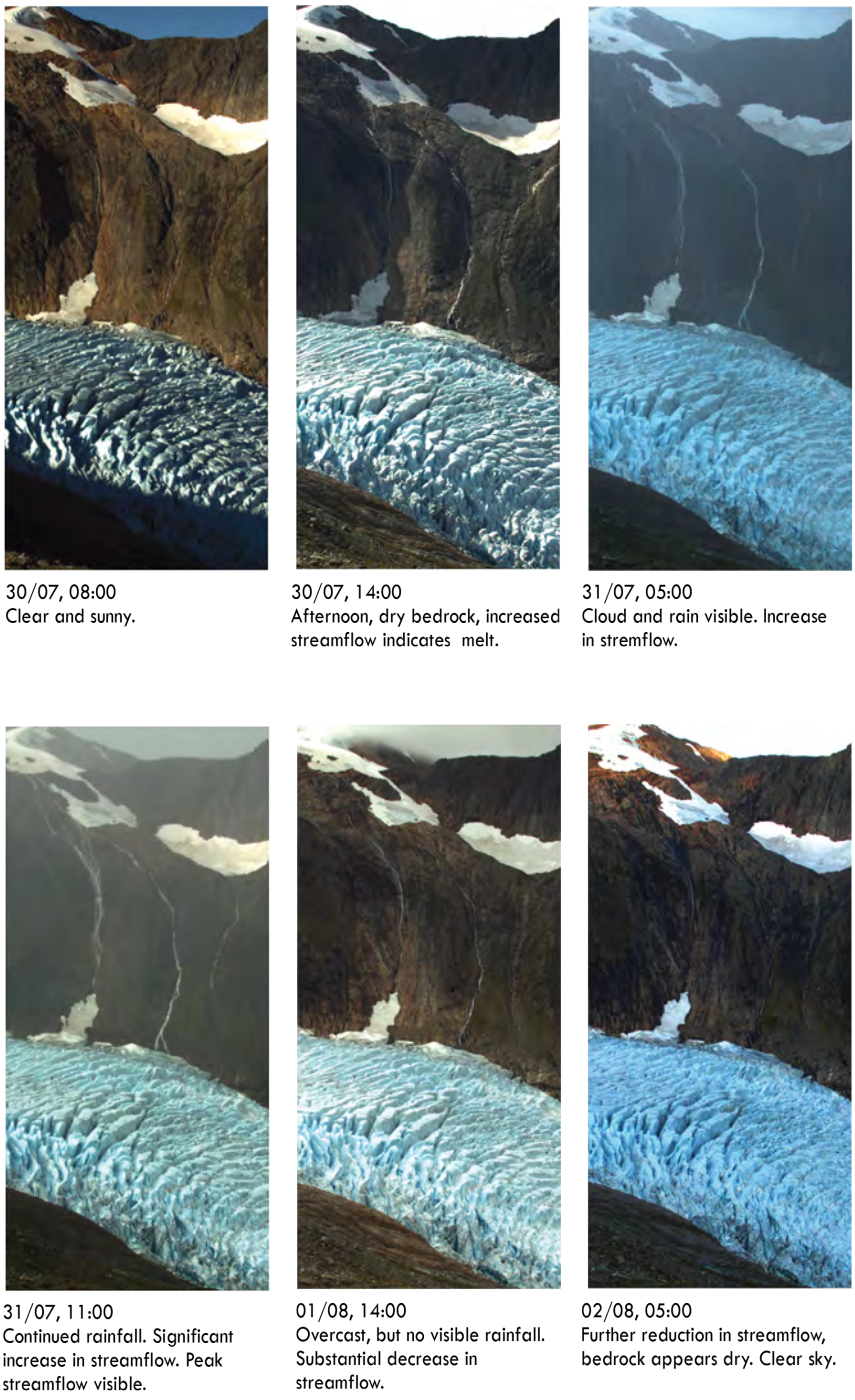

Figure 5.12: *Time-series of time-lapse images during the P1b event. The changing streamflow visible in the small streams on the opposing valley side provides indication of rain/melt conditions. Clear indications of rainfall are visible during poor visibility, and where the ground appears wet in the images. To make it easier for the reader to see the difference in the streamflow, the darker pictures have been lightened.*

at the gauging stations. It is a particularly useful set of observations at times where two or more datasets show opposing signals, for example the discrepancies between the two precipitation datasets during the P1b event. It is therefore suggested based on the evidence in Figure 5.12 that event P1b was most likely a rain induced, temperature

enhanced event, in spite of the evidence in the meteorological data.

5.4 Summary

An extensive set of observations has been presented that reflect the complex nature of the interaction between meltwater and the overlying ice. Many of the responses reflect well defined glacio-hydrological phenomena such as the spring-speed up event. A suit of methods and observations provide a complete overview of the season reorganisation of the hydrology at Engabreen. The reorganisation of the subglacial drainage system is a complex, transitional period where the drainage system adapts in order to facilitate the sudden influx of meltwater and higher background discharge. Previous studies by Lappegard et al. (2006) using pump tests and pressure transducers in boreholes at the SSL suggest that the region around the SSL is dominated by a linked-cavity system in winter and a more channelised (low pressure) configuration in summer (Lappegard et al., 2006). This is consistent with previous investigations of glacial-hydrological studies (Iken et al., 1983; Mair et al., 2001; Nienow et al., 1998).
Previous studies have suggested a Röthlisberger channel (R-Channel) configuration, however as discussed in Chapter 4 alternative lines of evidence indicate a possible combination of Nye-channel and R-channel structure during the melt season. Further insights and discussions on the subglacial drainage configuration are presented in Chapters 4 and 6. In light of the notion that the dominant channel under Engabreen is of a Nye-channel morphology, the activation of summer-channel drainage system could see the melting of ice that had in-filled the Nye-channel through creep closure during the winter. The resulting expression of the spring-event is therefore, a similar, almost indistinguishable expression of increased ice flow and subglacial pressurisation in response to the sudden influx of meltwater to the bed. A mean rate of ice creep under the ˜200m thick Engabreen ice at the SSL has been measured to exceed 25 $cm\ d^{-1}$.
Additional information provided by the time-lapse camera, further demonstrates the usefulness of such an imaging system in the monitoring of a glacial system. This is particularly the case during large, interconnected hydro-metoerological events, such as that in P1b, during which both velocity and supporting "visual meteorological" observations are available.

Chapter 6

Discussion: controls on Hydrology and Dynamics at Engabreen

This chapter summarises and discusses the the evidence and relationships presented in Chapter 4 and 5. Here we explore the impact of the geology and geomorphology at Engabreen on the response of the glacier to the evolution of the hydrological system.

The time-series data presented in Chapter 5 may be interpreted with a highly complex Nye-channel network in mind. When channels are incised into bedrock their capacity to route water efficiently is much higher than in other configurations, and it is often achieved at low pressures. This is because the Nye-channel must first completely fill with water before affecting the overlying ice. This is however not to say that their capacity is infinite, but instead that the large initial size of the channel provides an indication of what volumes of water must be routed through the system in order to reach ice overburden pressure and lead to ice-bed decoupling and enhanced sliding. During the winter months where meltwater discharge is negligible the creep of the overlying ice into the channel significantly reduces the capacity of the drainage system as the cross -sectional area of the channel is much smaller. By reducing the capacity of the Nye-Channels (similar to the roof/complete closure of R-channels) the threshold of water input needed to pressurise the system and lead to an increase in sliding also significantly lowers. This allows the glacio-hydrological system to respond like R-channel dominated systems, particularly during the spring-event. The re-activation of the subglacial drainage system following the low volume, linked cavity winter configuration is well documented in Alpine literature as discussed in chapter 5. The sudden influx of meltwater from the surface overloads the subglacial drainage system in its reduced capacity state and leads to regions of ice-bed decoupling, hydraulic jacking and enhanced sliding.

This can clearly be observed in the two velocity data sets from the GPS and the feature tracked velocity estimates during the spring-event (P1a). During this flooding and pressurisation at the base of the glacier a substantial reorganisation occurs in the drainage system which signifies the switching between the winter, distributed and the summer, channelised drainage structure. Due to the dominant geological features at Engabreen, the meltwater in the cavities flows and is likely to eventually intersect a Nye-channel, either a lateral or central channel and is routed to the terminus. The flow in the reactivated channels melts away the ice that has in-filled the Nye-channels during the low discharge months through the dissipation of heat from the turbulent melting on the roof of the channel. During this transition from Linked-Cavity to Nye-channel

system, the Nye-channels can act as orifices (Sharp et al., 1989) in the early melt season connecting cavities that have formed in the lee bedrock undulations. It is also possible that during the spring-event the immediate capacity of the perpendicular Nye-channels may increase. This leads to a very sudden drop in pressure and reduction in sliding. As the meltwater begins to flow more continuously the full activation of the Nye channels is achieved, thereby increasing the total threshold of the subglacial drainage system. Additionally, as sliding occurs throughout the summer, the perpendicular Nye-channels and cavities remain open. During this period where the Nye-channels are open one expects, that as seen in the GPS data in chapter 5 the relationship between discharge and basal sliding is thus somewhat independent (Walder and Hallet, 1979; Sharp et al., 1989). There appears to be no evidence for diurnal signals in the GPS data which supports the previous statement that diurnal variability in meltwater pulsing does not tend to exceed the capacity of the drainage system. This is somewhat unlike the typical response in R-channel dominated system.
The GPS shows a gradual slowdown throughout the summer where even sudden high discharge events such as event P1b does not appear to exceed the threshold during our observation period, further supporting the postulation that an extensive channelised system is dominant in summer under Engabreen below the bend.
Dye trace studies carried out at the glacier (see Appendix 1) suggest both efficient and inefficient components of the summer drainage system. Rapid peak dye returns during the latter part of the summer meltseason indicate an efficient routing of the water from injection to detection site. However, high dispersion coefficients calculated from the dye BTC suggest a more tortuous, inefficient routing of the water. This inconclusive dye return information could support the notion of a complex drainage network, enhanced by the influence of the perpendicular alignment of large Nye-channels on the routing of the subglacial water. In all cases high percentage tracer recovery in the return suggest minimal storage at the bed. However, recent studies suggest that traditional interpretations of dye BTC and dispersion coefficients can be misleading (Gulley et al., 2012).

The time-lapse camera velocity calculated throughout the entire GPS period do exhibit more variability than the GPS. Event P1b appears to affect the speed of the ice in the lower icefall but not on the lower tongue. The lower icefall appears to be more sensitive to meltwater pulses than the lower tongue, as a large discharge event later in August also generates a short-term speed up. It should be noted that the response recorded in the time-lapse velocities could also be an indication of longitudinal stresses from changes in flow speeds upstream. Unfortunately, no GPS data is available beyond the start of August and therefore it cannot be verified if the GPS responded to the water pulses from the large discharge event at the end of August or the two floods (natural flood and artificial jökulhlaup) in September.

The time-lapse data also indicated two further speed-up events outside of the GPS measurement period. These are both in response to the natural flood in August and the flood prior to the Jökulhlaup. It is unclear if the maintained higher velocity measured over the artificial jökulhlaup is in response to the preceding flood event or the jökulhlaup itself. Results from previous unpublished artificial jökulhlaup experiment, released in July 1997 (*J.Kohler pers. comm*) indicate a response in the surface velocity following the injection of water. However, the difference in timing and varying a priori conditions of the 2013 and 1997 jökulhlaups make it challenging to assess if a similar

response would have been recorded.
One possible indication for a difference in the two responses, is that in 1997 a large volume of the released water being backed-up at the entrance to the Nye-channel and subsequently overflowed along the margin of the glacier. Conversely, in the 2013 experiment all of the released water disappeared into the Nye-channel without any visible obstruction. This suggests that the drainage capacity a the Nye-channel was larger in September 2013 compared to July 1997. It should be noted that both experiments were of a similar volume of water, which is determined by the volume of the sediment chamber. It is therefore likely that if there was an increase in velocity on the lower tongue following the 2013 jökulhlaup it would have been of a lower magnitude to that in 1997. However, in the absence of GPS data on the tongue this is not certain. These unique experiments offer vital insights into the capacity and ability of the subglacial drainage system to accommodate large pulses of water. They also demonstrate the importance of an overview of the preceding hydro-meteorological conditions in inferring the subglacial response, as observed in the surface velocity data.

Other similar previous studies at Engabreen, that investigated the interaction of water ice flow on large glacier scales at Engabreen (Kohler, 1993, 1994, 1998) were carried out during the 1990's. The results published by (Kohler, 1998) in an internal NVE report, suggested that as the intakes began operating and tapping water from the subglacial environment there was a change in the velocity of the glacier downstream of the intakes. However, during this period the glacier had also begun its re-advance thus making it extremely difficult to distinguish between changes in velocity and ice thickness due to the re-advance as a result of positive mass balance or, as a result of the tapping of between 60 and 80 % of the subglacial water, as revealed by tracer studies (Kohler, 1994). A general consensus is that the increase in velocity directly after the activation of the intakes was likely driven by the positive mass balance, but enhanced by the dramatic changes in the subglacial drainage configuration directly downstream of the intakes following there activation. The degree to which each of the components played on the observed increase in velocity in the mid-1990's, is somewhat uncertain as both forcings are likely to have displayed changes in velocity on the same order of magnitude (Kohler, 1998) and *J.Kohler pers. comm.*. The challenge in distinguishing the effect of the intakes on ice flow is very much dependent on the most likely effect that the reduction of 60-80% of the water has on the ice flow. Kohler (1998) proposes three possible scenarios based on established theory, on the effect of changes in the subglacial-hydrological configuration and ice flow, all of which have components that rely heavily on knowledge of the subglacial topography. Whilst it is ultimately unclear of the sign and magnitude of the effects of intake construction on the immediate and more distal down-glacier regions of Engabreen (*J. Kohler pers.comm.*), the reduced water being transported from the upper glacier catchment to the lower catchment is likely to have had an effect on the configuration of the subglacial drainage system, at both short and longer time-scales. It has been suggested that the glacial hydrological system downstream of the intakes has been reset as a result of the extraction of water. Detailed observations of the exposed bedrock suggest that the upper limits of the capacity of the current drainage system is higher than the seasonal peaks in discharge. Nevertheless, it is likely that the resetting of the glacial hydrological catchment caused a shift in the dynamic equilibrium of the system, whereby the drainage evolution matched the lower background discharge levels following the tapping of the subglacial water. It

is likely that the long term effect of the intakes is negligible and any observable shifts are a likely longitudinal response from changes in the glacier dynamics upstream. The result of the intakes and reduction of water reaching the lower tongue of Engabreen is likely to have had an effect on the roof morphology of the Nye-channel. A lower volume of water in the channels would result in a decrease the upward incision of the Nye-channel roof. The response during high discharge events would therefore lead to the melting of the channel roof, and in doing so reduce the pressure. This can be seen in the Nye-channel example from before and after the jökulhlaup event (id 1i in Chapter 4).

6.1 Summary

The range of data presented in chapters 4 and 5 suggest an elaborate and heterogeneous subglacial drainage configuration that is a combination, of channels, cavities (N- and R- channels) and to some extent a TWF. Most glacial systems present complex hydrological network, however the unique geology at Engabreen amplifies the complexity. Whilst the GPS respond to some hydrological forcings but not others is attributed to the evolving subglacial drainage system, which under the lower tongue is dominated by a tortuous Nye-channel network. Discrepancies between responses observed from the time-lapse velocity and the GPS' velocity are likely to be in response to longitudinal influences from the region above the icefall, where a different drainage configuration is predicted. Whilst the Nye-channels are perpendicular below the bend in the glacier, knowledge of the dominant geological plan suggest that any existing Nye-channel like structures above the bend are likely to be parallel or unparalleled to the ice flow. Other studies suggest an R-channel dominated summer drainage in the upper reaches of Engabreen (Kohler, 1998; Lappegard et al., 2006). In the absence of recently exposed bedrock and limited GPR data in the region around the intakes, it is difficult to validate either hypotheses.

Chapter 7

Conclusions and outlook

7.1 Conclusions: Engabreen

This thesis presents a case study like investigation of the outlet glacier Engabreen, Norway. The thesis incorporates numerous techniques and methods, in order to understand the complex interaction between meltwater and ice flow. It is split into two main lines of research; firstly, the development and use of time-lapse camera techniques to estimate ice flow over a large spatial area and secondly, measurements using traditional glacial monitoring techniques, including GPS, discharge, meteorological and geomorphological data.

Recently it has been suggested that the hydro-dynamic responses at the margin of the land terminating sector of the GrIS is somewhat similar to that found in alpine settings (Andrews et al., 2014). It is anticipated that in a warming climate where the large ice masses are thinning and melt seasons extending, both temporally and spatially, similarities between the processes observed at valley glaciers and ice sheets will increase. It is therefore conceivable that, experiments such as the artificial jökulhlaup could allow for comparisons to be drawn between Engabreen and other large ice masses such as the marginal regions of the GrIS. Whilst operating at very different scales, the processes and interaction between water pulses and ice flow bear similarities to lake drainages on the GrIS. The advantage at Engabreen is that a good knowledge of the bed and the short term responses to controlled experiments has the potential for improving the interpretation of surface data, both at Engabreen and on other similar ice masses.

The importance and usefulness of time-lapse imagery is fully explored not only in the quantitative production of velocity fields but also the additional advantageous information obtained from the imagery. The use of time-lapse camera systems has seen a recent surge in use and deployment for a range of investigative purposes. These vary from the more complex feature tracking use as outlined in this thesis, to more aesthetic and informative tools in the case of documenting changes in the natural environment. Time-lapse systems often provide a cost-effective solution to monitoring changes at multiple spatial and temporal scales, in most environments. Their energy consumption is generally low and can be built to be self sustaining and depending on purpose, the data storage capacity high. They also have the additional benefit of acting as a stand alone system that can continuously operate in remote, harsh environments. In many respects they can been seen as the “CCTV” of the environment, offering a wealth of

data that would otherwise only be possible with full time manual observation.

From carrying out this thesis it is highly recommended that other similar studies should also consider using such a time-lapse system, for the primary reason of validating other geophysical datasets. The imagery has added a whole new dimension to the understanding of the study site at Engabreen and provided substantive layers of support to the interpretation of the time-series datasets presented in chapter 5, particularly in periods of contradicting lines of evidence.

7.2 Outlook and wider context

Many of the observations contained in this thesis have the potential to be applied to wider glacial settings, including the GrIS. The overall structure of subglacial hydrological systems are largely determined by on the local geology and geomorphology of the region. This is particularly apparent at hard-bedded glaciers where water routing is highly controlled by the rigid bed. The roughness of the bed and the ability for a cavity network to develop, have yet further influences on the meltwater at the base. The unique bed conditions at Engabreen, are punctuated by large Nye-channels that have led to a discontinuous, 'rough' bed, with many alternate water pathways. The influence of the bed conditions at Engabreen are discussed in this thesis within the framework of limited observations of hydrologically induced short-term speed up events. The responses recorded at Engabreen are somewhat variable. As shown in P1a the response is typical of a traditional valley glacier, where higher than average surface velocities correspond to changes in the meltwater input during spring. However, later in the season during the P1b event, the overall sensitivity to variable melt input appears to be significantly dampened on the lower tongue. Whilst the observation of summer slowdown in itself is consistent with other glacial studies. Where the summer slowdown of the ice is in response to a reorganisation and channelisation of the subglacial drainage system to accommodate the increased base flow of summer meltwater. Nevertheless, it is predicted, that short-pulses of meltwater input are likely to be expressed in short-term changes in the surface velocity, similar to the spring-event. This is due to the breaching of the thresholds in the hydrological system, leading to short periods of increased basal water pressures. These increased pressures are expected to be displayed as short-term speed-up events in the velocity data. This is not necessarily the case at Engabreen, with the most obvious cause, the rigid and high capacity of the Nye- channel dominated drainage system in the lower section of Engabreen. Previous studies have suggested that prior to activation of the subglacial intakes the glacial hydrological system accommodated up to 80% more meltwater. This is not to say that the lack of response is as a direct influence of the subglacial water extraction, as the subglacial drainage system is likely to have established a new dynamic equilibrium based on the lower volumes of water throughput; but rather that the maximum capacity of the system to accommodate rain induced flood events for example, has been increased, particularly during the summer meltseason.

This study highlights the importance of site specific interpretations of the relationship between subglacial water pressure and ice dynamics where a good knowledge of the bed is of utmost importance. Whilst it is a challenge (even on small glaciers) to obtain a high resolution bed data, that encapsulates sufficient detail to construct intricate flow pathways, researchers must seek to use a multidisciplinary approaches to exploit former glacial beds, as these provide an unequivocal dataset of the former, and most

likely present subglacial environment.
This is even more apparent in studies where only surface measurements are available. Many studies use complex inversions and models to infer the basal conditions that are ultimately expressed as changes in velocity at the surface. Whilst these provide useful information in the interpretation of the datasets, that are in no way a substitute for actual basal observations. Observations of basal processes assist in constraint of critical boundary conditions of the inversions that ultimately lead to a more representative outputs.
Case studies, such as the one presented at Engabreen can provide small scale analogies of these processes acting on large scale, at climatically important ice masses, especially in the light of a number of similarities being drawn between the Alpine glacial system and the margins of the GrIS.
Whilst a complete comparison of detailed responses of individual glacial system to hydrological forcings is somewhat limited, widespread glacier case studies highlight the range of possible responses of the glacial system to climatic and local forcings, which has further reaching implications. The effect of large Nye-channels at Engabreen, for example highlights a need for a clear understanding of the underlying bed to better interpret the hydrological (dye trace) and surface expression (velocity) of changes in the hydrology at hard-bedded glaciers. The inconclusive dye trace studies present a clear avenue for further investigation into the effect the perpendicular alignment of Nye-channels can have on water flow.
A lessons learnt from the process-based study at Engabreen, indicate at which scales inferences may be made between different glacial settings and strongly highlight the need for a complete survey at the site, including the recently deglaciated marginal area.

Following the findings of this thesis, numerous lines of further work at Engabreen are identified. These include a more detailed and comprehensive network of velocity measurements on all regions of the glacier. This will allow for a more complete overview of the variations in the surface velocity data, and may could lead to a better understanding of the most likely basal conditions. Surface data covering the area directly over the SSL would be of great benefit to understanding the links between the surface and the bed. By establishing a continuous network of surface measurements, the full potential of the subglacial datasets could be explored. For example by better constrain the surface expression of observed perturbations recorded at the bed.
A detailed finite-element model using Elmer Ice, has been applied to Engabreen by A. Solgaard (in prep.)[1]. The model uses the surface velocity data presented in this study to invert for basal conditions at Engabreen. Many of the details observed in this thesis are used to explain the variations in basal shear stress observed in the model, which form the basis for the development of the combined modelling and observation based study(Bartholomaus et al., 2008). Preliminary results from this study highlight regions where basal friction coefficients are low and indicate high proportions of sliding, and potential regions for water storage at the bed. The findings from the manuscript and this thesis aim to offer a more complete understanding of the different basal conditions at each subregion of the glacier, by exploring numerous dataset and a modelling approach in a multidisciplinary investigation.

[1] *Solgaard A., Messerli A., Grinsted A., Schellenberger T., Jackson M., Zwinger T. and Dahl-Jensen D., Basal conditions at Engabreen inferred from surface velocity fields, Manuscript in preparation*

7.3 Collaborations and outlook: Time-lapse and ImGRAFT

Since the release of ImGRAFT and its associated website http://imgraft.glaciology.net/ many inquiries have been made about applying the toolbox to a range of cryospheric and non-cryospheric applications, including landslides and radar datasets. Below is a small list of the currently known ImGRAFT users and the types of data they are using and which region they are applying it to.

- University of Edinburgh, United Kingdom, and University Centre on Svalbard (UNIS), Norway- Terrestrial Time-lapse data - Svalbard
- Aarhus University, Denmark,- Optical satellite data - Antarctica
- Geological Survey of Denmark and Greenland (GEUS)- Denmark- Optical satellite data - Greenland
- Extreme Ice Survey - Terrestrial time-lapse data - Numerous locations in Greenland
- University of Iceland - Terrestrial time-lapse and UAV data - Iceland
- Aberystwyth University, United Kingdom,- UAV data - Greenland
- Istanbul Technical University, Turkey,- Radar satellite data- ground deformation, Iran
- Polytechnical University of Turin, Italy, Terrestrial laser scan data- Landslides, Italy

Current close collaborations with many of the research groups listed above are developing rapidly with the preparation of manuscripts covering a range of research topics within the cryosphere. In particular, these includes studies where velocity mapping and associated products form a key component of the research.

Currently ImGRAFT has successfully been applied to the following data types:

- Terrestrial time-lapse imagery
- Optical Satellite imagery (Landsat MODIS)
- Aerial imagery (from UAVs, aircraft)
- Radar (Sentinal-1A data)

The diverse applications of ImGRAFT since its release in 2014, highlight a number of potential avenues for future development. One of the aims of ImGRAFT is to be able to collaborate with its users to channel its development. One area that we wish to develop is the use of ImGRAFT on radar data in combination with optical imagery. Radar satellite data, unlike optical imagery is not hampered by the presence of clouds or darkness. Thereby offering a much larger pool of data on which to perform feature tracking. Whilst ImGRAFT was developed for use with optical imagery, the principle of feature tracking radar data is similar. One current aim is to fill data gaps in optically

feature tracked data products with radar feature tracked products, thereby combining two datasets with different strengths to provide a more complete data coverage. An additional benefit of using multiple data sources, is that the temporal resolution and coverage is significantly increased. Furthermore, it is advantageous as only knowledge and installation of a single toolbox is needed in order to process a large, multi-platform datasets. It is also our aim to further increase the automation of ImGRAFT to process continuous datasets, for example automatic download, extraction and processing of newly acquired satellite data.

Further developments are also currently being investigated in relation to the terrestrial capacity of ImGRAFT. One obvious path is to include a stereo-imagery option, that would allow for the generation of DEMs. As mentioned, the DEM is a vital component of the terrestrial application and thus the greater the number available throughout the monitoring period, the more accurate the resulting output data is.

The application of ImGRAFT to a variety of data is only beginning to be realised. The planned future automation and data type adaptations to the ImGRAFT toolbox, open up the potential within numerous geoscientific applications not only within the realms of cryosphereic science. We hope to continue the tight collaboration with our users to channel our efforts in improving not only the toolbox but also its corresponding documentation.

Bibliography

Andreassen, L. M., Elvehøy, H., Jóhannesson, T., and others (2006). Modelling the climate sensitivity of storbreen and engabreen, norway. *NVE Rapp.*

Andreassen, L. M., Elvehøy, H., Kjøllmoen, B., Engeset, R. V., and Haakensen, N. (2005). Glacier mass-balance and length variation in norway. *Ann. Glaciol.*, 42(1):317–325.

Andrews, L. C., Catania, G. A., Hoffman, M. J., Gulley, J. D., Lüthi, M. P., Ryser, C., Hawley, R. L., and Neumann, T. A. (2014). Direct observations of evolving subglacial drainage beneath the greenland ice sheet. *Nature*, 514(7520):80–83.

Bartholomaus, T. C., Anderson, R. S., and Anderson, S. P. (2008). Response of glacier basal motion to transient water storage. *Nat. Geosci.*, 1(1):33–37.

Bartholomew, I., Nienow, P., Mair, D., Hubbard, A., King, M. A., and Sole, A. (2010). Seasonal evolution of subglacial drainage and acceleration in a greenland outlet glacier. *Nat. Geosci.*, 3(6):408–411.

Bartholomew, I., Nienow, P., Sole, A., Mair, D., Cowton, T., and King, M. A. (2012). Short-term variability in greenland ice sheet motion forced by time-varying meltwater drainage: Implications for the relationship between subglacial drainage system behavior and ice velocity. *Journal of Geophysical Research: Earth Surface*, 117(F3).

Benn, D. I. and Evans, D. J. A. (2010). *Glaciers and glaciation*. Hodder Arnold Publication. Hodder Education, 2nd edition edition.

Björnsson, H. (2003). Subglacial lakes and jökulhlaups in iceland. *Glob. Planet. Change*, 35(3–4):255–271.

Chandler, D. M., Wadham, J. L., Lis, G. P., Cowton, T., Sole, A., Bartholomew, I., Telling, J., Nienow, P., Bagshaw, E. B., Mair, D., Vinen, S., and Hubbard, A. (2013). Evolution of the subglacial drainage system beneath the greenland ice sheet revealed by tracers. *Nat. Geosci.*, 6(3):195–198.

Christianson, K. (2012). *Geophysical exploration of glacier basal processes and grounding line dynamics*. PhD thesis, Pennsylvania State University, Pennsylvania.

Clarke, G. K. C. (2005). Subglacial processes. *Annu. Rev. Earth Planet. Sci.*, 33(1):247–276.

Cohen, D. (2000). Rheology of ice at the bed of engabreen, norway. *J. Glaciol.*, 46(155):611–621.

Cohen, D., Hooke, R., Iverson, N. R., and Kohler, J. (1968). General theory of subglacial cavitition and sliding of temperate glaciers. *J. Glaciol.*, 7:21–58.

Cohen, D., Hooke, R., Iverson, N. R., and Kohler, J. (2000). Sliding of ice past and obstacle at engabreen, norway. *J. Glaciol.*, 46(155):599–610.

Cowton, T., Nienow, P., Sole, A., Wadham, J., Lis, G., Bartholomew, I., Mair, D., and Chandler, D. (2013). Evolution of the subglacial drainage system beneath the greenland ice sheet revealed by tracers. *Nature Geosc.*, 6(6).

Das, S. B., Joughin, I., Behn, M. D., Howat, I. M., King, M. A., Lizarralde, D., and Bhatia, M. P. (2008). Fracture propagation to the base of the greenland ice sheet during supraglacial lake drainage. *Science*, 320(5877):778–781.

Engeset, R. V., Elvehøy, H., Andreassen, L. M., Haakensen, N., Kjøllmoen, B., Roald, L. A., and Roland, E. (2000). Modelling of historic variations and future scenarios of the mass balance of svartisen ice cap, northern norway. *Ann. Glaciol.*, 31(1):97–103.

Flotron, A. (1973). Photogrammetirsche messungen von gletscherbewegunen mit automatischer kamera. *Schweizerische Zeitschrift fur Vermessung, Kulturtecknik und Photogrammetrie*, 71(15-17):1–73.

Flowers, G. E. (2010). Glacier hydromechanics: early insights and the lasting legacy of three works by iken and colleagues. *J. Glaciol.*, 56(200):1069–1078.

Flowers, G. E. and Clarke, G. K. C. (2002). A multicomponent coupled model of glacier hydrology 1. theory and synthetic examples. *J. Geophys. Res. [Solid Earth]*, 107(B11):ECV 9–1–ECV 9–17.

Fowler, A. (1987). Sliding with cavity formation. *J. Glaciol.*, 33:255–67.

Grinsted, A., Moore, J. C., and Jevrejeva, S. (2004). Application of the cross wavelet transform and wavelet coherence to geophysical time series. *Nonlinear Process. Geophys.*, 11(5/6):561–566.

Gulley, J. D., Walthard, P., Martin, J., Banwell, A. F., Benn, D. I., and Catania, G. (2012). Conduit roughness and dye-trace breakthrough curves: why slow velocity and high dispersivity may not reflect flow in distributed systems. *J. Glaciol.*, 58(211):915–925.

Hanna, E., Huybrechts, P., Steffen, K., Cappelen, J., Huff, R., Shuman, C., Irvine-Fynn, T., Wise, S., and Griffiths, M. (2008). Increased runoff from melt from the greenland ice sheet: A response to global warming. *J. Clim.*, 21(2):331–341.

Hoffman, M. and Price, S. (2014). Feedbacks between coupled subglacial hydrology and glacier dynamics. *Journal of Geophysical Research: Earth Surface*, 119(3):414–436.

Hoffman, M. J., Catania, G. A., Neumann, T. A., Andrews, L. C., and Rumrill, J. A. (2011). Links between acceleration, melting, and supraglacial lake drainage of the western greenland ice sheet. *Journal of Geophysical Research: Earth Surface*, 116(F4).

Hubbard, B., Bryn, H., and Alun, H. (1998). Bedrock surface roughness and the distribution of subglacially precipitated carbonate deposits: implications for formation at glacier de tsanfleuron, switzerland. *Earth Surf. Processes Landforms*, 23(3):261–270.

Hubbard, B. and Glasser, N. (2005). *Field techniques in glaciology and glacial geomorphology*. Wiley.

Hubbard, B. and Nienow, P. (1997). Alpine subglacial hydrology. *Quat. Sci. Rev.*, 16(9).

Iken, A. and Bindschadler, R. A. (1986). Combined measurements of subglacial water pressure and surface velocity of findelengletscher, switzerland: conclusions about drainage system and sliding mechanism. *J. Glaciol.*, 32(110).

Iken, A., Röthlisberger, H., Flotron, A., and W, H. (1983). The uplift of unteraargletscher at the beginning of the melt season - a consequence of water storage at the bed? *J. Glaciol.*, 29(101):28–47.

Iken, A., Röthlisberger, H., Flotron, A., and W, H. (1995). Intra-annual variations in glacier motion: a review. *Prog. Phys. Geog.*, 19(1):61–106.

Iverson, N. R., Hooyer, T. S., Fischer, U. H., Cohen, D., Moore, P. L., Jackson, M., Lappegard, G., and Kohler, J. (2007). Soft-bed experiments beneath engabreen, norway: regelation infiltration, basal slip and bed deformation. *J. Glaciol.*, 53(182):323–340.

Jackson, M., Brown, I. A., and Elvehøy, H. (2005). Velocity measurements on engabreen, norway. *Ann. Glaciol.*, 42(1):29–34.

Jansson, P., Kohler, J., and Pohjola, V. (1996). Characteristics of basal ice at engabreen, northern norway. *Ann. Glaciol.*, 22:114–120.

Joughin, I., Smith, B. E., Howat, I. M., Scambos, T., and Moon, T. (2010). Greenland flow variability from ice-sheet-wide velocity mapping. *J. Glaciol.*, 56(197):415–430.

Kamb, B. (1987). Glacier surge mechanism based on linked cavity configuration of the basal water conduit system. *J. Geophys. Res.*, 92(B9):9083–9100.

Kennett, M., Laumann, T., and Lund, C. (1993). Helicopter-borne radio-echo sounding of svartisen, norway. *Ann. Glaciol.*

Kohler, J. (1988). Kartlegging av istykkelse på vestre svartisen 1986. Technical Report 3, NVE-VHB Oppdragsrapport.

Kohler, J. (1993). Tracing at engabreen-august1993. Technical Report 17, NVE-HB Notat.

Kohler, J. (1994). Tracing at engabreen 1994. Technical Report 23, NVE-HB Notat.

Kohler, J. (1998). The effect of subglacial intakes on ice dynamics at engabreen. Technical Report 12, NVE-HB Notat.

Lappegard, G. and Kohler, J. (2005). Determination of basal hydraulic systems based on subglacial high-pressure pump experiments. *Ann. Glaciol.*, 40(1):37–42.

Lappegard, G., Kohler, J., Jackson, M., and Hagen, J. O. (2006). Characteristics of subglacial drainage systems deduced from load-cell measurements. *J. Glaciol.*, 52(176):137–148.

Lefeuvre, P.-M., Jackson, M., Lappegard, G., and Hagen, J. O. (2015). Interannual variability of glacier basal pressure from a 20 year record. *Ann. Glaciol.*, 56(70):33–44.

Mair, D., Nienow, P., Sharp, M., Wohlleben, T., and Willis, I. (2002). Influence of subglacial drainage system evolution on glacier surface motion: Haut glacier d'arolla, switzerland. *J. Geophys. Res. [Solid Earth]*, 107(B8):EPM 8–1–EPM 8–13.

Mair, D., Nienow, P., Willis, I., and Sharp, M. (2001). Spatial patterns of glacier motion during a high-velocity event: Haut glacier d'arolla, switzerland. *J. Glaciol.*, 47(156):9–20.

Mair, D., Willis, I., Fischer, U. H., Hubbard, B., Nienow, P., and Hubbard, A. (2003). Hydrological controls on patterns of surface, internal and basal motion during three"spring events": Haut glacier.

Meierbachtol, T., Harper, J., and Humphrey, N. (2013). Basal drainage system response to increasing surface melt on the greenland ice sheet. *Science*, 341(6147):777–779.

Menzies, J. (2009). Glacial geomorphology. In *Encyclopedia of Paleoclimatology and Ancient Environments*, pages 361–374. Springer Netherlands.

Messerli, A. and Grinsted, A. (2015). Image georectification and feature tracking toolbox: ImGRAFT. *Geoscientific Instrumentation, Methods and Data Systems*, 4(1):23–34.

Messerli, A., Karlsson, N. B., and Grinsted, A. (2014). Brief communication: 2014 velocity and flux for five major greenland outlet glaciers using ImGRAFT and landsat-8. *The Cryosphere Discuss.*, 8(6):6235–6250.

Moon, T., Joughin, I., Smith, B., and Howat, I. (2012). 21st-century evolution of greenland outlet glacier velocities. *Science*, 336(6081):576–578.

Moore, P. L., Winberry, J. P., Iverson, N. R., Christianson, K. A., Anandakrishnan, S., Jackson, M., Mathison, M. E., and Cohen, D. (2013). Glacier slip and seismicity induced by surface melt. *Geology*, 41(12):1247–1250.

Ng, F. and Hallet, B. (2002). Patterning mechanisms in subglacial carbonate dissolution and deposition. *J. Glaciol.*, 48(162):386–400.

Nienow, P., Sharp, M., and Willis, I. (1998). Seasonal changes in the morphology of the subglacial drainage system, haut glacier d'arolla, switzerland. *Earth Surf. Processes Landforms*, 23(9):825–843.

Nienow, P. W., Hubbard, A. L., Hubbard, B. P., Chandler, D. M., Mair, D. W. F., Sharp, M. J., and Willis, I. C. (2005). Hydrological controls on diurnal ice flow variability in valley glaciers. *Journal of Geophysical Research: Earth Surface*, 110(F4).

Pellikka, P. and Rees, W. G. (2009). *Remote Sensing of Glaciers: Techniques for Topographic, Spatial and Thematic Mapping of Glaciers*. A Balkema book. Taylor & Francis.

Rignot, E. and Kanagaratnam, P. (2006). Changes in the velocity structure of the greenland ice sheet. *Science*, 311(5763):986–990.

Ryser, C., Lüthi, M. P., Andrews, L. C., Hoffman, M. J., Catania, G. A., Hawley, R. L., Neumann, T. A., and Kristensen, S. S. (2014). Sustained high basal motion of the greenland ice sheet revealed by borehole deformation. *J. Glaciol*, 60(222):647–660.

Schoof, C. (2010). Ice-sheet acceleration driven by melt supply variability. *Nature*, 468(7325):803–806.

Schuler, T. V., Hock, R., Jackson, M., Elvehøy, H., Braun, M., Brown, I., and Hagen, J.-O. (2005). Distributed mass-balance and climate sensitivity modelling of engabreen, norway. *Ann. Glaciol.*, 42(1):395–401.

Sharp, M., Gemmell, J. C., and Tison, J.-L. (1989). Structure and stability of the former subglacial drainage system of the glacier de tsanfleuron, switzerland. *Earth Surf. Processes Landforms*, 14(2):119–134.

Sharp, M., Tison, J.-L., and Fierens, G. (1990). Geochemistry of subglacial calcites: Implications for the hydrology of the basal water film. *Arct. Alp. Res.*, 22(2):141–152.

Sundal, A. V., Shepherd, A., Nienow, P., Hanna, E., Palmer, S., and Huybrechts, P. (2009). Evolution of supra-glacial lakes across the greenland ice sheet. *Remote Sens. Environ.*, 113(10):2164–2171.

Walder, J. and Hallet, B. (1979). Geometry of former subglacial water channels and cavities. *J. Glaciol.*

Weertman, J. (1972). General theory of water flow at the base of a glacier or ice sheet. *Rev. Geophys.*, 10(1):287–333.

Worsley, P. (2007). The british geological survey's glaciological expedition to arctic norway in 1865. *Mercian Geologist*.

Yde, J. C., Hodson, A. J., Solovjanova, I., Steffensen, J. P., Nørnberg, P., Heinemeier, J., and Olsen, J. (2012). Chemical and isotopic characteristics of a glacier-derived naled in front of austre grønfjordbreen, svalbard. *Polar Res.*, 31(0).

Zwally, J., H Abdalati, W., Herring, . T., Larson, . K., Saba, . J., and Steffen, . K. (2002). Surface Melt–Induced acceleration of greenland Ice-Sheet flow. *Science*, 297.

Dye Tracing

Dye tracing Break through curves in 2012

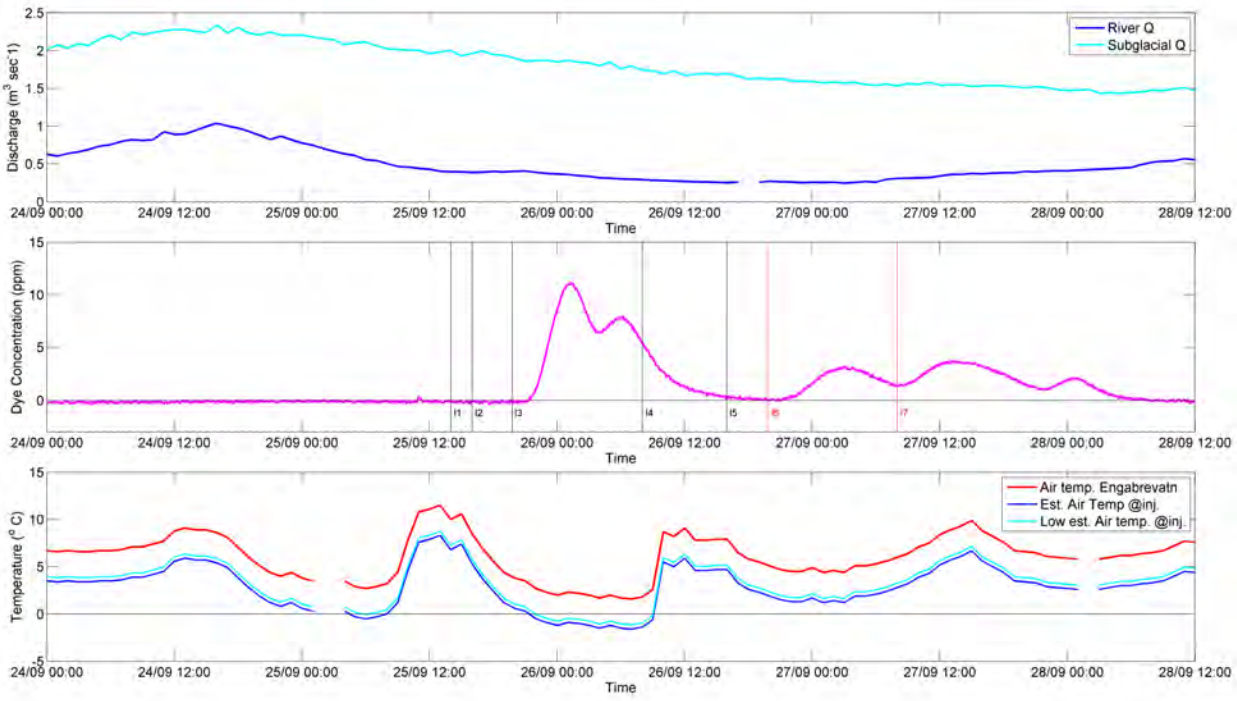

Dye tracing Break through curves September 2013 –Jökulhlaup experiment

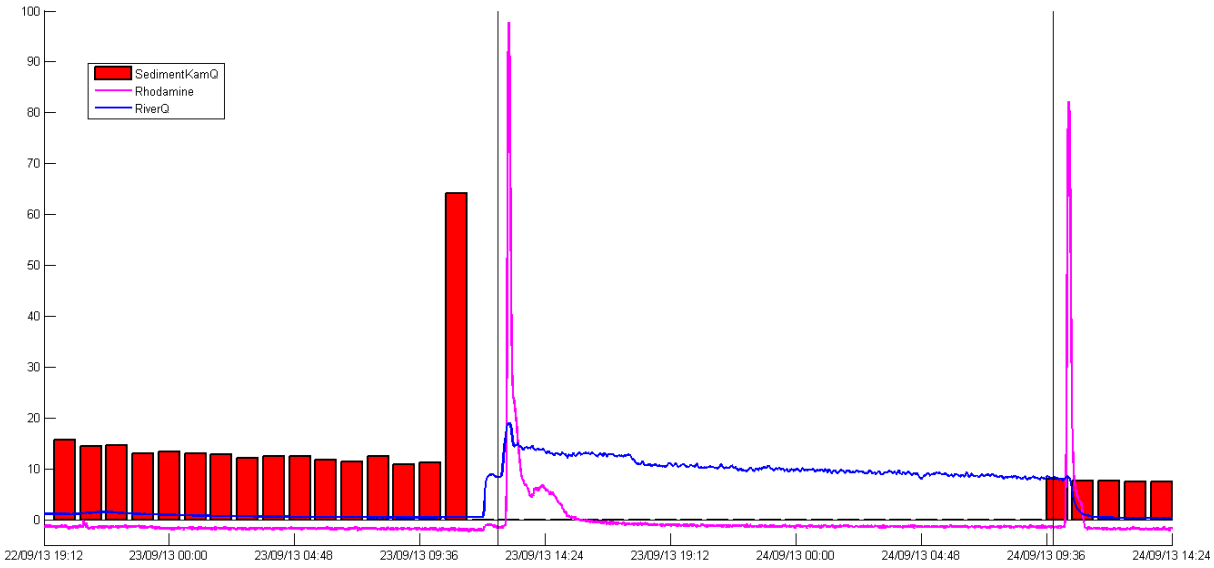

Overlapping Dye Break Through Curves (BTC)

Dye tracing dates: 25/09/2012 to 28/09/2012

Injection location: Engabreen bend, into ice dammed lake outflow stream

Date	Time	Dye Volume (conc.100g/l)	Distance (x) meters	Travel time -tm mins (secs)	Rising limb half peak –t1 Mins(secs)	Falling limb half peak –t2 Mins (secs)	Mean velocity m/sec	D	d	Amount dye returned	Q snout at detection	Local Q
29/08/2012	15:58	1000	1700	140 (8400)	120 (7200)	170 (10200)	0.2	3.95	19.75			0.8
			1700									
25/09/2012	14:00	400	1700	718 (43096)	615 (36916)	839 (50356)	0.04	0.57	14.42	For all 5 BTC 185.58g out of 190g injected		0.4
25/09/2012	16:00	400	1700	915 (62116)	757 (45453)	1106 (66376)	0.03	0.67	16.72			0.4
25/09/2012	19:47	400	1700	OVERLAP								0.4
26/09/2012	08:02	300	1700	OVERLAP								-
26/09/2012	16:00	400	1700	OVERLAP								-
26/09/2012	19:48	150	1700							DNR		-
27/09/2012	08:00	150	1700							DNR		-
Jokulhlaup	-------	-------		---------								
23/09/2013	13:36		2463	1491	1264	1729	1.7	35.95	21.12			
24/09/2013	10:52		2463	1539	1284	1808	1.6	41.56	24.44			